

POLITECNICO DI TORINO

CORSO DI LAUREA MAGISTRALE IN INGEGNERIA MECCANICA

Dipartimento di Ingegneria Meccanica e Aerospaziale



TESI DI LAUREA MAGISTRALE IN MECCANICA DEL VEICOLO

MULTIBODY MODELLING OF A HEAVY DUTY TRUCK AND ANALYSIS OF THE EFFECT OF FRAME FLEXIBILITY ON VEHICLE DYNAMICS

Relatore

Prof. Enrico GALVAGNO

Prof. Mauro VELARDOCCHIA

Tutor aziendale

Dott. Vladi Massimo NOSENZO

Laureando

Angelo Domenico VELLA

ANNO ACCADEMICO 2017 – 2018

all'Ing. Lodovico Paiotta

La logica vi porterà da A a B. L'immaginazione vi porterà dappertutto. (A.Einstein)

INDEX

INDEX.....	3
ABSTRACT	5
PICTURES INDEX.....	7
TABLE INDEX.....	10
INTRODUCTION	11
CNH Industrial and IVECO	12
Iveco Stralis.....	13
CHAPTER 1. ADAMS/CAR AND MULTIBODY APPROACH	15
1.1 Adams/Solver.....	15
1.2 Modelling in Adams/Car.....	23
CHAPTER 2. TRUCK MODELLING.....	27
2.1 Rear Suspension	30
2.2 Front Suspension.....	39
2.2.1 Leaf Springs	43
2.2.2 Steering System.....	49
2.3 Anti-roll Bars	51
2.4 Engine	55
2.5 Flexible Bodies.....	56
2.5.1 Chassis.....	57
2.5.2 Cabine	64
2.6 Front and Rear Cabine Suspensions.....	65

2.7 Tires.....	67
2.8 Semitrailer Subsystems	70
2.8.1 Semitrailer Suspensions	70
2.8.2 Semitrailer	75
2.9 Generation of the Assemblies and debugging.....	77
CHAPTER 3. SIMULATIONS	81
3.1 Open-loop test methods.....	82
3.2 Manoeuvres	84
3.2.1 Tractor Simulations	85
3.2.2 Full Truck Simulations.....	87
CHAPTER 4. POST-PROCESSING AND RESULTS	90
4.1 Tractor Results	92
4.2 Full Truck Results	102
CONCLUSIONS	112
APPENDIX A	114
Modal Superposition	114
Flexibility in Adams/Solver	116
BIBLIOGRAPHY	118
RINGRAZIAMENTI	119

ABSTRACT

This *Master of Science* Thesis is the result of an eight-month internship in the *CNH Industrial* headquarter located in *Turin, Italy*.

The main target of the work was the development of a multibody model of an on-road heavy commercial vehicle, i.e. *Iveco Stralis model year 2019*. The main programming environment used in this activity was *MSC Adams/Car 2015.1*. The significance of a complete and updated multibody model is clear since it provides the starting point of several studies within the Engineering Office of the Company, for instance the handling and the comfort ones as well the extrapolation of the dynamic loads which work on the mechanical elements in order to compute their fatigue life. To achieve this goal, intermediate steps were required, like the building of the little subsystems which were finally assembled to generate the full-vehicle. The most relevant innovations of this model compared to the previous ones is represented by the integration of some flexible bodies, such as the frame, and the use of a specific tool to model the leaf spring suspension. Normally, the validation of the model, thanks to the experimental data coming from on-road tests, should follow. Regretfully, it was not possible to carry out this phase since *Iveco Stralis my2019* is not in production yet. Thus, the focus of the activity was shifted on studying the influence of the flexible bodies in a multibody model which typically consists of rigid parts. This paper is made of four main chapters. In the Introduction, an overview of *CNH Industrial* and *Iveco* is given; then, the attention is focused on the object of the activity, the *Iveco Stralis my2019*. In the first chapter *Adams/Car* Software is discussed as regards both the modelling and the solving phase. The second one deals with the realization of the subsystems which compose the vehicle and the methodology employed. Afterwards, in the third chapter, the manoeuvres according to ISO standard, performed both on the tractor and the complete vehicle, are described. Finally, in the fourth chapter, the results are shown in order to get the difference between a fully rigid heavy vehicle model and a partially flexible one.

Besides *Adams/Car*, other softwares have been required: *Altair Hypermesh*, *MSC Nastran* and *MSC Adams/View* were used to create the flexible bodies; the 3D starting model was available in *Dassault Catia* while *Siemens Team Center* was used like 2D drawings database; *Matlab* was chosen as the post-processing environment.

PICTURES INDEX

Pic. 1 - Iveco Stralis my2019	13
Pic. 2.1 - Previous multibody model (ADAMS/CAR).....	27
Pic. 2.2 - 3D model (CATIA).....	28
Pic. 2.3 – 3D model of the rear suspension (CATIA)	30
Pic. 2.4 – Example of Bushing	32
Pic. 2.5 – Example of Bushing characteristics	33
Pic. 2.6 – Damper characteristic in Adams/Car.....	33
Pic. 2.7 – Isobar curves for four pressure levels.....	34
Pic. 2.8 – Air Spring charactertic	36
Pic. 2.9 – Axle Bumpstop.....	36
Pic. 2.10 – Axle Bumpstop characteristic.....	37
Pic. 2.11 – Rear suspension in Adams/Car.....	38
Pic. 2.12 - 3D model of the front suspension (CATIA)	39
Pic. 2.13 – Front suspension template	40
Pic. 2.14 – Iterative procedure on the front suspension template (ADAMS/CAR)	42
Pic. 2.15 – Toe Angle in function of the Wheel Travel (ADAMS/CAR)	42
Pic. 2.16 – Leaf Beam Elements.....	43
Pic. 2.17 – Leaf Springs 3D drawing (CATIA).....	44
Pic. 2.18 – “OG Profile Generator” panel (LeafToolKit).....	45
Pic. 2.19 – Leaf Spring Parameters	46
Pic. 2.20 – “Create Leafspring” panel (LeafToolKit)	47
Pic. 2.21 – “Create the attachments” panel (LeafToolKit).....	47
Pic. 2.22 – Vertical Force in function of vertical travel (ADAMS/CAR).....	48
Pic. 2.23 – Leaf springs of first attempt (ADAMS/CAR)	49
Pic. 2.24 – Steering System (ADAMS/CAR).....	50
Pic. 2.25 – 3D drawing of the rear anti-roll bar (CATIA).....	51
Pic. 2.26 – Rear Anti-roll Bar on the first attempt (ADAMS/CAR).....	53
Pic. 2.27 – Final Rear Anti-roll Bar (ADAMS/CAR)	54
Pic. 2.28 – Front Anti-roll Bar (ADAMS/CAR)	54
Pic. 2.29 – Engine template (ADAMS/CAR)	56
Pic. 2.30 – FEM model of the chassis (HYPERMESH)	57
Pic. 2.31 – Example of RBE2 entity (HYPERMESH).....	58
Pic. 2.32 – Chassis template (ADAMS/CAR).....	59

Pic. 2.33 – Flexible Body Panel (ADAMS/CAR)	60
Pic. 2.34 – Damping Ratio in function of the frequency	61
Pic. 2.35 – Mass Matrix.....	61
Pic. 2.36 – First shape mode of the frame (ADAMS/CAR).....	62
Pic. 2.37 – Second shape mode of the frame (ADAMS/CAR)	63
Pic. 2.38 – Third shape mode of the frame (ADAMS/CAR)	63
Pic. 2.39 - Fourth shape mode of the frame (ADAMS/CAR)	64
Pic. 2.40 – Cabine template (ADAMS/CAR)	65
Pic. 2.41 – Front Cabine Suspension Template (ADAMS/CAR)	66
Pic. 2.42 – Rear Cabine Suspension Template (ADAMS/CAR)	67
Pic. 2.43 – Example of the lateral force trend in function of the drift angle ^[7]	68
Pic. 2.44 – 2D drawing of the semitrailer suspension	70
Pic. 2.45 – Creation of the mesh (ADAMS/VIEW)	71
Pic. 2.46 – Definition of the master nodes (ADAMS/VIEW).....	72
Pic. 2.47 – Semitrailer suspension (ADAMS/CAR)	73
Pic. 2.48 - First and second shape modes of the axle (ADAMS/CAR).....	73
Pic. 2.49 - Third and fourth shape modes of the axle (ADAMS/CAR)	74
Pic. 2.50 - Fifth shape mode of the axle (ADAMS/CAR).....	74
Pic. 2.51 – Semitrailer drawing and technical Specifications	75
Pic. 2.52 – Semitrailer subsystem (ADAMS/CAR)	76
Pic. 2.53 – Rear Suspension Assembly (ADAMS/CAR).....	78
Pic. 2.54 – Front Suspension Assembly (ADAMS/CAR).....	78
Pic. 2.55 – Tractor Assembly (ADAMS/CAR).....	79
Pic. 2.56 – Full Truck Assembly (ADAMS/CAR).....	79
Pic. 4.1 - Geometrical characteristics of Iveco Stralis MY2019	90
Pic. 4.2 – Tractor, Ramp Steer: steering-wheel angle against lateral acceleration.....	92
Pic. 4.3 – Tractor, Ramp Steer: side-slip angle against lateral acceleration.....	93
Pic. 4.4 – Tractor, Ramp Steer: time evolution of the roll angle.....	93
Pic. 4.5 - Tractor, Step Steer1: time evolution of the lateral acceleration.....	94
Pic. 4.6 - Tractor, Step Steer2: time evolution of the lateral acceleration.....	94
Pic. 4.7 - Tractor, Step Steer1: time evolution of the side-slip angle.....	95
Pic. 4.8 - Tractor, Step Steer2: time evolution of the side-slip angle.....	95
Pic. 4.9 - Tractor, Step Steer1: time evolution of the yaw rate	96
Pic. 4.10 - Tractor, Step Steer2: time evolution of the yaw rate	96

Pic. 4.11 - Tractor, Step Steer1: time evolution of the roll angle	97
Pic. 4.12 - Tractor, Step Steer2: time evolution of the roll angle	97
Pic. 4.13 - Tractor, Sweep Steer1: time evolution of the lateral acceleration	98
Pic. 4.14 - Tractor, Sweep Steer2: time evolution of the lateral acceleration	98
Pic. 4.15 - Tractor, Sweep Steer1: time evolution of the side-slip angle	99
Pic. 4.16 - Tractor, Sweep Steer2: time evolution of the side-slip angle	99
Pic. 4.17 - Tractor, Sweep Steer1: time evolution of the yaw rate	100
Pic. 4.18 - Tractor, Sweep Steer2: time evolution of the yaw rate	100
Pic. 4.19 - Tractor, Sweep Steer1: time evolution of the roll angle	101
Pic. 4.20 - Tractor, Sweep Steer2: time evolution of the roll angle	101
Pic. 4.21 – Full Truck, Ramp Steer: steering-wheel angle against lateral acceleration	102
Pic. 4.22 - Full Truck, Ramp Steer: time evoluion of the roll angle	103
Pic. 4.23 – Full Truck, Ramp Steer: side-slip angle against lateral acceleration	103
Pic. 4.24 – Full Truck, Step Steer1: time evoluion of the lateral acceleration	104
Pic. 4.25 – Full Truck, Step Steer2: time evoluion of the lateral acceleration	104
Pic. 4.26 – Full Truck, Step Steer1: time evoluion of the side-slip angle	105
Pic. 4.27 – Full Truck, Step Steer2: time evoluion of the side-slip angle	105
Pic. 4.28 – Full Truck, Step Steer1: time evoluion of the yaw rate.....	106
Pic. 4.29 – Full Truck, Step Steer2: time evoluion of the yaw rate.....	106
Pic. 4.30 – Full Truck, Step Steer1: time evoluion of the roll angle	107
Pic. 4.31 – Full Truck, Step Steer2: time evoluion of the roll angle	107
Pic. 4.32 – Full Truck, Sweep Steer1: time evoluion of the lateral acceleration	108
Pic. 4.33 – Full Truck, Sweep Steer2: time evoluion of the lateral acceleration	108
Pic. 4.34 - Full Truck, Sweep Steer1: time evoluion of the side-slip angle	109
Pic. 4.35 - Full Truck, Sweep Steer2: time evoluion of the side-slip angle	109
Pic. 4.36 - Full Truck, Sweep Steer1: time evoluion of the yaw rate.....	110
Pic. 4.37 - Full Truck, Sweep Steer2: time evoluion of the yaw rate.....	110
Pic. 4.38 - Full Truck, Sweep Steer1: time evoluion of the roll angle	111
Pic. 4.39 - Full Truck, Sweep Steer2: time evoluion of the roll angle	111

TABLE INDEX

Tab. I – CNH Brands and their applications	12
Tab. II – Rear Suspension Part List.....	30
Tab. III – List of constraints in Rear Suspension template	31
Tab. IV – Front Suspension Part List	39
Tab. V – List of constraints in Front Suspension template	41
Tab. VI – List of constraints in Leaf Spring template	48
Tab. VII – Steering System Part List.....	50
Tab. VIII – List of constraints in Rear Anti-roll Bar.....	52
Tab. IX – List of RBE2 Nodes	58
Tab. X – Main Invariants and their meanings	61
Tab. XI – Tractor Ramp Steer parameters.....	85
Tab. XII – Tractor Step Steer parameters.....	86
Tab. XIII – Tractor Swept-Sine Steer parameters	87
Tab. XIV – Full Truck Ramp Steer parameters.....	88
Tab. XV – Full Truck Step Steer parameters	88
Tab. XVI – Full Truck Swept-Sine Steer parameters.....	89

INTRODUCTION

The dynamics of an on-road vehicle, is an extremely important subject of study since the design phase. The vehicle provides a single closed-loop system together with its driver and the environment. Thus, the purpose of evaluating the dynamics turns out to be really difficult: in fact, there is a mutual interaction between these three elements, each of which is complex in itself. An exhaustive and detailed characterization of the dynamic behaviour needs to gather several data coming from different type of manoeuvres, each of them performed many times. Nevertheless, these tests are able to consider a small part of the on-road behaviour. Other relevant aspects, which can not be ignored, are the test conditions and the tires: only the results collected under identical tests and tire conditions can be compared.

Any vehicle approach involves three main study instruments: virtual simulation, bench testing and on-road testing. In this thesis, the attention is focussed on the virtual testing, which occurs since the first phases of the design of a new vehicle. In this context, multibody softwares, like *Adams/Car*, have had a widely spread. Its task consists of solving in a fast way the constituent equations which rule the kinematics and the dynamics of a vehicle. Compared to the stress analysis by FEM approach, on the one hand, the level of detail and so the accuracy of the results is lower, on the other one the simulations are faster since the system is composed by rigid bodies and have to help only to provide global information. Multibody and FEM do not constitute two different options but they parallelly work in the Engineering Office of any automotive Company influencing each other. For instance, by multibody simulations, the loads acting on the components are extrapolated and then used in FEM analysis. Multibody studies can also replace the bench and the on road tests: compared to them, virtual approach ensures identical test conditions and a driving which is able perfectly to follow the standard directives. Notice that it is possible as long as the model under analysis was calibrated on the basis of previous experimental data. This allow to get also an economic savings.

CNH Industrial and IVECO

CNH Industrial is an Italian and American worldwide operative Company which projects, produces and commercializes capital goods. The main examples are agriculture and construction machines, industrial and commercial vehicles, buses and vehicles for special missions, all including their powertrains, and a wide range of propulsion systems.

The Company is made of twelve brands, located in sixty-six sites, in which more than sixty-three thousands employees work.

Main Brands	Applications
<i>Case IH, New Holland Agriculture</i>	Agriculture machines
<i>Case Construction Equipment, New Holland Construction</i>	Earth-moving equipments
<i>Iveco, Iveco Bus, Heuliez Bus, Iveco Astra, Magirus, Iveco Defence Vehicles</i>	Commercial Vehicles and buses
<i>FPT Industrial</i>	Powertrains

Tab. 1 – CNH Brands and their applications

CNH Industrial was born in 2012 thanks to the fusion of *CNH Global*, previously enestablished by the union of *New Holland* and *Case Corporation*, with *Fiat Industrial*.

Nowadays, it is considered the leader in its trade.

Iveco is an Italian Company with its headquarter located in *Turin (Italy)*, completely controlled by *CNH Industrial* group. The name stands for *Industrial Vehicles Corporation*. The core business is the design and the manufacturing of light, medium and heavy on-road commercial vehicles, construction machinery, urban and interurban buses and other vehicle for specific applications. It was created by the union of some Italian, French and German brands in 1975.

Iveco Stralis



Pic. 1 - Iveco Stralis my2019

Iveco Stralis belongs to Iveco heavy on-road gamma (over than 18 tons). Its production has started since 2002 in order to replace the old model called Eurostar.

Current European standard sets 44 tons as the maximum weight for the ordinary on-road trucks. It is commercialized both as lorry and as articulated vehicle.

According to Iveco norm, the Stralis model is identified by an alphanumeric code, which could be for instance AT 440 S 45 T Z /P -HM.

where:

- AT means the cabine type;
- 440 is the maximum weight on the ground (MTT) [$tons \cdot 10$];
- S means the model, which in this case stands for Stralis;
- 45 is the engine power [$kW \cdot 10^{-1}$];
- T distinguishes the tractor from the lorry model;
- Z gives directions about the number and the type of axes;
- /P deals with the type of the front and the rear suspensions;
- -HM is a specific version.

The configuration of a commercial vehicle can be also defined according to ISO standard by a three numbers acronym, for instance 6x2(x2). In this case:

- 6 is the total number of the wheels;
- 2 is the number of the driving wheels;
- 2 is the number of the steering wheels.

Notice that a couple of twinned wheels is considered only as two wheels according to this rule.

Iveco Stralis mounts a straight-six engine: there are three different displacements each of them available with different powers. The manual transmission includes six-teen gears while the automatic only twelve. More details, as regards the vehicles under analysis, will be given in the introduction of Chapter 2.

CHAPTER 1. ADAMS/CAR AND MULTIBODY APPROACH

The aim of this Chapter is to introduce *Adams* to the reader, firstly deepening the theory and the methods that underlines the solver, secondly discussing the modelling principles.

Adams is the main working environment in which this *Master Degree* work was produced. It represents the software by *MSC* of multibody dynamic simulation; it is equipped with *Fortran* and *C++* solver. *Adams* stands for *Automated Dynamic Analysis of Mechanical Systems*. By *Adams*, several tools were created: for instance, in this work the vehicle simulation one, named *Adams/Car*, and the generic purpose one, called *Adams/View*, were used.

1.1 Adams/Solver

The following theoretical discussion is from the *Adams/Solver Primer* ^[1].

The solver, implemented by *MSC*, is common to every *Adams* tool. The equations on the basis of any mechanical system are non-linear ones. Thus, it is necessary a numerical fast and robust algorithm in order to solve them. In *Adams* it is the *Newton-Raphson Method*. In one dimension, it finds the root x^* of the non-linear equation

$$f(x) = 0 \quad (1)$$

where the function $f: \mathbb{R} \rightarrow \mathbb{R}$ is assumed to be differential. The algorithm requires an initial approximation $x^{(0)}$ of x^* ; a new configuration $x^{(1)}$, closer to x^* is computed as:

$$x^{(1)} = x^{(0)} - \frac{f(x^{(0)})}{f'(x^{(0)})} \quad (2)$$

where $f(x)'$ is the derivative of f respect to x .

This strategy of updatating the value x is achieved linearizing the function f at the point $x^{(0)}$.

The algorithm continues by setting $x^{(0)} \leftarrow x^{(1)}$ and performing a new iteration following Eq.

(2). The strenght of this method is that it leads to a quadratic rate of convergence to the root $x^{(*)}$, while the weakness is that each iteration requires the evaluation of the function and its

derivative, which is considered an expensive cost. An alternative version consists of updating the derivative once in a while, recycling the computed one for several iterations: this algorithm is named *Newton-like* and the convergence rate turns out to be linear. In the *PATTERN SETTINGS* of the *ADAMS/INTEGRATOR SOLVER*, the user can choose how often the derivative needs to be updated. The derivative, called Jacobian, is an expensive operation: computing it seldom is supposed to lead to advantages in terms of time simulation but the convergence rate degrades: more iterations are required. In general, exit criteria of the algorithm are used, i.e. a specified threshold of the $f(x^{(n)})$. Thus, iteration by iteration, the computed configuration gets closer and closer to the point where the non-linear function $f(x)$ vanishes. Normally, *ADAMS/Solver* deals with several non-linear equations in which multiple unknowns figure: the root consists of a n . dimensional vector, $q \in \mathbb{R}^n$.

The system to be solved can be written as:

$$f(q) = [f_1(q) \ f_2(q) \ ... \ f_n(q)]^T = [0] \quad (3)$$

The approach is very similar to the one-dimensional case and will be not discussed.

Since this moment, the vector and matrix entities in the equation will be noticed by bold font.

Adams/Solver task consists of simulating the time evolution of a mechanical system in order to get, at each moment, the position, the orientation and their derivatives associated with each body in the model. The position and the orientation are monitored by the generalized coordinates, whose choice is not unique: there are cartesian and spherical ones or global and relative ones; nevertheless, a set of generalized coordinates uniquely describes the configuration of a body in the model in time.

For instance, the Cartesian coordinates can define the position of a rigid body

$$\mathbf{p} = [x \ y \ z]^T \quad (4)$$

while the Euler angles its orientation

$$\boldsymbol{\varepsilon} = [\psi \ \varphi \ \theta]^T \quad (5)$$

In *Adams*, as regards the Euler sequence rotation, the 3-1-3 one is used by default. The user has eventually the possibility to work on another one.

The set of the generalized coordinates of the rigid body i , can be written by \mathbf{q}_i vector.

$$\mathbf{q}_i = [\mathbf{p}_i \ \boldsymbol{\varepsilon}_i]^T \quad (6)$$

The longitudinal and the angular velocity of a body, expressed in the body-fixed coordinate system, can be written as:

$$\mathbf{u} = \dot{\mathbf{p}} \quad (7)$$

$$\bar{\boldsymbol{\omega}} = \mathbf{B}\dot{\boldsymbol{\varepsilon}} = \mathbf{B}\boldsymbol{\zeta} \quad (8)$$

where \mathbf{B} is a matrix which defines the relationship between the angular velocity and the choice of the generalized coordinates.

$$\mathbf{B} = \begin{bmatrix} \sin\varphi \sin\theta & 0 & \cos\varphi \\ \cos\varphi \sin\theta & 0 & -\sin\varphi \\ \cos\theta & 1 & 0 \end{bmatrix} \quad (9)$$

If nb is the number of the bodies in the model, the vector \mathbf{q} will describe position and orientation of the system:

$$\mathbf{q} = [\mathbf{q}_1^T \ \mathbf{q}_2^T \ \dots \ \mathbf{q}_{nb}^T]^T = [q_1 \ q_2 \ \dots \ q_n]^T \quad (10)$$

$$n = 6 \cdot nb \quad (11)$$

where n is the number of the degrees of freedom of the entire system.

Between coordinates q_i , joints can act. In a mathematical point of view, each of them is traduced in one or more algebraic equations.

The set of all the constraints related to the joints in the model is denoted by $\boldsymbol{\Phi}$.

$$\boldsymbol{\Phi} = [\boldsymbol{\Phi}_1(\mathbf{q})^T \ \boldsymbol{\Phi}_2(\mathbf{q})^T \ \dots \ \boldsymbol{\Phi}_{nj}(\mathbf{q})^T]^T = [\Phi_1(\mathbf{q}) \ \Phi_2(\mathbf{q}) \ \dots \ \Phi_m(\mathbf{q})]^T = \mathbf{0} \quad (12)$$

nj represents the number of joints in the model and m the number of the constraint equations.

Notice that $\mathbf{q} \in \mathbb{R}^n$ and $\boldsymbol{\Phi} \in \mathbb{R}^m$. Generally $m < n$ which means that the generalized coordinates are more than the constraints induced by the joints.

Computing one and two time derivative of Eq. (12), the velocity and the acceleration kinematic constraints follow.

The generalized coordinates array \mathbf{q} must also satisfy this other two conditions.

In *Adams* model, even motions can be included: according to a mathematical point of view, they establish that a generalized coordinate explicitly depends on time: it is traduced into a time dependent constraint equation.

$$\Phi(\mathbf{q}, t) = \mathbf{0} \quad (13)$$

The discussion is similar to the previous case.

In order to perform any kind of test, *Initial Condition Analysis (IC)* is required: a consistent configuration for the model at the beginning of the simulation is computed. The mechanism must be already assembled and the generalized coordinates \mathbf{q} and their derivatives must follow all the constraint equations at time t_0 .

$$\Phi(\mathbf{q}, t_0) = \mathbf{0} \quad (14)$$

During *IC Analysis*, the user can set the value of some generalized coordinates and the solver do its best to satisfy these new constraints. This phase is solved by *Adams* thanks to an optimization approach, minimizing a cost function in which weight factors w_i figure. It is required that the configuration \mathbf{q}^0 has to be consistent. Large weights corresponds to prescribed entries in \mathbf{q}^0 , while 1 is associated with generalized coordinates which the user did not specify.

In matrix notation, the stage consists of minimizing the following cost function.

$$f(\mathbf{q}) = \frac{1}{2}(\mathbf{q} - \mathbf{q}^0)^T \mathbf{W}(\mathbf{q} - \mathbf{q}^0) \quad (15)$$

subject to Eq. (14), where \mathbf{W} is the diagonal matrix of weights.

In *IC Analysis*, the solver verifies the compatibility of all the constraints induced by the joints and the motions included in the model: some of them might be recognized as redundant. Redundant and consistent constraint represents a benign case: *Adams* will monitor this equation in order to make sure that the redundant constraint continues to be consistent. Otherwise the solver will stop the simulation and inform the user about this situation. Using too

many joints in the model is the main responsible of this problem: the number of the constraint equations exceeds the number of the generalized coordinates.

The *Velocity IC Analysis* is a direct and simple application of the algorithm employed for the *Position IC Analysis*.

Thanks to *Adams*, several types of analysis can be performed: one of the most interesting is the *Kinematic* one. To be performed, it requires a number of independent constraint equations equal to the number of generalized coordinates.

Defined the position of the bodies in the system at time t_0 , the problem consists of determining the position of each at time $t_j > t_0$. Since the non-linear nature of the constraint equations, *Newton-Raphson* algorithm is used to compute q_j at time t_j .

Firstly, at time t_1 , the non-linear constraint equations are rewritten thanks to the *Taylor-expansion*.

$$\Phi(\mathbf{q}_1, t_1) = \Phi(\mathbf{q}_0, t_1) + \Phi_q(\mathbf{q}_0, t_1)(\mathbf{q}_1 - \mathbf{q}_0) \quad (16)$$

The matrix Φ_q is square, since the number of equations is equal to the generalized coordinate one. The matrix is also invertible, if the equations were assumed to be independent. Usign an explicit integrator, for instance *Forward-Euler*, an initial starting configuration $q_1^{(0)}$ is determined and the iterative algorithm is repeated at each iteration $j > 0$ searching the correction $\Delta^{(j)}$.

$$\mathbf{q}_1^{(j+1)} = \mathbf{q}_1^{(j)} + \Delta^{(j)} \quad (17)$$

The iterative procedure goes on until the correction turns out to be small enough.

After the position analysis, even the velocity and acceleration ones can be performed.

Probably the most powerful analysis which can be carried out in *Adams* is the *Dynamic* one. In addition to the notation previously used, other quantities will figure in the equations of motion:

M is the generalized mass matrix;

J is the generalized inertia matrix expressed in the main local reference frame;

K is the kinetic energy defined as

$$K = \frac{1}{2} \mathbf{u}^T \mathbf{M} \mathbf{u} + \frac{1}{2} \boldsymbol{\omega}^T \mathbf{J} \boldsymbol{\omega} \quad (18)$$

U is the potential energy due to the gravity;

L is the Lagrangian term, computed as

$$L = K - U \quad (19)$$

$\boldsymbol{\lambda} \in \mathbb{R}^m$ is the array of Lagrange multipliers and the number is given by the number of constraint equations induced by joints;

$\mathbf{F} \in \mathbb{R}^6$ is the vector of applied forces: f are the forces in the global reference frame, while n the torque in the local Cartesian reference frame

$$\mathbf{F}(\mathbf{q}, \dot{\mathbf{q}}, t) = \begin{bmatrix} \mathbf{f} \\ \mathbf{n} \end{bmatrix} \quad (20)$$

$\mathbf{Q}(\mathbf{q}, \dot{\mathbf{q}}, t) \in \mathbb{R}^6$ is the generalized force, obtained by projecting F upon the generalized coordinates.

Notice that, except for gravity, all the other potential forces are included in Q.

The Lagrange formulation take the form of the following second order differential equation:

$$\frac{d}{dt} \left[\left(\frac{\partial L}{\partial \dot{\mathbf{q}}} \right)^T \right] - \left(\frac{\partial L}{\partial \mathbf{q}} \right)^T + \boldsymbol{\Phi}_q^T \boldsymbol{\lambda} = \mathbf{Q} \quad (21)$$

For a rigid body, in vector notation, Eq. (20) becomes:

$$\frac{d}{dt} \begin{bmatrix} \left(\frac{\partial L}{\partial \mathbf{u}} \right)^T \\ \left(\frac{\partial L}{\partial \boldsymbol{\zeta}} \right)^T \end{bmatrix} - \begin{bmatrix} \left(\frac{\partial L}{\partial \mathbf{p}} \right)^T \\ \left(\frac{\partial L}{\partial \boldsymbol{\varepsilon}} \right)^T \end{bmatrix} + \begin{bmatrix} \boldsymbol{\Phi}_p^T \boldsymbol{\lambda} \\ \boldsymbol{\Phi}_\varepsilon^T \boldsymbol{\lambda} \end{bmatrix} = \begin{bmatrix} (\boldsymbol{\Pi}^P)^T \mathbf{f} \\ (\boldsymbol{\Pi}^R)^T \mathbf{n} \end{bmatrix} \quad (22)$$

where $(\boldsymbol{\Pi}^{P/R})^T$ is the projecting operator.

By collecting all the differential equations, the solver produces a system of 15 equations for each body which is enough to reach a numerical solution.

Since

$$\frac{d}{dt} \left(\frac{\partial K}{\partial \mathbf{u}} \right)^T = \mathbf{M} \dot{\mathbf{u}} \quad (23)$$

$$\left(\frac{\partial K}{\partial \mathbf{p}} \right)^T = \mathbf{0} \quad (24)$$

$$\boldsymbol{\Gamma} \equiv \left(\frac{\partial K}{\partial \boldsymbol{\zeta}} \right)^T = \mathbf{B}^T \mathbf{J} \mathbf{B} \boldsymbol{\zeta} \quad (25)$$

The *EOM* (equation of motion), namely Eq. (22), is rewritten as:

$$\mathbf{M} \dot{\mathbf{u}} - \frac{\partial L}{\partial \mathbf{p}} + \boldsymbol{\Phi}_p^T \boldsymbol{\lambda} - (\boldsymbol{\Pi}^P)^T \mathbf{f} = \mathbf{0} \quad (26)$$

$$\boldsymbol{\Gamma} - \mathbf{B}^T \mathbf{J} \mathbf{B} \boldsymbol{\zeta} = \mathbf{0} \quad (27)$$

$$\dot{\mathbf{r}} - \frac{\partial L}{\partial \boldsymbol{\varepsilon}} + \boldsymbol{\Phi}_\varepsilon^T \boldsymbol{\lambda} - (\boldsymbol{\Pi}^R)^T \mathbf{n} = \mathbf{0} \quad (28)$$

$$\dot{\mathbf{p}} - \mathbf{u} = \mathbf{0} \quad (29)$$

$$\dot{\boldsymbol{\varepsilon}} - \boldsymbol{\zeta} = \mathbf{0} \quad (30)$$

Eq. (26) to Eq. (30) describe the variation in time of the generalized coordinates, the reaction forces and the applied ones. The set of equations must also include the constraint equations. There are many methods to solve this system composed by differential and algebraic equations (*DAE*). A *DAE* must be differentiated as many time until to become an *ODE*. The higher the index of derivatives is, the more challenging the numerical solution of the *DAE* turns out to be. Generally, the *DAE* of a dynamic problem has index 3, which is considered high. The common and fastest method which is implemented in *Adams* to solve the set of equations is called *GSTIFF-I3*. A method which is considered more accurate and robust but also slower is called *SI2*: it directly works on the differential equations. What is common to each method is that the approach consists of turning the *DAE*'s into a set of algebraic equations. An example of that is the *Backward-Euler formula*, which is an implicit integration method. For instance, in order 1, at time t_1 , the derivative \dot{y}_1 can be replaced as:

$$\dot{y}_1 = \frac{1}{h}y_1 - \frac{1}{h}y_0 \quad (31)$$

where h represents the time step used in the simulation.

Derivative $\dot{y} = g(t, y)$ is almost always non-linear and needs to be solved by *Newthon-Raphson* iterative algorithm. Thus, the Eq. (26) to Eq. (30) are discretized in their derivative in order to produce a non-linear algebraic system.

Naming the vector of the unknown \mathbf{y} ,

$$\mathbf{y} = [\mathbf{u} \ \Gamma \ \zeta \ \mathbf{p} \ \varepsilon \ \lambda \ \mathbf{f} \ \mathbf{n}]^T \mathbf{0} \quad (32)$$

the non-linear system can be denoted as:

$$\Psi(\mathbf{y}) = \mathbf{0} \quad (33)$$

If an initial guess of the solution is provided, the algorithm is carried out iteration by iteration until the corrections $\Delta^{(j)}$ are small enough

$$\Psi_{\mathbf{y}}(\mathbf{y}_0)\Delta^{(j)} = \Psi(\mathbf{y}^{(j)}) \quad (34)$$

$$\mathbf{y}^{(j+1)} = \mathbf{y}^{(j)} + \Delta^{(j)} \quad (35)$$

Note that if the initial condition, found in a *IC Analysis*, is far away from the real solution, the iterations might fail to converge: a solution can be the reducing of the step size.

To improve the integration, *Adams* sometimes replaces $\frac{1}{h}$ with $\frac{1}{\beta h}$ where β is an specific coefficient of the integration formula. The using of more complex formula helps to replace the first order time derivative in the equations with a linear combination of future and past values of the unknowns: backward Euler formula operates it in a very basic way.

The last Analysis which *Adams* is able to performe is the *Static* one. It consists of finding the equilibrium configuration of a mechanical system: the solution of a non-linear system composed by algebraic equations is required. The set of equations is the same of the *Dynamic Analysis* although the time derivatives of any quantity should be set at zero: in fact, at the equilibrium, there is no change in time in the value of the variables. The Eq. (26) to (30) become:

$$-\frac{\partial L}{\partial \mathbf{p}} + \Phi_{\mathbf{p}}^T \boldsymbol{\lambda} - (\Pi^P)^T \mathbf{f} = \mathbf{0} \quad (36)$$

$$\boldsymbol{\Gamma} - \mathbf{B}^T \mathbf{J} \mathbf{B} \boldsymbol{\zeta} = \mathbf{0} \quad (37)$$

$$-\frac{\partial L}{\partial \boldsymbol{\varepsilon}} + \Phi_{\boldsymbol{\varepsilon}}^T \boldsymbol{\lambda} - (\Pi^R)^T \mathbf{n} = \mathbf{0} \quad (38)$$

$$\mathbf{u} = \mathbf{0} \quad (39)$$

$$\boldsymbol{\zeta} = \mathbf{0} \quad (40)$$

In the Appendix, at the end of this paper, it will be explained how *Adams/Solver* find and solve the equations in a mechanical system composed even by flexible bodies.

1.2 Modelling in Adams/Car

As previously said, *Adams/Car* represents the more specific tool by *MSC* to model a vehicle. Even though it was thought to manage passenger cars, in Iveco Engineering Office it is used for other applications, for instance, the commercial vehicles.

The peculiarity of a multibody approach is that the bodies belonging to the mechanical system are modelled like rigid parts, i.e. 6 dof bodies.

Adams/Car modelling is devised in subsystem, linked each other only in the final phase in order to create more and more complex systems until getting the full-vehicle. This task allows to have an extreme flexibility since, on the same vehicle, it is easier to modify, add, replace or delete parts, then moving to evaluate the differences in terms of results and performance.

The subsystem, named *template*, takes place in a specific programming environment called *template builder*. In this phase, the user defines the topology of the *template*, not caring about the real data: it will be possible to update the geometry and the properties in the next steps.

The design of a new body starts off on the basis of two different entities, the *Hardpoints* and the *Construcion Frames*: the first ones represent a geometric point equipped with three coordinates in the space, which the user has inevitably to define; the second ones own position

and orientation properties, settable in several ways, for instance using other *Hardpoints* or *Construction Frames*, previously defined.

Modelling in this phase takes two important advantages: firstly, each variable is parametric and can depend on the other ones; secondly, the software symmetrically works in the default mode, generating a right-side entity if the user has done the left-side one and viceversa. By staying in *template builder*, next step is the creation of the bodies, which are called *Parts*. Several type of *Parts* in *Adams/Car* are available.

The most common is the *General Part*, characterized by a center of mass and an orientation, set from a scratch or on the basis of *Hardpoints* and *Construction Frames* by different ways, the mass and the main moments of inertia. The last two properties can be manually included, if they are known data, or computed by the software if a *Geometry* is built together with the *Part*. Note that, in *Adams*, shapes are not fundamental since only spatial and mass properties are required to solve the equations of motion.

An other important kind of *Part* is the *Mount Part*: it serves as interface with an other *template* in the assembling phase. Together with its building, *Adams/Car* automatically creates an *Input Mount Comunicator*. It is required to the user to build an *Output Mount Comunicator* on the second *template*. Note that, linking two *templates*, only one has to own an *Input Comunicator* and the other the output one.

Generally, communicator entities are used to move information from a *template* to an other one, for instance positions, orientations, links, ecc: a specific comunicator is required for any kind of information.

The *Parts* belonging to the same or different *templates*, are linked each other by joints which are able to lock one or more relative degrees of freedom. In *Adams/Car* it is possible to use ideal joints, characterized by an infinite stiffness, or real ones, which own a user defined stiffness: the first are used in *Kinematic* studies while the second are more suitable for evaluating the *Dynamics* of the bodies. Generally, at the same interface between two bodies,

both the types are used in order to switch one to the other depending on the analysis which will be performed.

Other relevant elements which is easier to put inside the vehicle model are represented by forces, for instance, due to spring or shock absorber actions. In this two cases the force exchanged between two bodies is a function respectively of the relative displacement or velocity: the relationship between the forces and these two quantities is defined by the user thanks to a property file which contains a spline. The solver, during the simulation, will interpolate the current value.

An other kind of force which is implemented in a similar way is the one produced by the travel limits of the springs and the shock absorbers in compression (*Boundstop*) and in expansion (*Reboundstop*) or by the axle buffers (*Boundstop*).

Finally, the user can define generic forces or toques applied on the mechanical system, function of the time or other variables. An example is the engine subsystem: it is represented like a box, equipped with inertia, from which an output torque is trasmitted to the trasmission subsystem, function of *rpm* and the accelerator pedal travel.

To make the model even more pliable, *Parameter Variables* can be included in the model: they allow, even after the assembling phase, to change a lenght or a mass or a gear ratio or to controll the switch from a configuration to an other one.

After the modelling phase, it is necessary to move to the second programming environment, named *Standard Interface*. Firstly, each *template (.tpl)* has to be converted in a *Subsystem (.sub)*. At this point, it is still possible to modify the previously created entities; otherwise, it is not allowed to build or to delete something. Generally, in *Template Builder*, *Adams* default data are used while in *Standard Interface* real ones are included.

After this step, in *Standard Interface* mode, the assembly is created collecting many *Subsystems*. An *Assembly* can belong to three different categories: *Suspension Assembly*, *Full-Vehicle Assembly* and *Generic Assembly*. In this paper the attention is focussed only on the first

two ones. Depending on the kind of Assembly, the software will simulate a different bench test (*Testrig*). For instance, a suspension test bench will be associated to a *Suspension Assembly* or a driver and a track to a *Full-Vehicle Assembly*.

According to the *Assembly*, *Adams/Car* requires the presence of specific *Subsystems*.

For instance, a *Full-Vehicle Assembly* needs at least two suspension, a front and a rear one, two pairs of wheels, a chassis and a steering system; other *Subsystems* like the engine, the brakes or the anti-roll bars are optional but necessary to perform specific tests.

In addition to this, depending on the type of *Assembly*, only a small range of tests are available.

Completed the simulation phase, Post-Processing follows. It is possible both to display the performed manoeuvres like animations and to plot the *Adams/Car* default results. If the user is interested in evaluating forces, displacements, ecc of a specific point in the system, in *Template Builder*, a *Request* has to be set in order to monitor the variable in time.

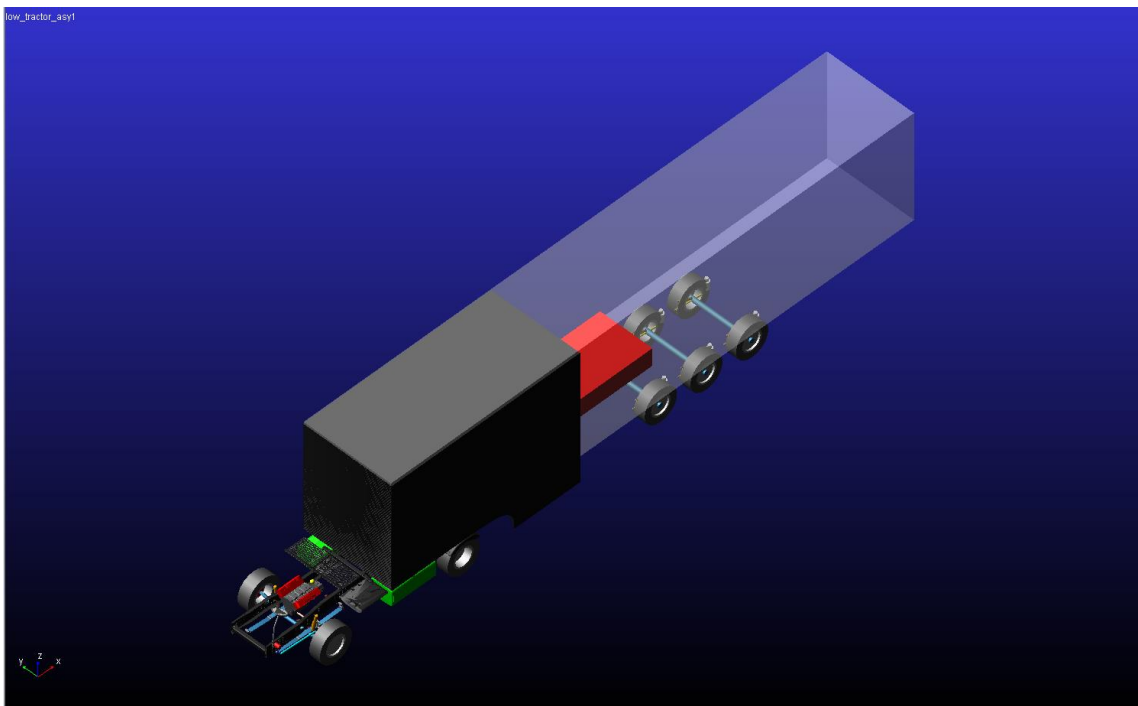
More details will be given in the next Chapter as for the modelling of the truck under analysis.

CHAPTER 2. TRUCK MODELLING

The first purpose of this work was to build a multibody model in *Adams/Car 2015.1* of the *Iveco Stralis my2019*, the more complete and updated as possible.

Since the input data of the problem are covered by industrial and commercial secrecy, some information are hidden within this paper.

The starting point of the activity was a multibody model of an on-road truck, built by Iveco Engineering Office in 2008: it was reported in the following pictures.



Pic. 2.1 - Previous multibody model (ADAMS/CAR)

The track had been developed in order to simulate longitudinal tests, like the downhill ones, to evaluate the contact forces among the frame of the tractor and the trailer: thus, it missed some parts, not necessary to achieve this aim, for instance, the front and the rear anti-roll bars, the cabine and its own suspension (the steering system was both upperly and lowerly linked to the tractor chassis).

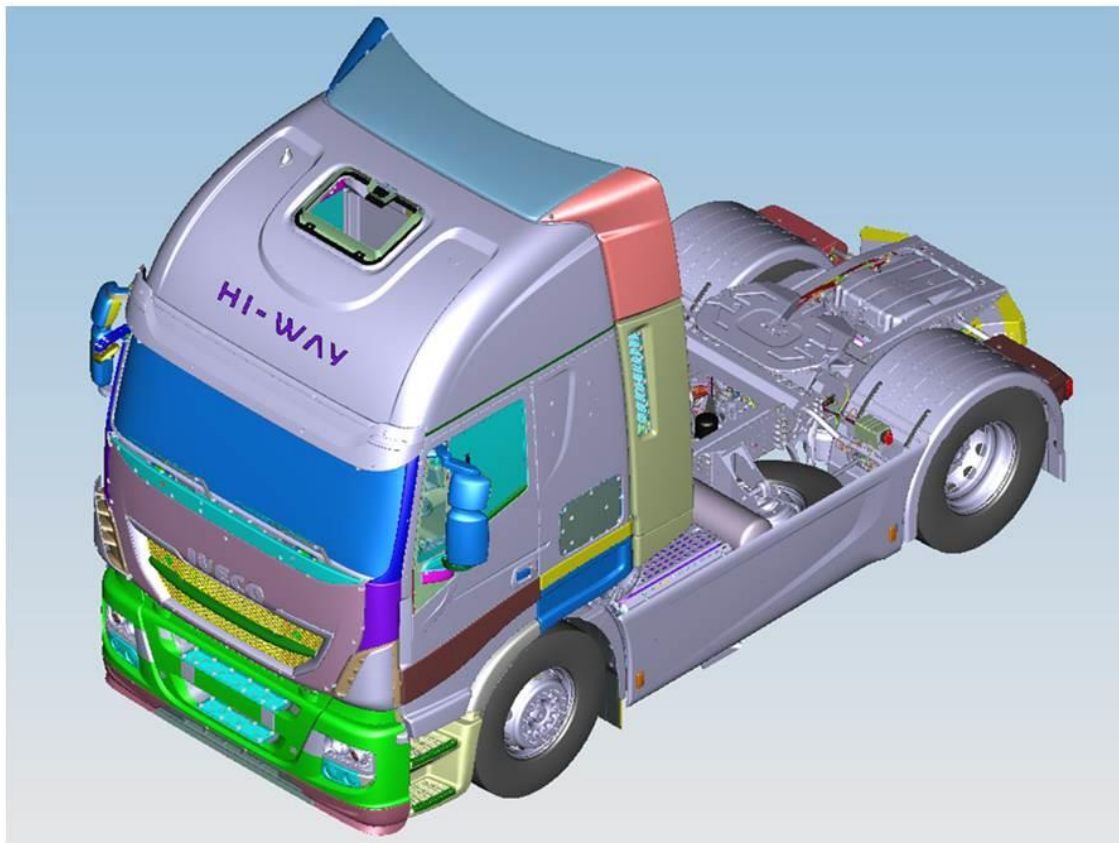
Naturally, mass, spring and shock absorber properties belongs to the previous version of the *Iveco Stralis*.

Moreover, the leaf springs, which constituted part of the front suspension, had been generated in a simplified way: each of them was represented like three rigid bodies, connected by two bushings, in order to simulate the torsional stiffness.

All this simplifying assumption were resonable in the past, when some tools did not exist, and only for this low-speed longitudinal manoeuvres.

In this activity, some *templates* were completely replaced by new ones while others were just updated.

In addition to the multibody model in Pic. 2.1, other data were available: the main one consisted of a 3D model of the tractor in Cad Software *Catia*. A view is reported below.



Pic. 2.2 - 3D model (CATIA)

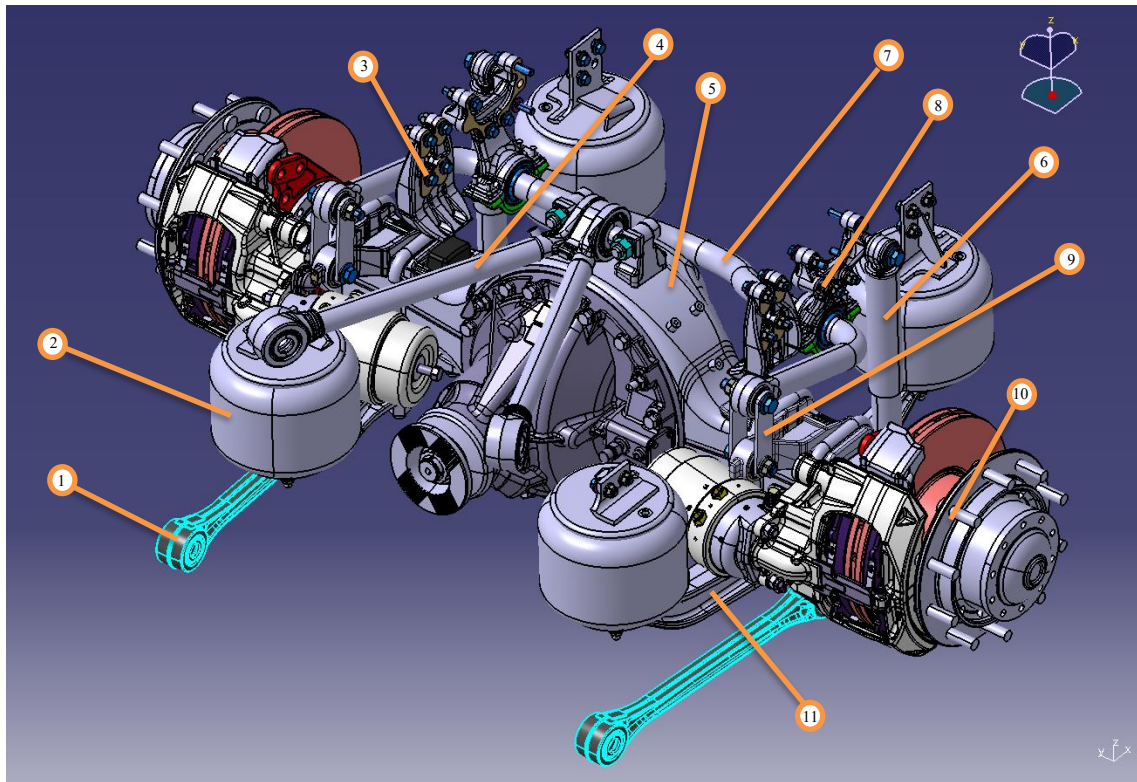
From the entire model, thanks to the Catia structure, it was possible to isolate 3D subsystems at different levels, until the single geometries. Each level of each subsystem is characterized by an alphanumeric code, by which the corresponding 2D drawing can be found.

Notice that, both in *Catia* and in *Adams/Car*, the reference frame is such orientated that the x-axis coincides with the vehicle one and is rearwards, the z-axis is perpendicular to the road surface and is upwards while the y-axis forms a right-handed frame.

In addition to this, in *Catia* the origo of the global reference frame do not match a particular point of the vehicle: it was chosen the same in *Adams* modelling both for semplicity and for consistency in the Company.

2.1 Rear Suspension

The first component existed in the starting model: thus, it was just updated.



Pic. 2.3 – 3D model of the rear suspension (CATIA)

Part Number	Part Name	Quantity
1	<i>Tierod</i>	2
2	<i>Air Spring</i>	4
3	<i>Axle Bumpstop</i>	2
4	<i>V rod</i>	1
5	<i>Axle</i>	1
6	<i>Shock Absorber</i>	2
7	<i>Rear Anti-roll Bar</i>	1
8	<i>Link from Bar to Frame</i>	2
9	<i>Link from Bar to Suspension</i>	2
10	<i>Hub</i>	2
11	<i>Spring Beam</i>	2

Tab. II – Rear Suspension Part List

The task of any suspension is to link the wheels to the chassis, trying to dampen the vibrations and to avoid the detachment of the tires from the ground. In this case, the rear suspension is mainly formed by a rigid axle (5), clutched to two longitudinal elements (11) on which two shock absorbers (6) and two couples of air springs (2) are mounted. In addition to this, the suspension is linked to the chassis by a *V rod* (4) in the upper zone, by two *tierods* (1) in the lower zone and by an anti-roll bar (7) in the middle; the *hubs* (10) are constrained to the axle by ball-bearings. The rear anti-roll bar will form an independent *template* and will be discussed later. As regards the original *template*, it had been modelled by ten *General Parts*, i.e a single body including the axle and the two spring beams, two hubs, a V rod, two upper shock parts, two lower shock parts and two tierods. In order to update the *template*, the first step consisted of reading from the 3D rear suspension model the construction coordinates, the mass and the main moments of inertia of each body and including them in *Adams* model. Preparatory to this phase, the main body, which forms the suspension in the original model, had been divided in three *General Parts*, an axle and two spring beams: this allowed an accurate and efficient evaluation of the mass properties. As concerns the constraints, no changes were performed. A list of the joints in the model follows.

Constraint Name	Kinematic Mode	Dynamic Mode
<i>Hub to Axle</i>	Revolute	
<i>V rod to Axle</i>	Bushing	
<i>V rod to Chassis</i>	Bushing	
<i>Upper Shock</i>	Spherical	Bushing
<i>Lower Shock</i>	Convel	Bushing
<i>Shock Absorber</i>	Cylindrical	
<i>Tripot to Axle</i>	Planar	
<i>Tierod to Axle</i>	Spherical	Bushing
<i>Tierod to Chassis</i>	Convel	Bushing

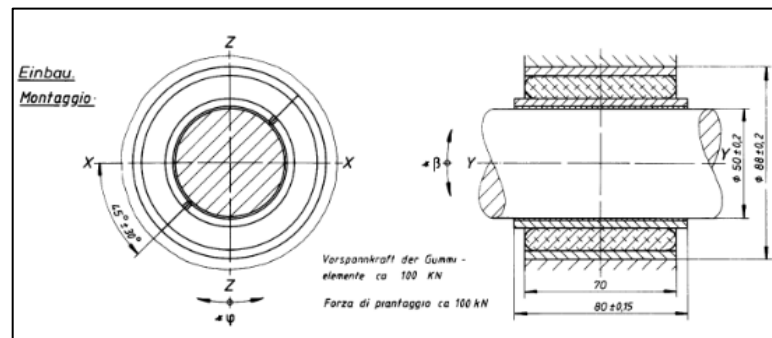
Tab. III – List of constraints in Rear Suspension template

Notice that, in some cases, different joints were used for the kinematic and the dynamic analysis, while, in other ones, a single type of constraint was included.

Then, the attention was focussed on the wheel position and orientation: although the wheels will form an independent *template*, their layout closely depends on the hubs and so on the suspension. Note that, at the back, the tractor mounts a couple of twinned wheels. In the previous model, the wheels occupied a fixed location in the space and there was not the possibility to change it, as even the static toe and camber angle.

Firstly, the reference *hardpoints* were replaced by four *construction frames*, one for each wheel, whose positions were related to the hubs. Four *parameter variables* called lateral distance (from the hub), one inside and one outside, toe and camber were created. Thus, the *construction frames* were parameterized thanks to these new entities. Note that the twinned wheels are locked each other and were set up together: thus, a single toe and a single camber angle was defined, while two distance were necessary since the wheels are not symmetrical to the hub. Finally, the *Output Communicators* were included in the model.

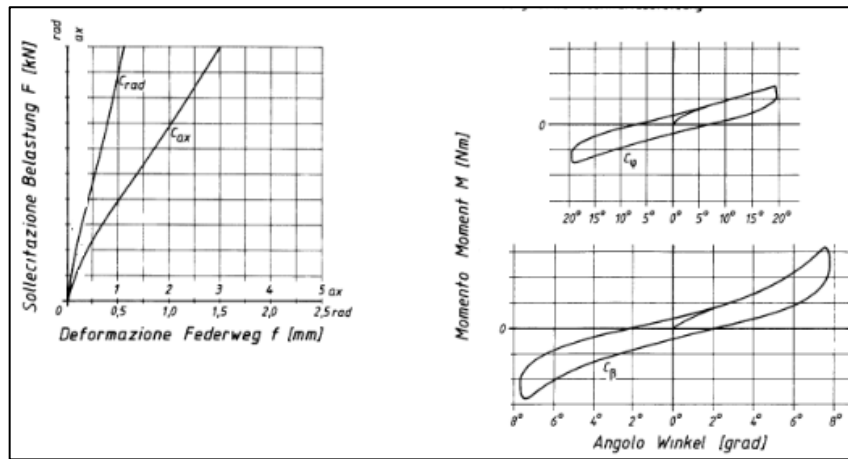
Next, property files of bushings were updated. An example of bushing is reported below.



Pic. 2.4 – Example of Bushing

This mechanical element consists of two cylindrical metallic surface, an internal and an external one, among which there is a rubber layer.

In 2D drawings of each bushing, the Force-Displacement characteristics were available, i.e. the Axial, the Radial, the Cardanic and the Flessional ones.

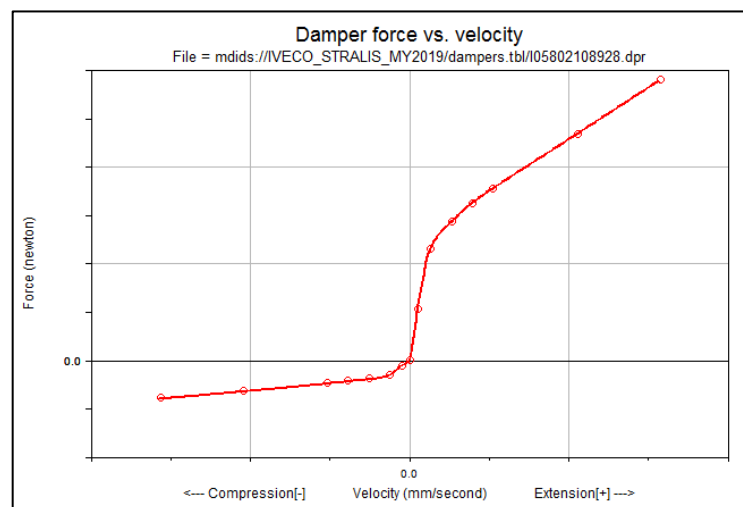


Pic. 2.5 – Example of Bushing characteristics

The splines were read and put in the multibody model.

Note that, the curves show only the pseudo-linear tract, corresponding to the rubber displacement: an huge value was additionally included at the end in order to simulate the metal contact of the two opposite surfaces.

The next elements to be updated were the shock absorbers. Note that, in *Adams/Car*, each of them consists of two *Generic Parts*, an upper and a lower, which can move one inside the other thanks to a cylindrical joint. Thus, they can eventually own mass properties. Besides, an *Adams/Car damper* entity was required among the *Parts*. The Force-Velocity characteristic was got from the 2D drawing and included in *Adams*. The values of the spline were available within a tolerance margin. The average values were computed before.



Pic. 2.6 – Damper characteristic in *Adams/Car*

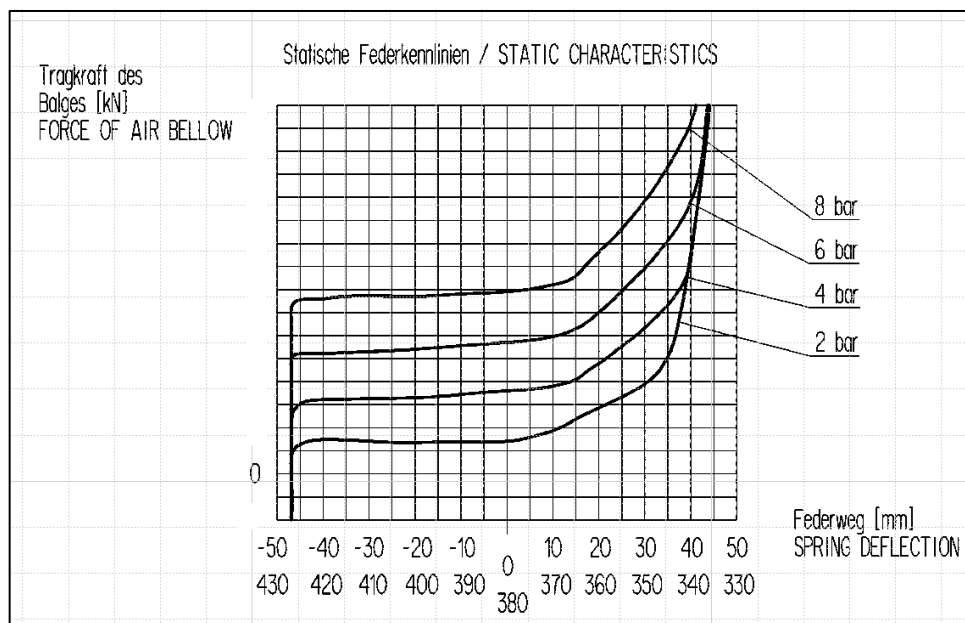
Note the different trend in compression and in expansion.

Other important elements that needed to be modified were the air springs. In *Template Builder*, *Adams/Car* allows the user only to manage helical springs, while in *Standard Interface*, they can be eventually replaced by air ones. Just for greater clarity, their discussion was anticipated in this paragraph. In the real drive, each air spring was connected to the pneumatic system of the vehicle and was inflated by air at a level of pressure among an upper and a lower limit in order to guarantee the project height in the static configuration: changing the track load, the pressure level will be automatically adjusted.

Adams/Car requires the polytropic Force-Displacement trend at least for three different pressure levels: it will provide the interpolation in pressure and in displacement.

In the 2D Air Springs drawings, the isobar curves are available: they represent the force values, for several pressure levels, in function of the displacement. Since the splines are got by quasi-static state changes, the force maintains almost constant along a spline.

An example was reported below.



Pic. 2.7 – Isobar curves for four pressure levels

For each pressure \bar{P}_j in the diagram, the static force \bar{F}_j and the spring volume $V_{j,0}$ corresponding to the design height h_0 were read, where j is one of the splines. Then, the effective area of the air spring in the static configuration was computed:

$$A_{ef,j} = \frac{\bar{F}_j}{\bar{P}_j} \quad (41)$$

The effective area was assumed constant along a spline: this ipothesis is quite realistic in the middle of the Pic. 2.7 where the force is almost costant; the effective area changes at the right and at the left: it is clear by the fact that the force trend changes at the same pressure level.

After, it was assumed that the compression and the expansion of the fluid inside the spring is a polytropic one with exponent $m = 1,35$.

Thus, the air spring travel was discretized from the static configuration to the upper and the lower limits by a step of 20 [mm].

The volumes, at each pressure level, were computed as:

$$V_{j,i} = V_{j,0} + A_{ef,j} \cdot (h_i - h_0) \quad (42)$$

The polytropic formula was applied:

$$P_{j,i} = \bar{P}_j \cdot \left(\frac{V_{j,0}}{V_{j,i}} \right)^m \quad (43)$$

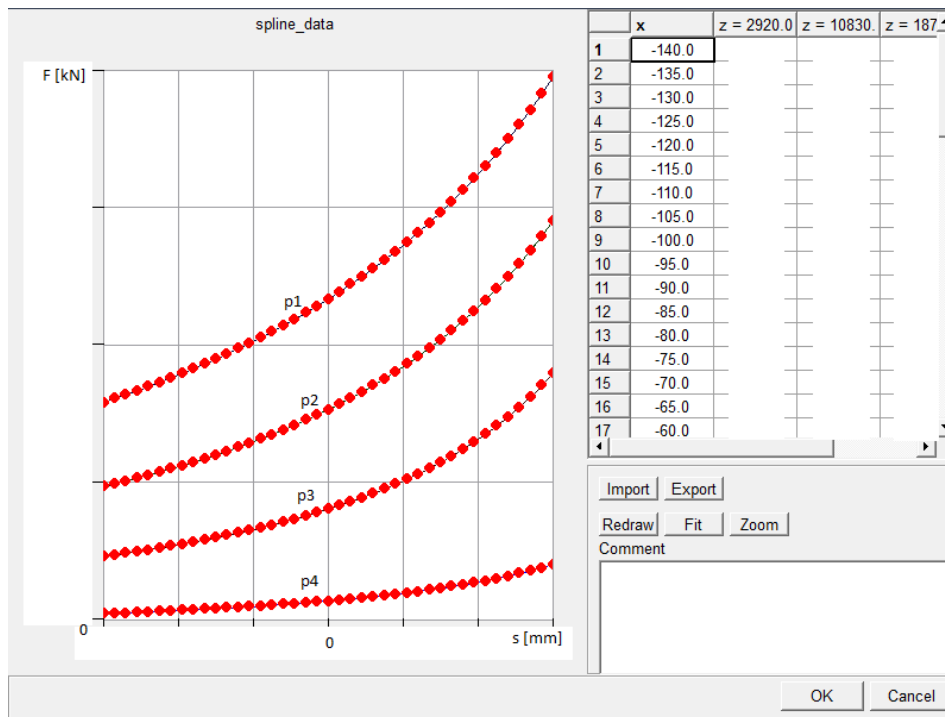
Known the pressures at the different heights, the forces were computed as:

$$F_{j,i} = P_{j,i} \cdot A_{ef,j} \quad (44)$$

Adams/Car requires the force splines in function of the difference between the current height and the static one: according to its covenant, the compression value of height are considered positive; thus, they are computed as:

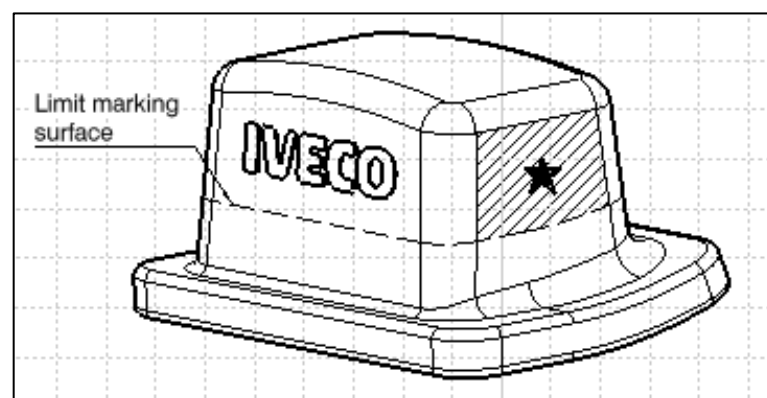
$$x_j = h_0 - h_j \quad (45)$$

The resultant diagram was included in *Adams/Car* model like a property file. In this, the trim lenght, i.e. the static height, and the design diameter were manually added.



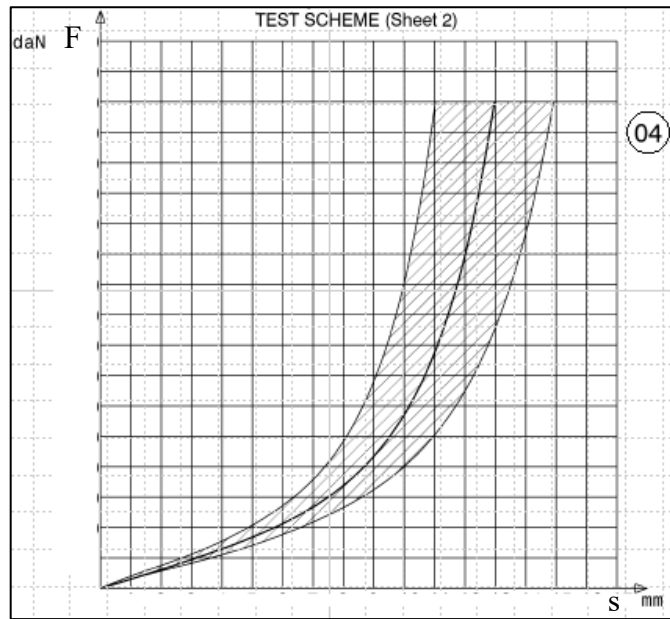
Pic. 2.8 – Air Spring characteristic

The last force entities to be included in the model were the *bumpstop* and *reboundstop* corresponding to the upper and the lower travel limits of the *shock absorbers*, the ones of the *air springs* and the ones of the *axle*. As concerns the ones of the first two elements, no data were available: thus, the default ones in *Adams/Car* were included. More information were present concerning the axle bumpstop. The 2D drawing is reported below.



Pic. 2.9 – Axle Bumpstop

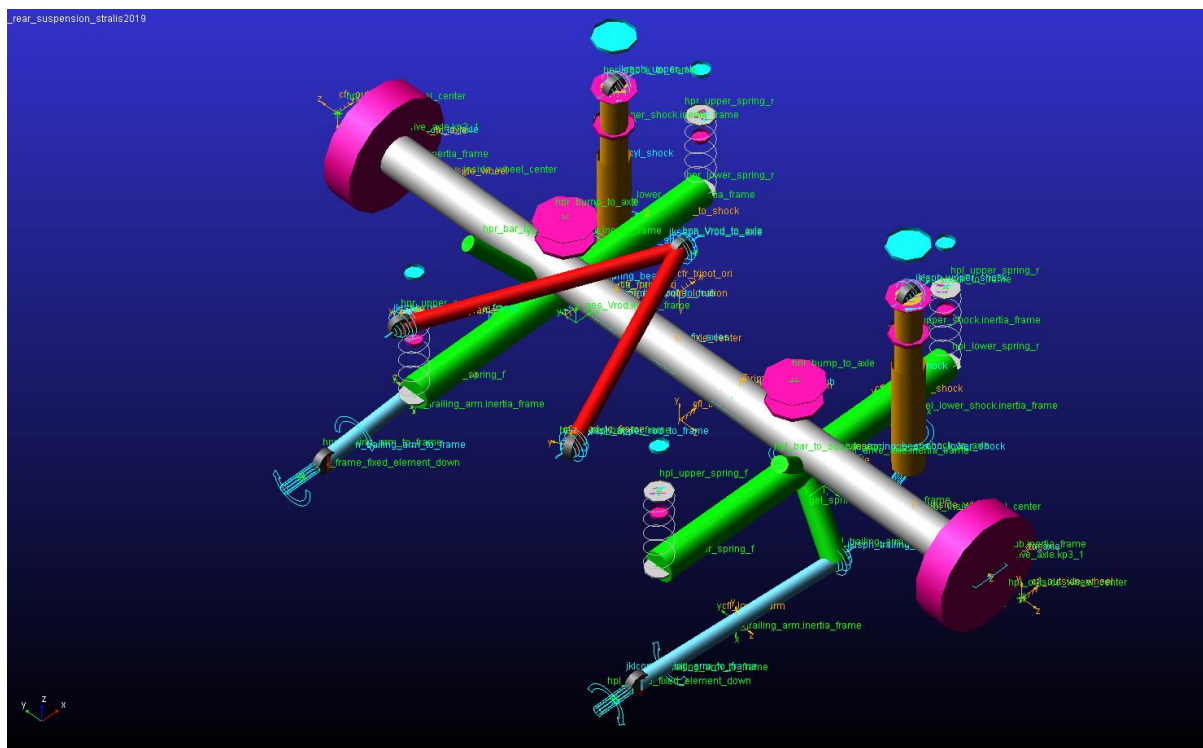
Its characteristic was available in terms of tolerance margin: the average spline was included.



Pic. 2.10 – Axle Bumpstop characteristic

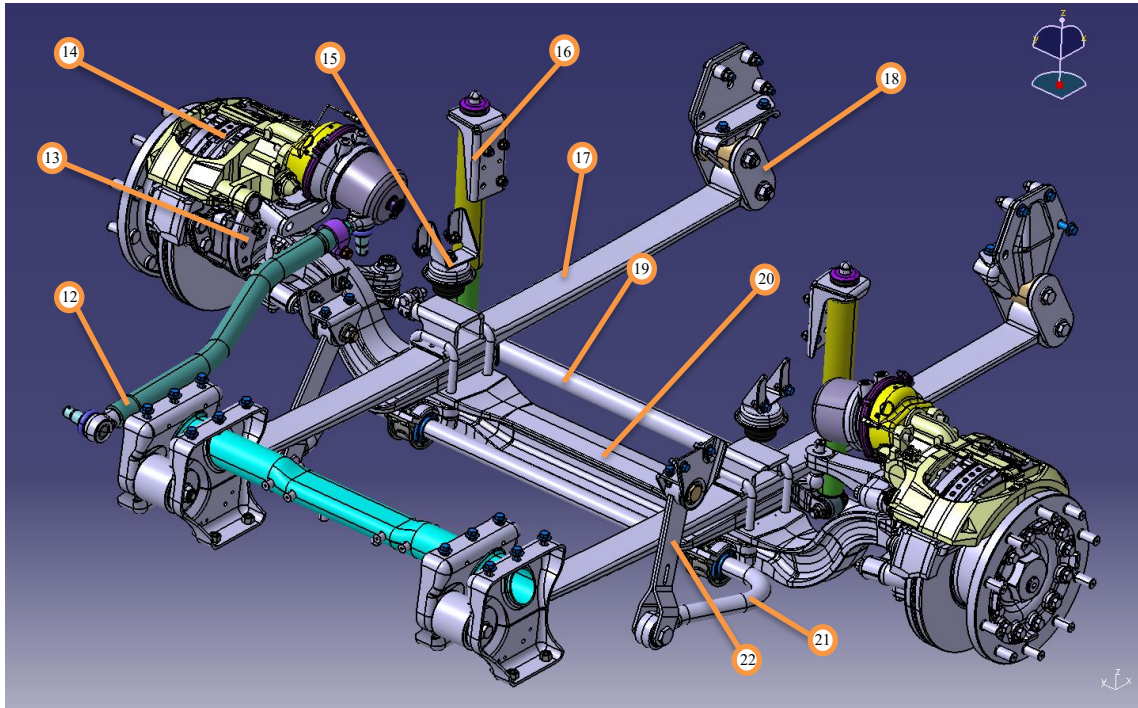
Notice that in the rear suspension *template*, two *Mount Parts* named Tripots were originally defined: their purpose was to transfer the motion in this case from the engine, since there was not the driveline, to the driving hub, which in this vehicle are the ones at the rear. Besides the constraints to the axle, described in Tab. III, it was required to implement the differential which is represented in *Adams/Car* by nothing but a set of equations: it was decided to use the formulation of the *Open* differential.

The picture of the resulting rear suspension *template* follows.



Pic. 2.11 – Rear suspension in Adams/Car

2.2 Front Suspension



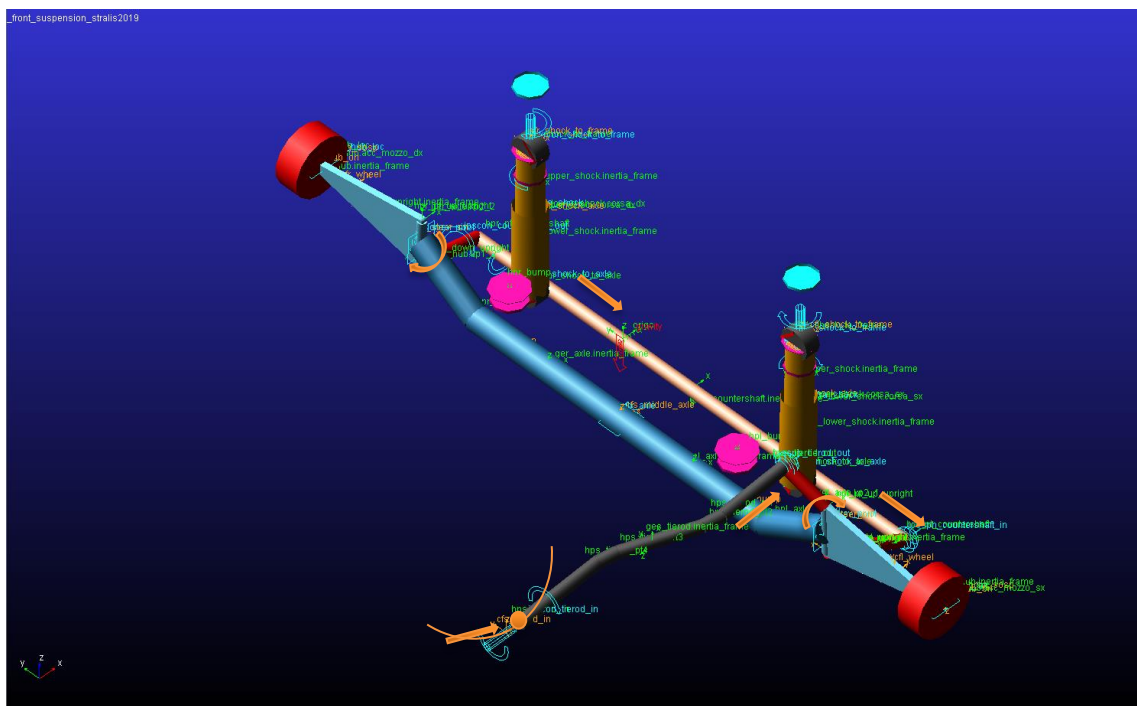
Pic. 2.12 - 3D model of the front suspension (CATIA)

Part Numeber	Part Name	Quantity
12	<i>Longitudinal Steering Tierod</i>	1
13	<i>Upright</i>	2
14	<i>Hub</i>	2
15	<i>Axle Bumpstop</i>	2
16	<i>Shock Absorber</i>	2
17	<i>Leaf Spring</i>	2
18	<i>Shackle</i>	2
19	<i>Transversal Steering Tierod</i>	1
20	<i>Axle</i>	1
21	<i>Anti-roll Bar</i>	1
22	<i>Link from Bar To Frame</i>	2

Tab. IV – Front Suspension Part List

The front suspension was mainly formed by two leaf springs (17), rigidly clamped to the axle (20), which is linked to the chassis even by a couple of shock absorbers (16) and a front anti-roll bar (21). The hubs (14) are mounted on the axle thanks to two uprights (13), one left and one right, which are necessary in order to steer. From Pic. 2.13, it is even evident the way by which the vehicle achieves the steering: firstly, the longitudinal tierod (12), linked on one side to a steering lever and on the other one to the right upright is moved; secondly, the translational x-component of motion is communicated to the left upright and to the relative hub like a rotation; then, the revolution is even assigned to the other upright thanks to the transversal tierod (19) which can move along y-axis.

The modelling was splitted in four *templates*, indipendently managed: the first one, called front suspension, is the one which contains the front axle, then the leaf springs, the front anti-roll bar and the steering system. The discussion starts with the first part of the front suspension, then paragraphs 2.2.1 and 2.2.2 respectively deal with leaf spring modelling and steering system updating. The front anti-roll bar will be discussed in paragraph 2.3 together with the rear one.



Pic. 2.13 – Front suspension template

Constraint Name	Kinematic Mode	Dynamic Mode
<i>Hub to Axle</i>	Revolute	
<i>Axle to Upright</i>	Revolute	
<i>V rod to Chassis</i>	Bushing	
<i>Upper Shock</i>	Convel	Bushing
<i>Lower Shock</i>	Spherical	Bushing
<i>Shock Absorber</i>	Cylindrical	
<i>Long. Tierod to Lever</i>	Convel	
<i>Long. Tierod to Upright1</i>	Sperical	
<i>Upright1 to Trans. Tierod</i>	Spherical	
<i>Trans. Tierod to Upright2</i>	Convel	

Tab. V – List of constraints in Front Suspension template

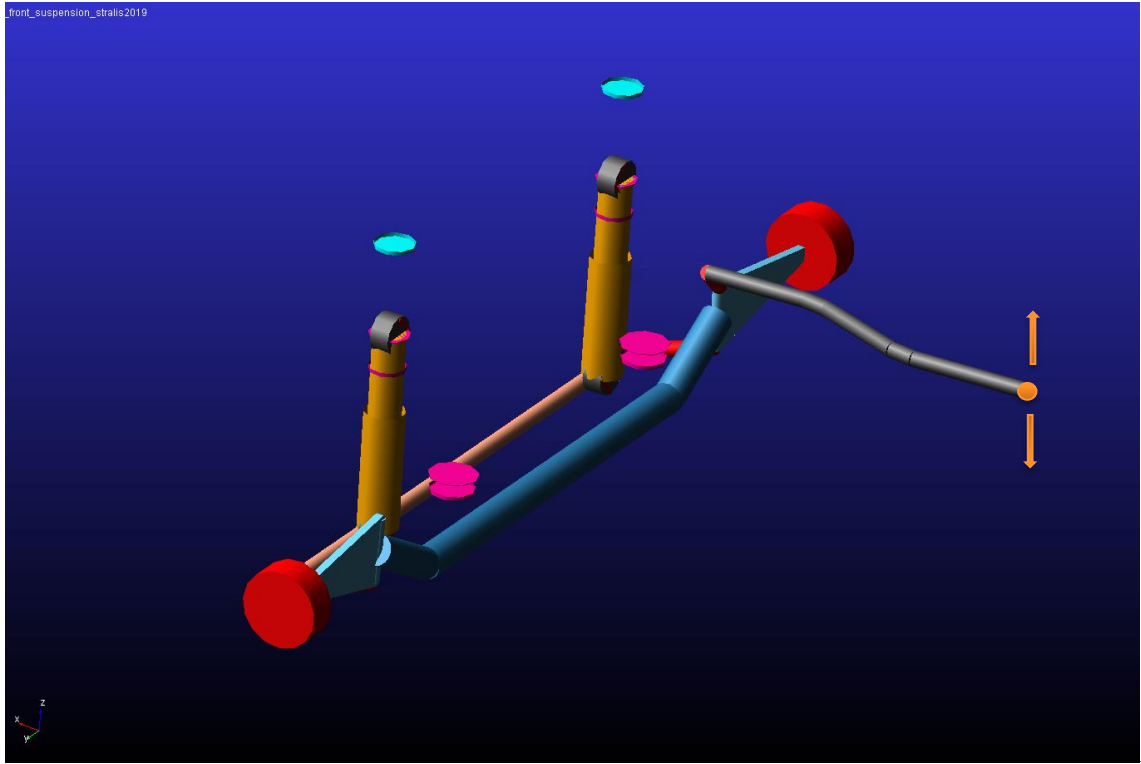
Basically, no change to the topology was performed compared to the previous model.

The property files belonging to the shock absorbers, to the bushings and to the axle boundstops were updated. Even the positions, the masses and the moments of inertia of each part were checked and if necessary modified.

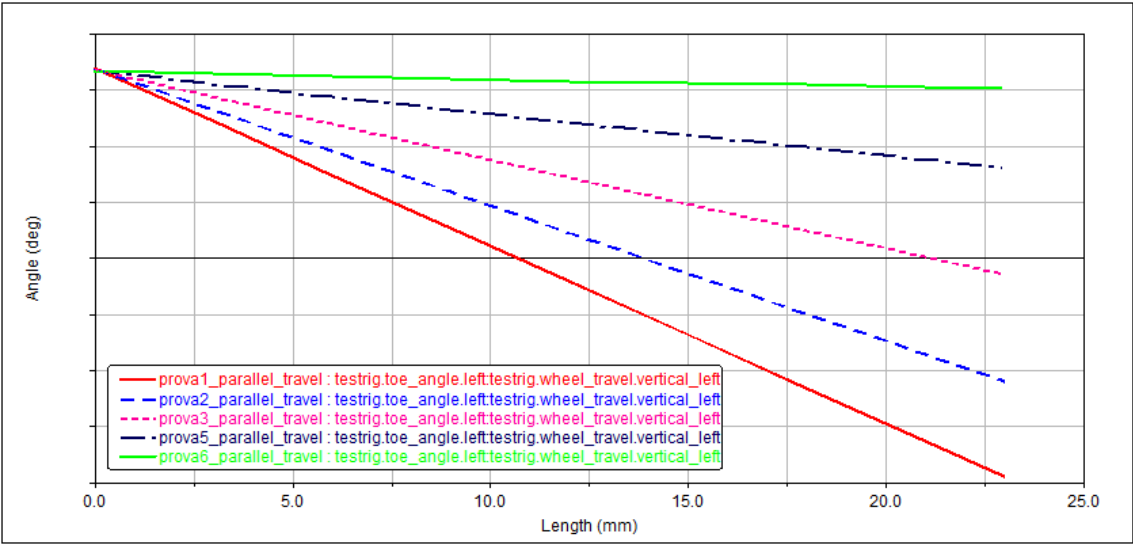
Moreover, the shock absorber *boundstops* and *reboundstops* were added: their contains the default property files by *Adams/Car* since no info were available.

By contrast, it will be described an adjustment of particular interest, anticipating it from Chapter 3. Since the Kinematics of the leaf springs realized in *Adams/Car* in the attempt to replicate the real one is imperfect, the wheels tend to have variable toe angle if subject to a parallel vertical shaking. It was evident, if a *Suspension Assembly* is created and a *Parallel Wheel Travel Test* is performed. Thus, it was made a *Suspension Assembly* formed by the Leaf Springs, the Front Suspension and Front Anti-roll Bar and a test was launched. Plotting the toe angle of the left wheel in function of the travel of the same one, the rate of the curve is not zero. In the attempt

to decrease it, the *hardpoint* of the steering tierod (in orange), which serves as link among the suspension and the steering subsystem was iteratively set in an upper and lower location to bring the rate to zero.



Pic. 2.14 – Iterative procedure on the front suspension template (ADAMS/CAR)



Pic. 2.15 – Toe Angle in function of the Wheel Travel (ADAMS/CAR)

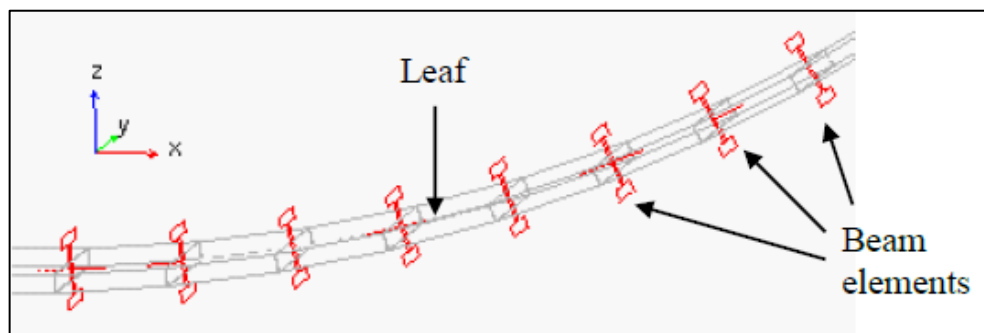
The curve in red represents the original rate while the green one shows the final one: an alteration of more or less 100 *mm* has brought to a decrease of two order of magnitude in the rate. Note that the starting point of the curve was not zero like in the real mechanical system: checking a mark in the full-vehicle simulation panels, as it will be shown later, the fictional driver of the *testrig* will set a specific steering angle in order to move straight forward the vehicle, offsetting this and other phenomena.

2.2.1 Leaf Springs

The most innovative components of the front suspension modelling were represented by the leaf springs which constitutes an independent *template*.

To generate the leaf springs, the Japanese tool named *MSC LeafToolKit* was used. The steps to be done, suggested by the User's Guide, were followed [3].

The toolkit which is used in this activity provides some benefits: it is a high quality environment for creating virtual leaf spring model, using an advanced discrete beam approach.



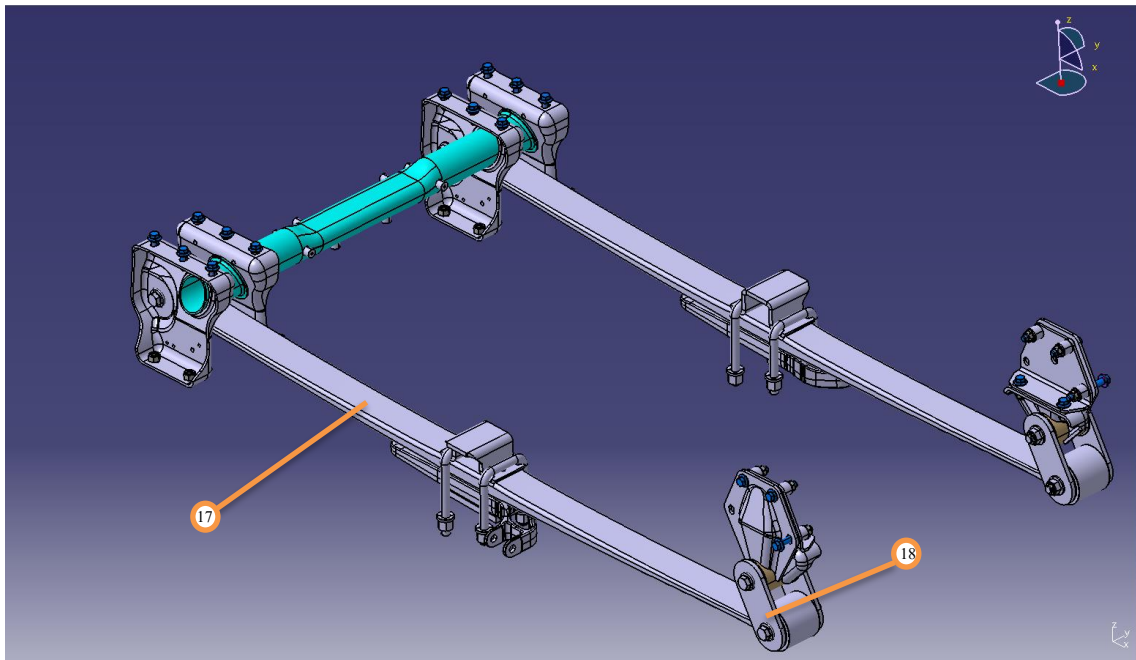
Pic. 2.16 – Leaf Beam Elements

LeafToolKit divides each leaf into a user-defined number of rigid parts. The parts are connected to each other through *Adams* beam element. Note that, adding parts do not produce an increasing of degrees of freedom since each flexible beam is framed to two rigid parts but it provides only to approximate the leaf profile with a better quality.

The virtual leaf spring model can be analyzed as a stand-alone subsystem or can be part of a leaf spring suspension model, eventually assembled in a Full-Vehicle Assembly.

The *Toolkit* works in both *Adams/View* and *Adams/Car*: by its own programming environment, the leaf model can be automatically converted in a *template* with *Adams/Car* attachments and *Communicators*.

The 3D and 2D drawings of the leaf springs under analysis were available, from which the main data were collected.

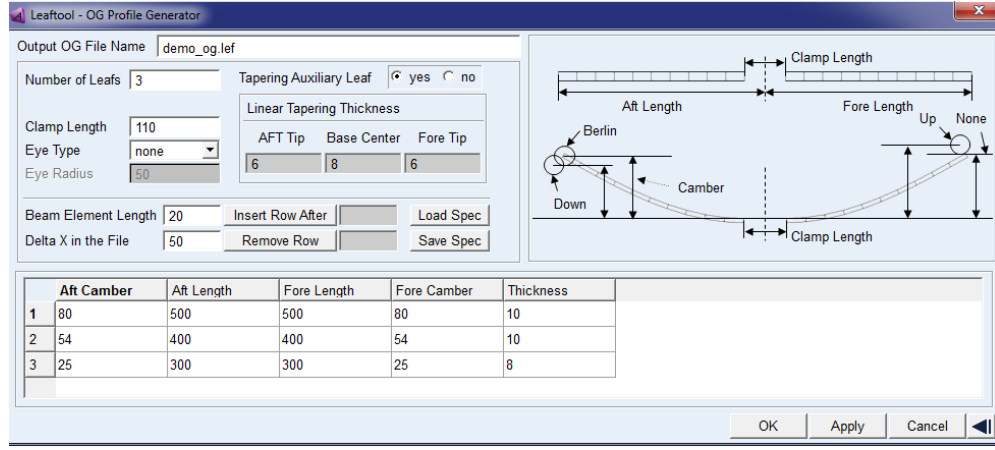


Pic. 2.17 – Leaf Springs 3D drawing (CATIA)

Each leaf springs (17) is directly connected at the front eye and by a shackle (18) at the rear eye to the tractor frame. The axle mounts are located in the middle of the top leafs.

The first step consisted of the creation of the original geometry of the leaf and it was called *OG Profile*: it allows the user to generate the leaf profile from the configuration at drawaing. The profile will be summarized in an output file containing the x and z coordinates and the thickness s, sampled with a defined step.

As example, the default *OG Profile* panels will be reported.



Pic. 2.18 – “OG Profile Generator” panel (LeafToolKit)

To do this, some geometrical data are required, as seen in Pic. 2.18:

- the number of leafs: in the case under analysis is 1;
- the Clamp Length, which can be eventually set to zero;
- the Fore and the Aft Camber heights of the leaf which are defined as the distance from the center of the fore and the aft eye to the inner top surface of the leaf which is parallel to the clamp plane. The data required are the pre-load one while, at drawing, it was possible to read only the value after the pre-load application. Naming h_F [mm] and h_A [mm] the values after the pre-load application, knowing the pre-load F_0 [N] and the stiffness of the leaf k [N/mm] which is almost linear, the *Camber heights* before pre-load application, $h_{F,0}$ [mm] and $h_{A,0}$ [mm], were computed as:

$$h_{F,0} = h_F + \frac{F_0}{k} \text{ [mm]} \quad (46)$$

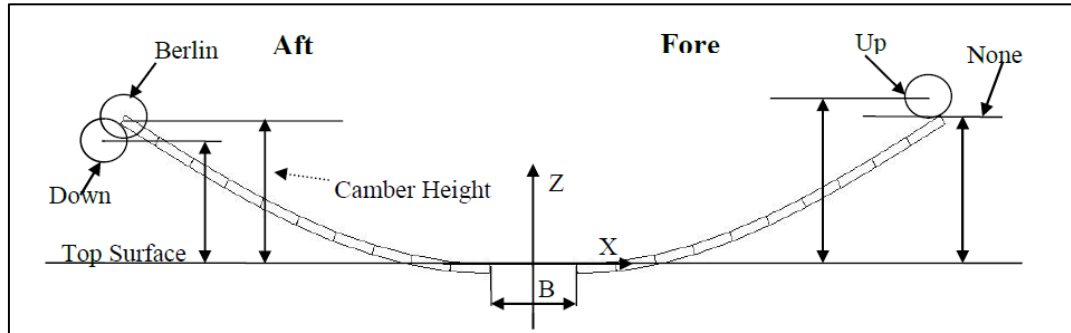
$$h_{A,0} = h_A + \frac{F_0}{k} \text{ [mm]} \quad (47)$$

In this case, $h_A = h_F$ and so even $h_{A,0} = h_{F,0}$.

- the Aft and the Fore Lengths of the leaf, read in the flat configuration;
- the Thickness of each leaf, assuming a constant value in this phase;
- the Eye types: in this case both are Berlin;

- Beams Element Lenght, which consists of the step thanks to which the leaf was discretized;
- Delta X in the file which is the sampling step of the profile in the output file.

The following picture summarized the most important definitions.



Pic. 2.19 – Leaf Spring Parameters

The Beams Element Lenght was set to 20, which is the maximum possible partition while the Delta X in the file was set to 5 [mm], which is considered a small value. This two choise allowed to approximate the thickness and the leaf profile in a good way: it will be evident later.

Since each spring owns one leaf, the interleaf contact force and the clip application will not be discussed. Note that *LeafToolKit* follows the *Adams/Car* convention as concern the global reference frame: thus, assuming the origin of the pseudo-*template* on the center of the main leaf top surface, Fore is the side with the positive x-coordinate and Aft the one with negative.

Before moving to the next step, it was necessary to modify manually the OG profile output file (*.lef*) in order to allocate the correct thickness to each section: to do this, an Excel spreadsheet was used. In fact, in the first phase, a constant value was assigned to the whole leaf while the profile is made of constant and linear tracts.

After this, the next panel in *LeafToolKit* was completed: in particular, the clip and the friction fields were set to zero and the type and the diameter of the Aft and Fore Eyes were assigned. This phase strictly requires the (*.lef*) file.

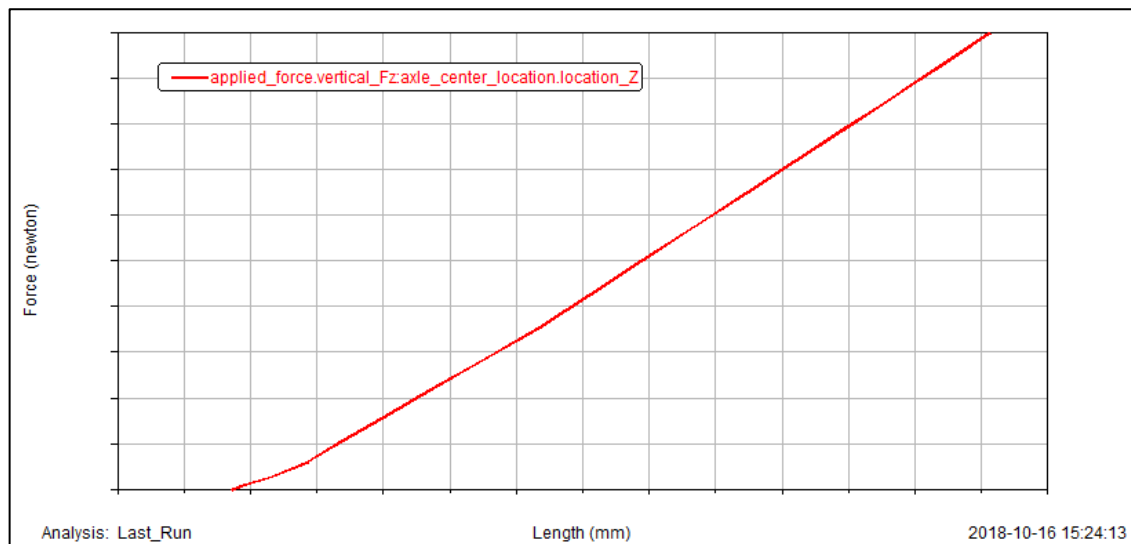
Pic. 2.20 – “Create Leafspring” panel (LeafToolKit)

The next panel deals with the shackle info, i.e. the type (Up or Down), the position (Aft or Fore), and the length. In this case, it is a Fore-Up one.

Pic. 2.21 – “Create the attachments” panel (LeafToolKit)

Before testing the leaf spring generated, it is possible to modify some material properties like E and G modulus and the damping. This parameters will be varied in a second stage.

Before moving to the *Adams/Car* environment, a quasi static vertical test was performed on the mechanical subsystem in order to verify the right behaviour. In particular, a *roller plate test* with $F_z[N] = F_0$ is used to check the characteristic. Then, in the Post-Processing environment, the vertical applied Force in function of the vertical displacement was plotted in order to read the rate which corresponds to the leaf spring stiffness.



Pic. 2.22 – Vertical Force in function of vertical travel (ADAMS/CAR)

An iterative procedure was used in order to find the stiffness at drawing. The floating values has been the profile of the leaf-spring, in particulare the Clamp length which is the most thick section and the E modulus.

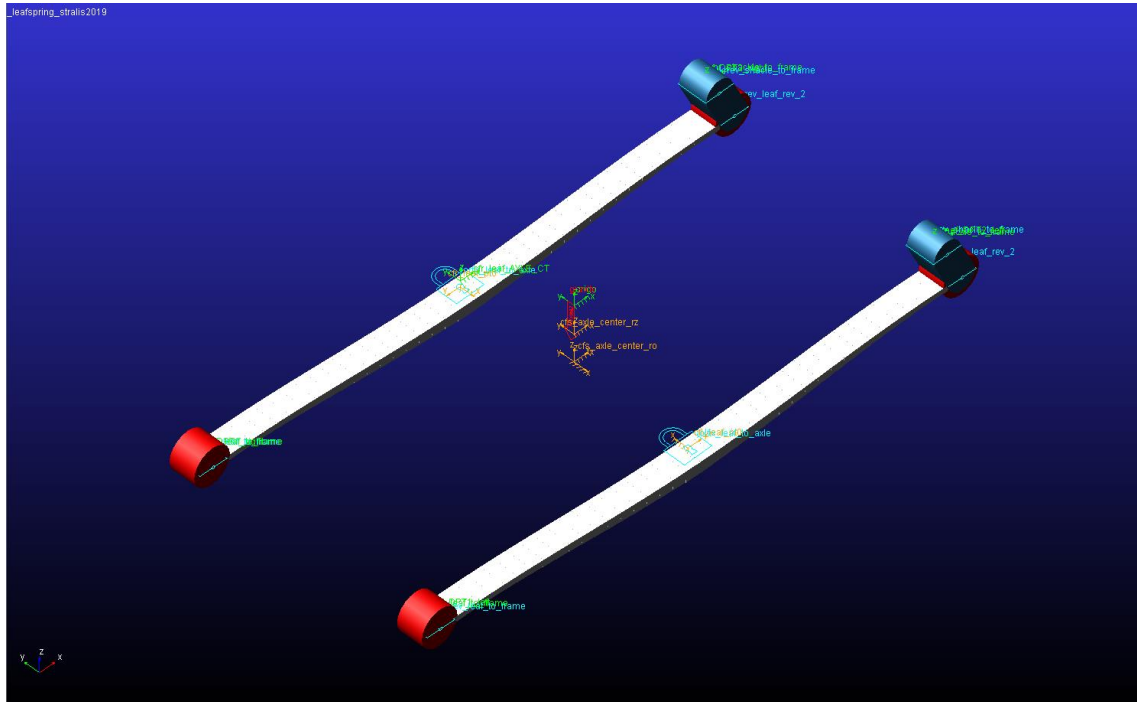
The vertical pre-load F_0 was set thereafter.

In the Assembling phase, on the basis of the single leaf spring, a right and a left one were generated. The last things to do, moving to *Adams/Car Template Builder* environment, were the updating of the bushing property files and the position in the space of the two objects.

Constraint Name	Kinematic Mode	Dynamic Mode
<i>Leaf to shackle</i>	Revolute	Bushing
<i>Leaf to Shackle</i>	Revolute	Bushing
<i>Leaf to Frame</i>	Revolute	Bushing
<i>Leaf to Axle</i>	Fixed	

Tab. VI – List of constraints in Leaf Spring template

The resulting subsystem was reported below.



Pic. 2.23 – Leaf springs of first attempt (ADAMS/CAR)

2.2.2 Steering System

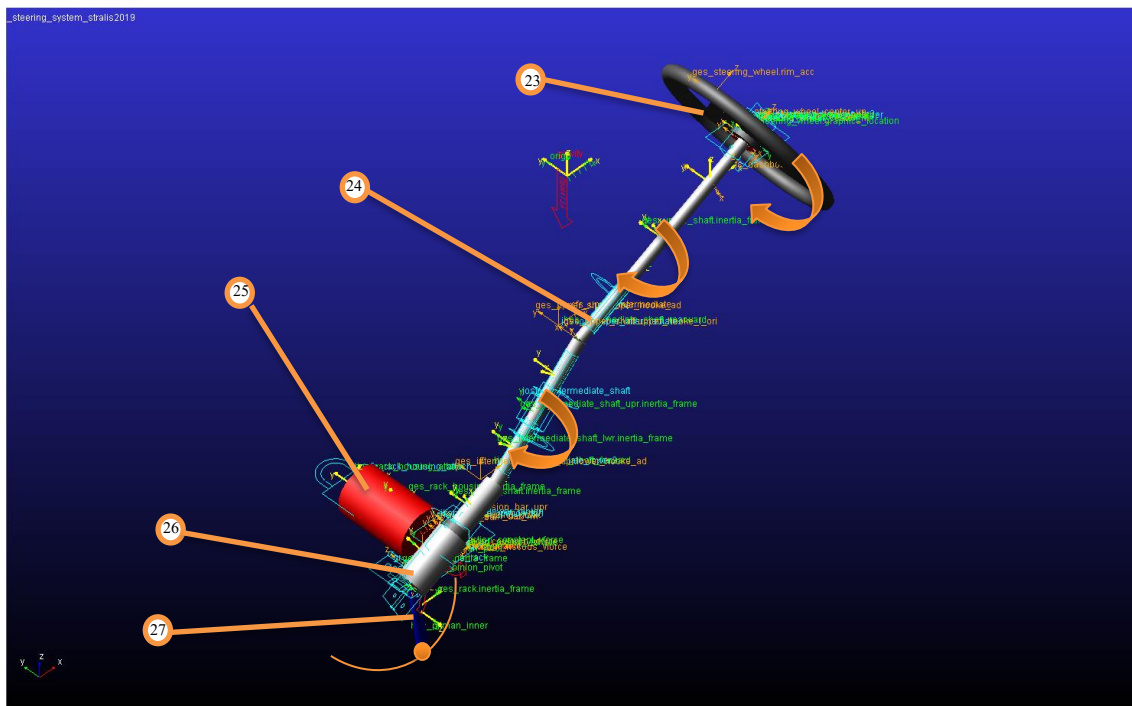
The steering system belonging to the previous model was included in the new one.

It mainly consists of a series of shafts (24), linked each other by convel joints; the upper shaft is connected to the steering wheel (23) by a bushing which simulates the torque stiffness while the last one was linked to a pinion (26) whose spinning is related to the pivot elements (27) by a reduction ratio. The top end of the lever (27) is hinged to the rack housing (25), which is fixed to the chassis.

No substantial change in the topology was performed exept for transfer the driving position from the right to the left side.

Note that the entire system is always connected both in the upper zone to the cabine and in the lower zone to the chassis: the system was made switchable in order to have the steering wheel

linked to the cabine if this *subsystem* was included in the model, otherwise it will be linked to the chassis.



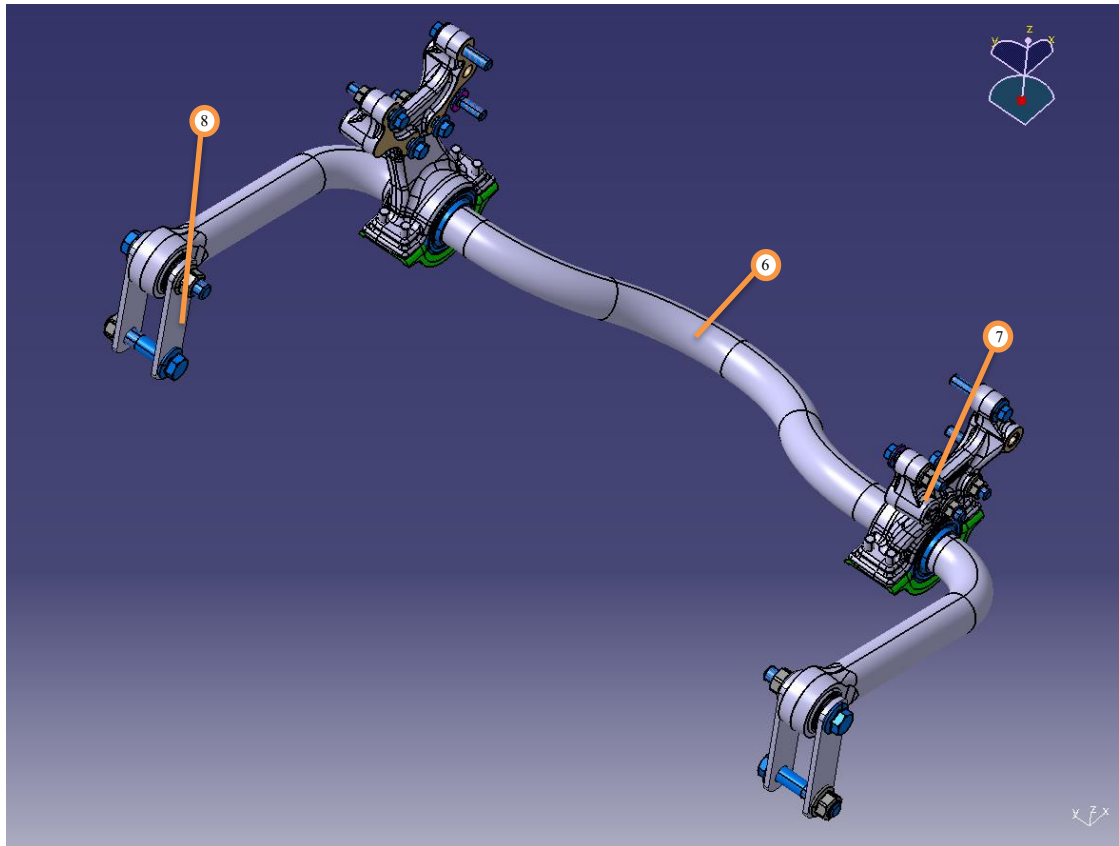
Pic. 2.24 – Steering System (ADAMS/CAR)

Part Numeber	Part Name	Quantity
23	<i>Steering Wheel</i>	1
24	<i>Shaft</i>	3
25	<i>Rack Housing</i>	1
26	<i>Pinion</i>	1
27	<i>Steering Lever</i>	1

Tab. VII—Steering System Part List

2.3 Anti-roll Bars

The front and the rear anti-roll bars represent two totally new *templates*. Like example, the modelling of the rear one will be described; only the difference will be shown as regard the front one. The 3D and the 2D drawings of each one were available.



Pic. 2.25 – 3D drawing of the rear anti-roll bar (CATIA)

It is essentially composed by a cylindrical hollow bar, whose profile is curved, and two couple of linking elements, the lowers to the rear suspension and the uppers to the chassis.

First of all, the *hardpoints*, on the basis of which the *Parts* were generated, were defined, one in the middle of the bar, simmetrically four for the linking elements and other eight to approximate the bar pofile. Note that, as concern the elements connected to che chassis, a single fictious hardpoint was put instead of the two screws.

Then, the two couple of connection elements were created as *General Part*: they were characterized by the appropriate mass and moments of inertia.

On the contrary, the bar was built like a Non-Linear Beam: it will not be managed by the software like a rigid part but like a flexible element using the Eulero-Bernoulli formulation.

It requires more data compared to a common *General Part*:

- *Beam Method*: discrete flexible link was chosen;
- *Beam Formulation*: it was chosen the linear one;
- The collection of *hardpoints* to define the profile;
- some info about the material like the type, which owns a specific stiffness (E and G modulus), and the damping;
- some info about the geometry: it was chosen an hollow circular section characterized by a constant d_{in} and a d_{out} .

Then, the *Mount Parts* corresponding to the chassis and to the rear suspension were included.

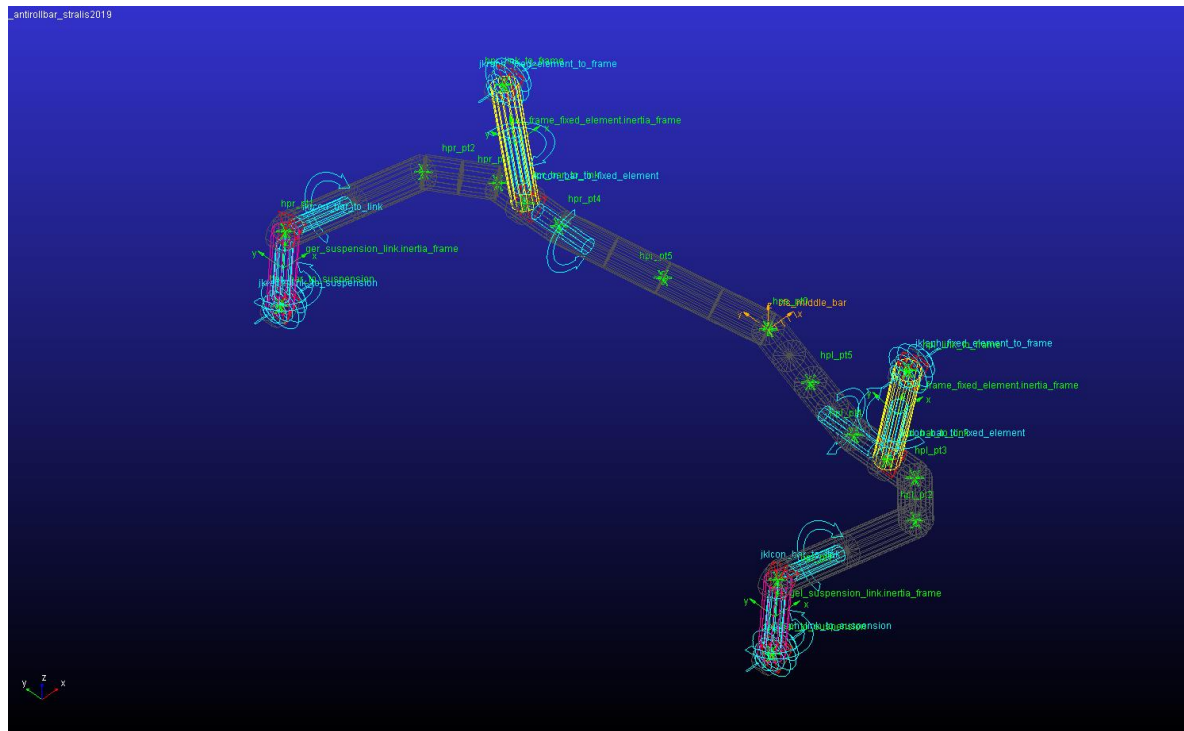
Final step consisted of the template attachments, which were summarized in the follow table.

Joint Name	Kinematic	Dynamic
<i>Lower Arm to Rear Susp.</i>	Spherical	Bushing
<i>Lower Arm to Bar</i>	Convel	Bushing
<i>Bar to Upper Arm</i>	Convel	Bushing
<i>Upper Arm to Chassis</i>	Fixed	

Tab. VIII – List of constraints in Rear Anti-roll Bar

Finally, the right property files of the bushing were included.

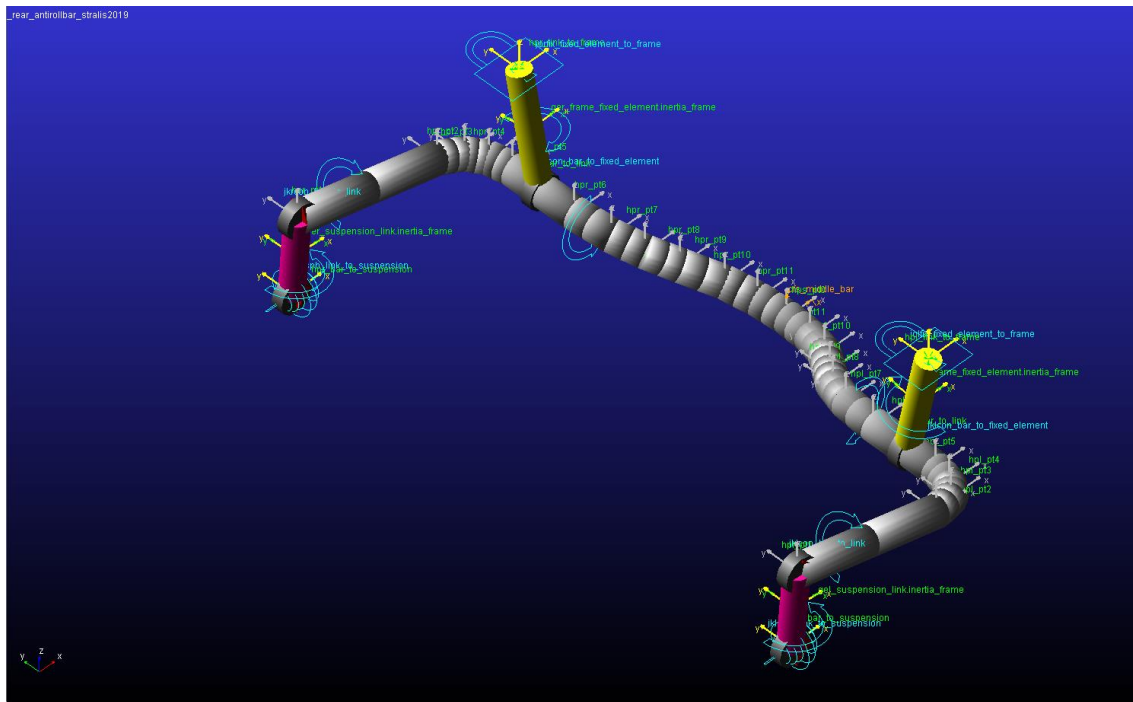
The resulting *template* was reported below.



Pic. 2.26 – Rear Anti-roll Bar on the first attempt (ADAMS/CAR)

In a second time, it was decided to improve the profile approximation in order to make more realistic the bar characteristic.

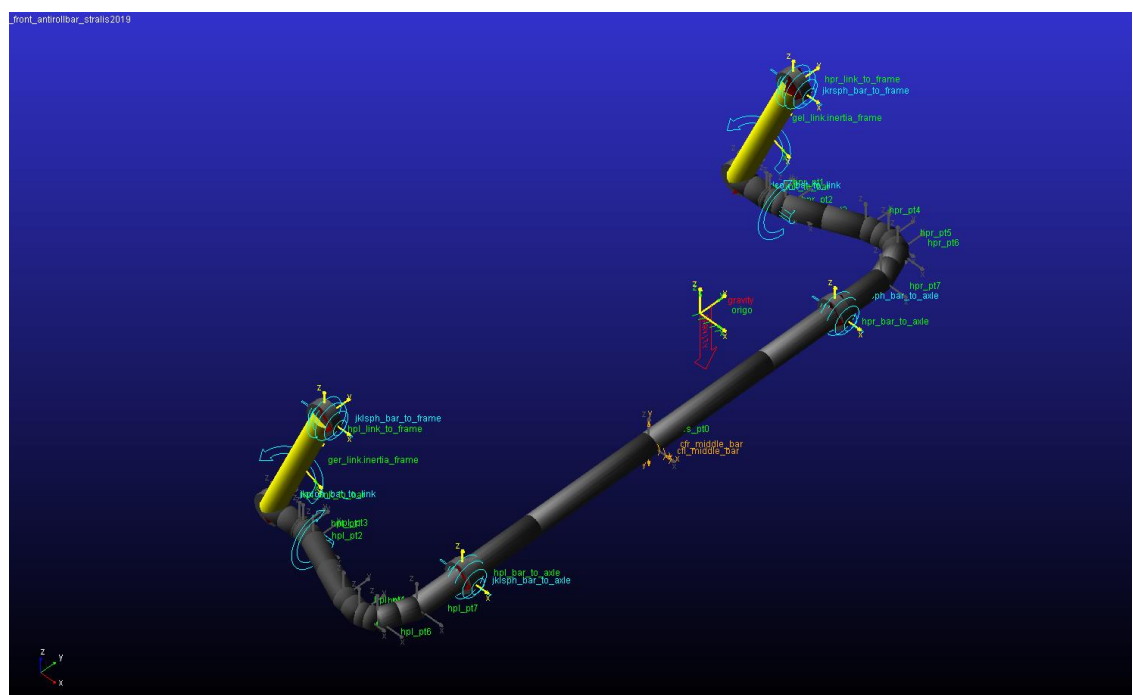
To achieve this aim, more intermediate points in the bar were necessary. Preliminarily, other points were put into the 3D *Catia* model on the middle line by which the solid was extruded. Then, the coordinates of these new points were read and included in the *Adams/Car* model. Finally the *Beam* Panel was updated. The final *template* follows.



Pic. 2.27 – Final Rear Anti-roll Bar (ADAMS/CAR)

Thereafter, the attention was focussed on the front anti-roll bar. It is formed by a bar, modelled again as a Linear Beam and a couple of links which connects it to the chassis; the connections to the front suspension are just two bushings.

Exept for the topology, the modelling followed the previous steps.



Pic. 2.28 – Front Anti-roll Bar (ADAMS/CAR)

2.4 Engine

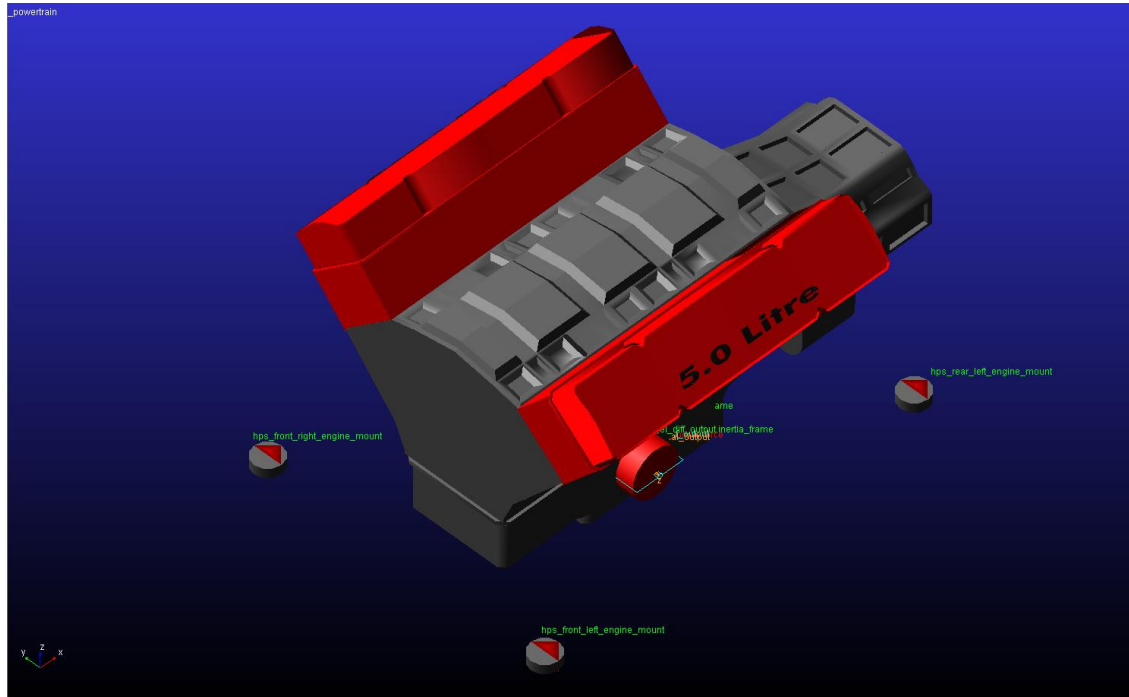
This *template* is not essential in order to realize a *Full-Vehicle Assembly* in *Adams/Car*; despite this, it was decided to include it in order to perform a large range of manoeuvres. In fact it turns out to be necessary as concern the constant velocity and the constant accelerator pedal travel ones. The default *template* by *Adams/Car* was used like starting point: it is constituted by a box (characterized by inertia properties), four bushings which stand for the engine mounts (all of which are linked to a single *Mount Part*, i.e. the chassis) and an output torque (function of rpm, accelerator pedal travel and the gear) which is transmitted to the rear suspension where the equations of the differential were computed. Note that in this simplified model, the real transmission misses, thus the reduction ratios of the gear and the differential are included in this *template* like *parameter variables*.

First of all, the effective mass and moments of inertia were read from *Catia* model and put in the *Adams/Car* one.

A crucial difference between the default *Adams/Car* vehicle model and the one under analysis is represented by the kind of element used to model the chassis: in fact the first frame is rigid while the second one is flexible. Thus, it was fundamental to replace the single *Mount Part* of the chassis with four independent element in order to let the engine mount transmit loads and deform on their own. Note that the engine mount were modelled like bushing in order to include a specific characteristic in terms of stiffness and damping, previously studied within the Engineering Office. Thus, the bushing property files corresponding to the engine mount were included. Even though the Iveco Stralis has 12 or 16 gears ratios, according to the specific version, while the example of engine *template* only 6 ones, no changes were done: on the one hand, *Adams/Car* was implemented for passenger cars and so it is quite difficult to perform this kind of adjustments, on the other hand the results coming from the engine subsystem were only used as a verification of the correct behaviour of the model and so they are not normally

required. The mechanical characteristic was not modified while the six gear ratios were allocated in a fictitious way in order to perform test from the 20km/h to the 100km/h both at full-load and when the vehicle was unladen.

The resulting *template* follows.



Pic. 2.29 – Engine template (ADAMS/CAR)

2.5 Flexible Bodies

At first, it was decided to implement two flexible bodies: in the previous model, one was entirely lacking, namely the cabine, while the other one was rigid, the chassis.

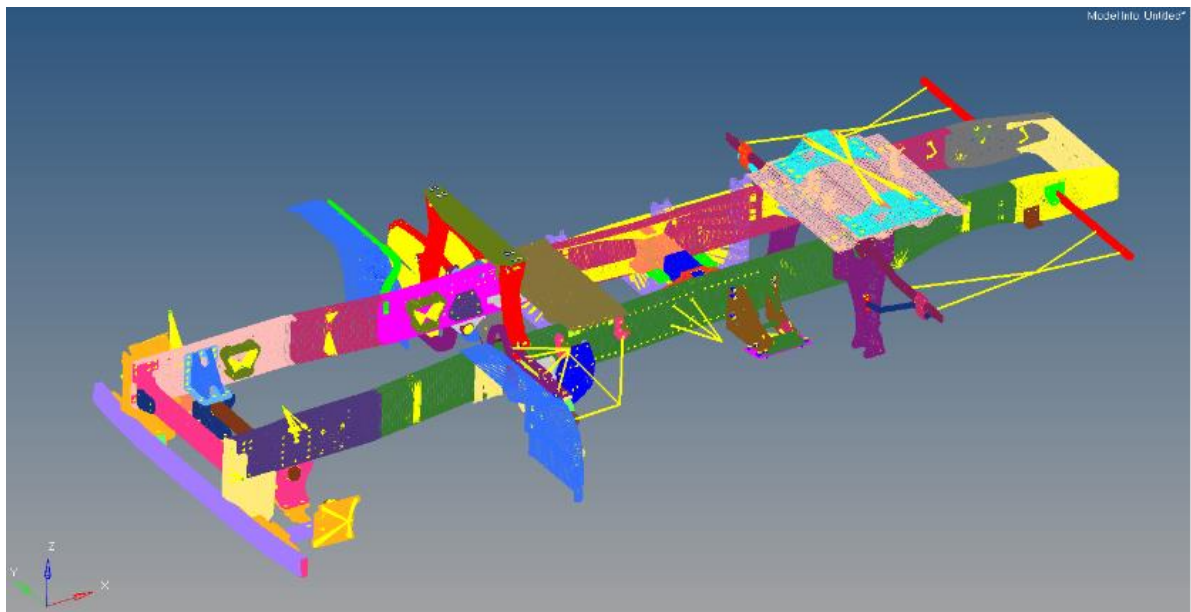
In the vehicles of a certain size, like in this case, the larger components can have a direct influence on the dynamic behaviour of the entire mechanical system in terms of stiffness and damping. Note that more details about the theory which underlines the flexible body were given at the end of this paper, in the Appendix.

The discussion starts from the chassis modelling, the same steps were applied even to the other elements.

2.5.1 Chassis

This element was the longest to be modelled: thus, it was expected that its greater contribution, as flexible body, would be in the torsional and flexional vibration modes.

First of all, a FEM model of the new Iveco Stralis chassis was collected from the Engineering Office. It had been previously generated, with shell elements from the 3D *Catia* model in order to perform other FEM analysis. The procedures used to create the mesh, which was already available, will not be discussed in this sheet.



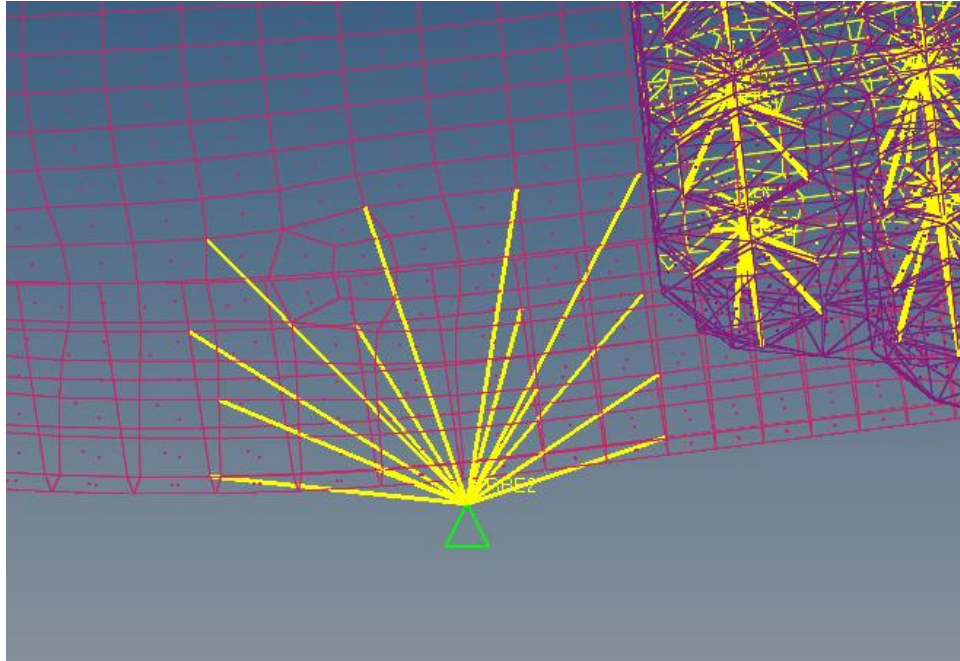
Pic. 2.30 – FEM model of the chassis (HYPERMESH)

It was used *Hypermesh* by *Altair* as Pre-Processing environment.

Before launching any FEM computation, some adjustments were necessary on the mesh, i.e. the creation of the interface nodes. These will be the geometrical points in the space by which the chassis subsystem sends to and receives from the outside forces. Note that, these interface nodes do not belong to the mesh ones.

In order to model them, RBE2 entities were used: thanks to this *Hypermesh* option, each interface node displacement was related to some mesh nodes nearby and viceversa. In fact, the

interface node are called *master* while the relative mesh nodes *slaves*. The reason of this step is represented by the fact that in mechanical system, forces are never concentrated in a point but they are normally exchanged across a surface; useful example can be the force transmitted by a screw or by a bushing.



Pic. 2.31 – Example of RBE2 entity (HYPERMESH)

A list of the RBE2 entity in the model follows.

Chassis interfaces	N. of interface nodes
<i>Engine Mount</i>	4
<i>Cabine Suspension</i>	8
<i>Fifth Wheel</i>	1
<i>Leaf Springs</i>	4
<i>Front Shock Absorbers</i>	2
<i>Front Anti-roll Bar</i>	2
<i>Air Springs</i>	4
<i>Rear Shock Absorbers</i>	2
<i>Rear Anti-roll Bar</i>	2

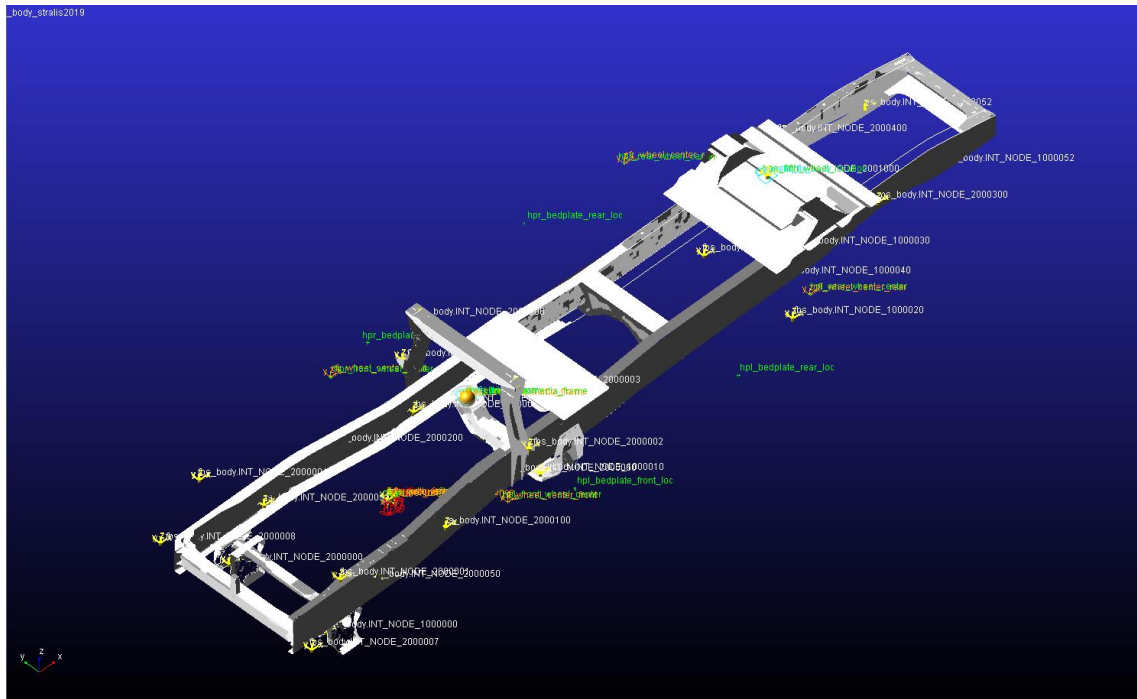
Tab. IX – List of RBE2 Nodes

The fifth wheel is the term in technical jargon used to indicate the point and also the mechanism used to connect the semitrailer onto the tractor

Then, a modal analysis, using *Nastran* by *MSC Software*, was launched using the resulting *Hypermesh* file (.dat) which is a list of nodes and elements. More details about the modal analysis will be given in Appendix A.

Moving again in *Adams/Car*, the example *template* of chassis by *Adams* was imported: thanks to the *switch to flexible* comand it was replaced by a flexible one in which the *Nastran* output file (.mnf) was included. The *modal neutral file* contains the vectors of the mode shapes (eigenvectors) and the natural frequencies (eigenvalues).

A picture from *Adams/Car* is reported below.

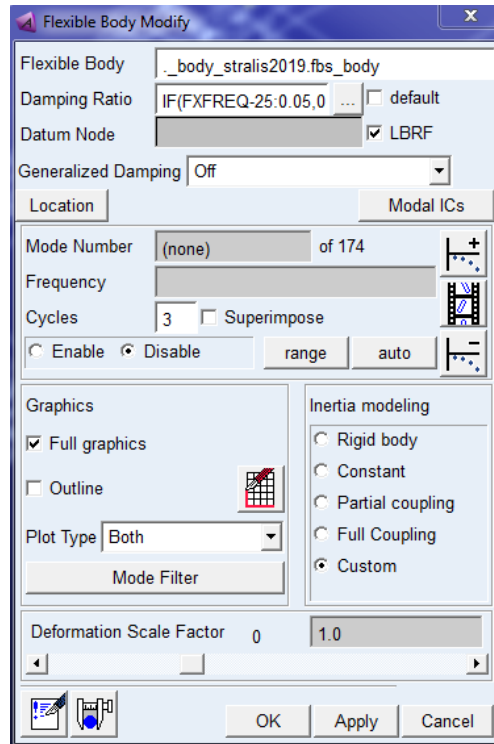


Pic. 2.32 – Chassis template (ADAMS/CAR)

First of all, the geometry was associated to a *construction frame*, moving which the chassis was placed in the correct position and orientation.

Secondly, the *Interface Parts* were created on the master nodes previously defined in *Hypermesh*: this allowed not only to build the *Communicators* on them but also to take advanges from the symmetrical functions by *Adams/Car*.

Opening the Flexible Body Panel, reported below, some data were required.



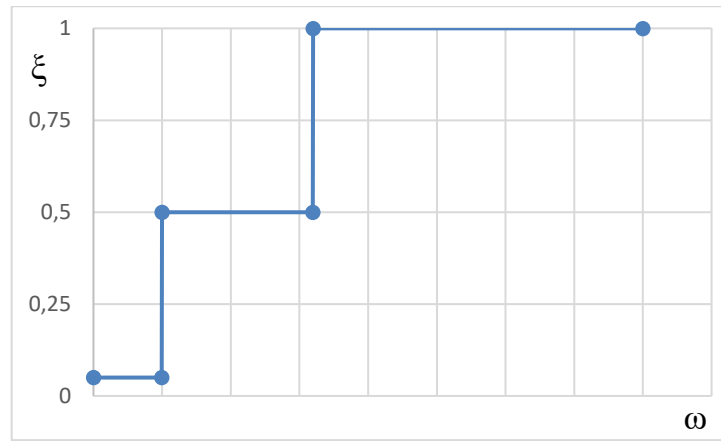
Pic. 2.33 – Flexible Body Panel (ADAMS/CAR)

Firstly, the damping ratio was included in the model as the following function, previously studied in the Iveco Engineering Office:

$$\begin{aligned} \xi &= \xi_1 \quad \text{if } \omega < \omega_1 \\ \xi &= \xi_2 \quad \text{if } \omega_1 \leq \omega < \omega_2 \\ \xi &= \xi_3 \quad \text{if } \omega \geq \omega_2 \end{aligned} \quad (48)$$

where

- ω is the frequency of the force;
- ω_1 and ω_2 are two frequency threshold;
- ξ_1 , ξ_2 and ξ_3 are three constant values of damping ratio.



Pic. 2.34 – Damping Ratio in function of the frequency

The trend is such that the damping is very small at the low frequencies, increases in the middle and become 100% over a certain value.

Thanks to the same panel, it is possible on the one hand to animate all the shape vectors, on the other hand to switch from the flexible body configuration to others like the rigid one, flattening an Inertia Modelling option: it acts on the nine inertia invariants used to compute the time varying mass matrix of the flexible body.

$$\begin{bmatrix} \mathbf{I}^1 & -\tilde{\mathbf{I}}^2 - \tilde{\mathbf{I}}_j^3 q_j & \check{\mathbf{I}}^3 \\ & \mathbf{I}^7 - \check{\mathbf{I}}_j^8 q_j - \check{\mathbf{I}}_{ij}^9 q_i q_j & \check{\mathbf{I}}^4 + \check{\mathbf{I}}_j^5 q_j \\ & & \check{\mathbf{I}}^6 \end{bmatrix} \begin{bmatrix} \ddot{\mathbf{x}} \\ \dot{\omega} \\ \ddot{\mathbf{q}} \end{bmatrix}$$

Pic. 2.35 – Mass Matrix

Pic. 2.36 represents the flexible body mass matrix in which nine invariants figure and the acceleration state vector.

Invariants	Meaning
1	Total Mass
2	Center of Mass location multiplied by the mass
7	Moments of Inertia
8 and 9	1st and 2nd order modification to the Moments of Inertia

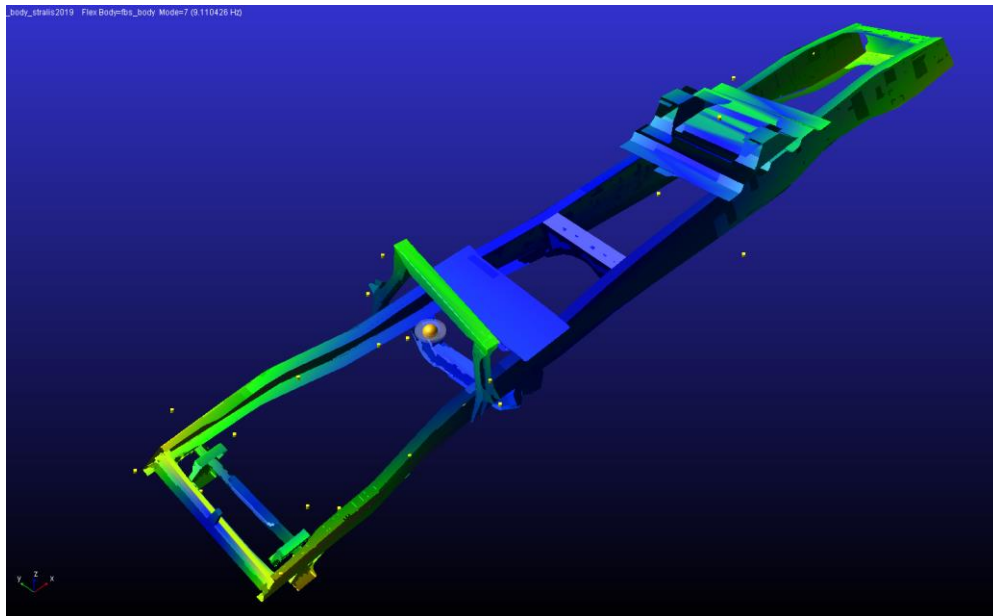
Tab. X – Main Invariants and their meanings

A short overview about the several options is now offered to the reader:

- Rigid Body: Invariant 6 is disabled, Adams/Car ignores all the modes during the simulation, so the body is totally considered rigid;
- Constant: Invariants 3, 4, 5, 8 and 9 are disabled which means that inertia properties are unaffected by deformation;
- Partial Coupling: Invariants 3, 4, 5 and 9 are disabled. The last two provide a 2nd order correction to the mass matrix, imposing a great computational overhead with a small impact on the results;
- Full Coupling: only Invariants 3 and 4 are disabled;
- Custom: the user has the possibility to select the Invariants to disable.

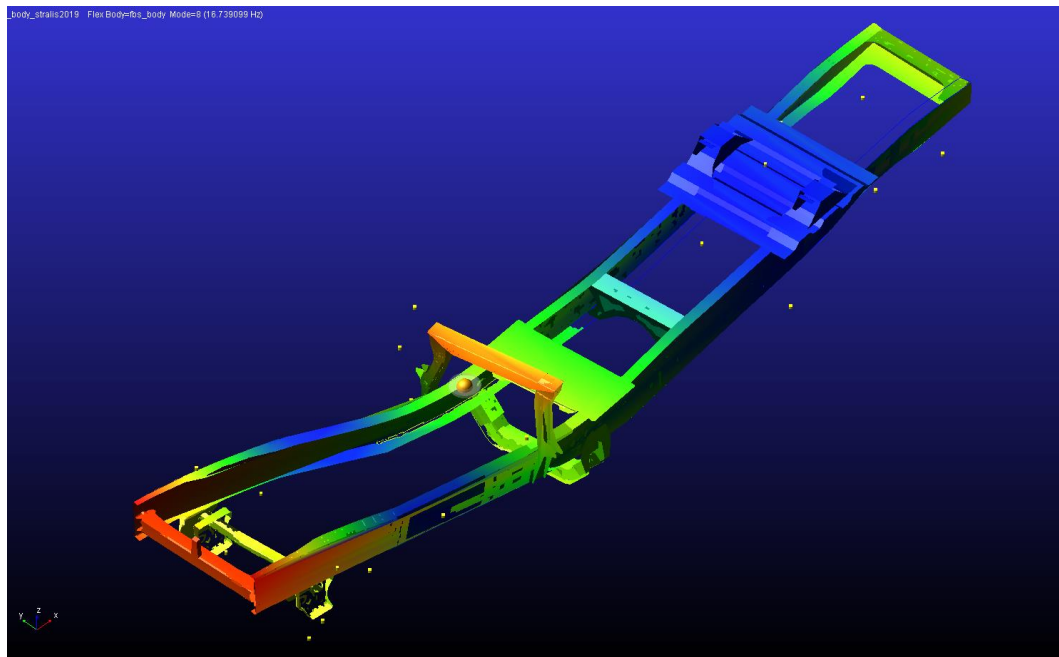
In order to get the simulation quicker and more efficient, the flexible body simulations will be performed with Partial Coupling configuration instead of the Full Coupling.

The four following pictures refers to the first no zero shape modes; note that the first six ones correspond to the six rigid motions of the structure.



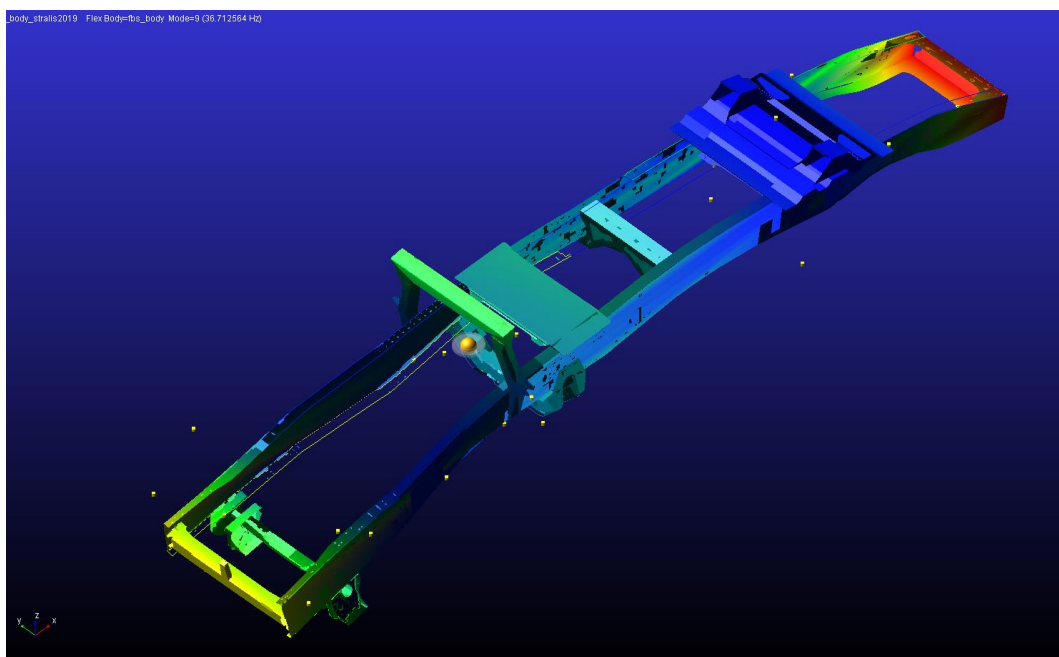
Pic. 2.36 – First shape mode of the frame (ADAMS/CAR)

The first shape mode, plotted in Pic. 2.37, is a torsional one (around x-axis): its natural frequency is less than 10 Hz.



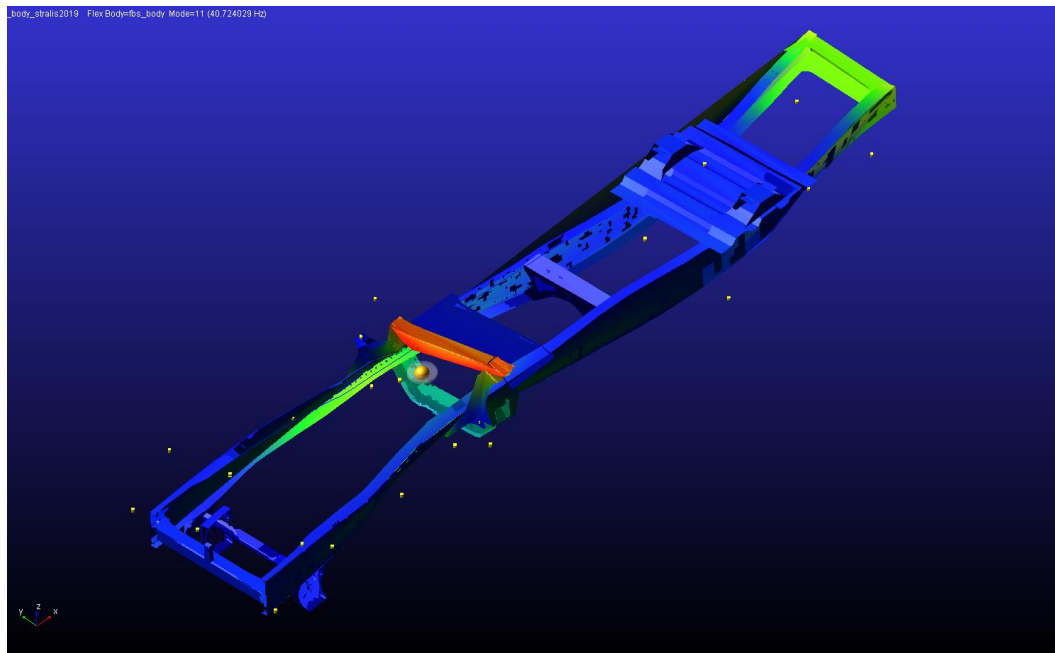
Pic. 2.37 – Second shape mode of the frame (ADAMS/CAR)

The second shape mode, plotted in Pic. 2.38, is a flessional one and it is around the z-axis: its natural frequency is between 10 and 20 Hz.



Pic. 2.38 – Third shape mode of the frame (ADAMS/CAR)

The third shape mode, plotted in Pic. 2.39, is a flessional one and it is around the y-axis: its natural frequency is between 30 and 40 Hz.



Pic. 2.39 - Fourth shape mode of the frame (ADAMS/CAR)

The fourth shape mode, plotted in Pic. 2.40, is a shearing one and it is in the xy-plane: its natural frequency is between 30 and 40 Hz.

The further shape mode are still flessional, torsional, shearing or a combination of them but they refer to higher natural frequencies and so they affect less mass of the system: this is the reason why it was decided to cut the number of the shape modes not considering all of them.

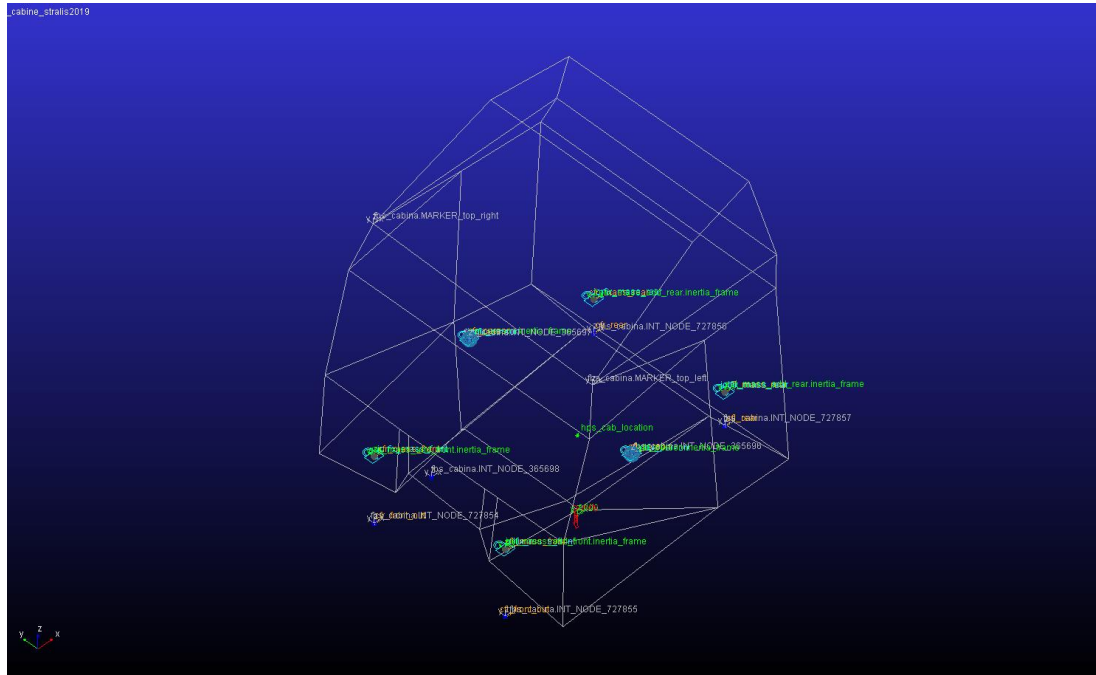
2.5.2 Cabine

The second *template* which is useful to make flexible in order to achieve better results is surely the cabine. A *template* containing a flexible cabine was already available since it had been just created to perform comfort studies on the Stralis my2019.

The same procedure discussed in Paragraph 2.5.1 was followed. This *template* contains eight *Interface Parts* since both the front and the rear cabine suspensions own four attachment each.

In the cabine *template*, two *General Parts*, fixed to the flexible body, were included in order to simulate two people. All the *Output Comuniators* were renamend to make the model consistent and a new one, corresponding to the attachment of the steering wheel, was created.

The resulting *template* was reported below.



Pic. 2.40 – Cabine template (ADAMS/CAR)

Note that the first two natural frequencies of the cabine are under 10 Hz while the third and the fourth ones are between 10 and 20 Hz.

2.6 Front and Rear Cabine Suspensions

The front and the rear cabine suspensions were already available since they were collected from the same database which contained the cabine *template*.

The discussion starts from the front element. The front cabine suspension is substantially composed by a couple of shock absorbers and air springs, included in a single body each, linked to two arms. The arms are connected each other thanks to a torsional bar fixed on them. The connections to the chassis are at the lower ends of the shock absorbers and at the rear ends of the arms while the link to the cabine takes place in the middle of each arm. All the joints in the *template*, except for the bar ones, are spherical and can be replaced by bushings in the dynamic mode.

The equations used to describe the tire performances have a specific structure, i.e. they are based on some coefficients obtained by experimental tests. The Magic Formula of Pacejka was updated over the years and has taken more and more variables in order to describe more carefully the tire. The original formula is able to get the longitudinal force F_x , the lateral force F_y and the moments of self-alignment M_z in function of the vertical load F_z , the longitudinal slip s , the drift angle α , the grip μ and the camber angle γ .

The simple formula is the *Pacejka 89*, which, thanks to a $\sin(\text{atg})$ function, compute F_x in function of s , F_y and M_z in function of α .

As example, the formula used to obtain the longitudinal force is reported below.

$$F_x = \mu_x (b_1 F_z^2 + b_2 F_z) \cdot \sin \left\{ b_0 \cdot \arctg \left[Bx - (b_6 F_z^2 + b_7 F_z + b_8) \cdot (Bx - \arctg Bx) \right] \right\} \quad (49)$$

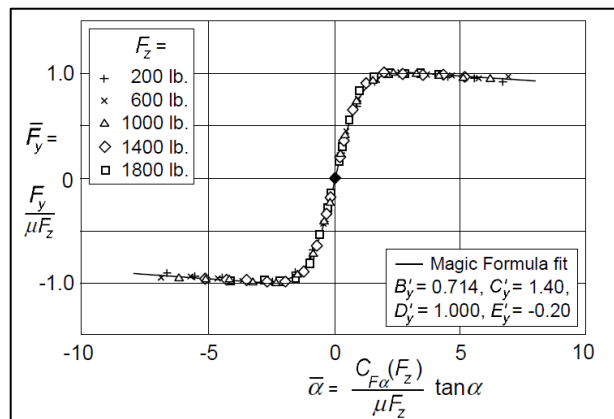
where

$$B = \frac{(b_3 F_z^2 + b_4 F_z) \cdot e^{-b_5 F_z}}{b_0 (b_1 F_z^2 + b_2 F_z)}$$

$$x = (100s + b_9 F_z + b_{10}) \quad (50)$$

The lateral force and the moment of self-alignment formulae have the same structure but different coefficients.

An example of trend which can be obtained by this approach was reported below.



Pic. 2.43 – Example of the lateral force trend in function of the drift angle ^[7]

The next versions of the formula consider the interaction among the longitudinal and the lateral forces in addition to other parameters.

Turning again to *Adams/Car*, as concerns the front, the rear and the semitrailer tires, the example *templates* were used like starting point. The *multibody* software gives the possibility to use a specific version of the Magic Formula according to the version of *Adams*.

In this case, since *Adams/Car 2015.1* was used to model the truck, Pacejka 5.2 Formula will be included. The tires constitute a specific *Part* in the template characterized by:

- a location and an orientation;
- a mass, sum of the tire and the rim;
- the moments of inertia I_z and $I_x = I_y$;
- a property file (*.tir*) containing the Pacejka coefficients and other features like the maximum value of the independent variables.

In this work, the Iveco Engineering Office provided the *.tir* files for the front and the rear tires at three different pressure levels, i.e. 7, 8, 9 bar. The property files corresponding to 8 bar were used in the simulation:

- Rear Tires: ContiEcoPlus/HD3M+S_Truck 315/70R225;
- Front Tires: ContiEcoPlus/HS3_Truck 385/55R225.

Note that the tires and the pressure levels used in the virtual simulations were the same of the real test ones. As regards the inertia properties, they were read from the Continental technical sheets and included in the model, while location and orientation were referred to a *construction frame* guided by *input communicators*.

Notice that the tire model adopted in this activity is particularly suitable in order to perform handling studies ($f < 4\text{Hz}$). Since the fact that the flexible bodies contemplate a wider frequency range, it is advisable in the future the using of other tire models which are normally used for comfort and durability test.

The *template* will be framed on the correct suspension during the assembling phase.

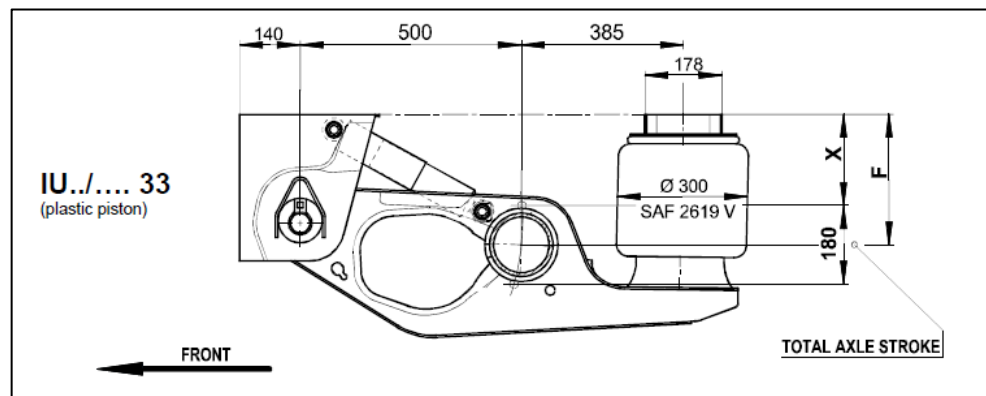
2.8 Semitrailer Subsystems

The semitrailer, together with its suspensions and its tires, is not an Iveco product, thus the majority of the data were obtained by the suppliers while other ones were assumed.

As starting point, *Adams/Car* example *template* was used.

2.8.1 Semitrailer Suspensions

A sketch of the semitrailer suspension was reported below.



Pic. 2.44 – 2D drawing of the semitrailer suspension

It consists of an axle hinged into two arms connected to the semitrailer frame by a couple of shock absorbers and air springs.

First of all, the position of the *harpoints* and so the lengths of the bodies were updated. As regards the inertia properties, which were unknown, they were computed by the software thanks to the geometry which was known and assuming steel as materials.

Since the air spring isobar diagram was available, the procedure described in paragraph 2.1 was followed again in order to achieve the Force-Displacement characteristic.

Concerning the shock absorbers, no info was available, thus the *Adams* default one was left.

Then, the default *Bumpstop* and *Reboundstop* were included.

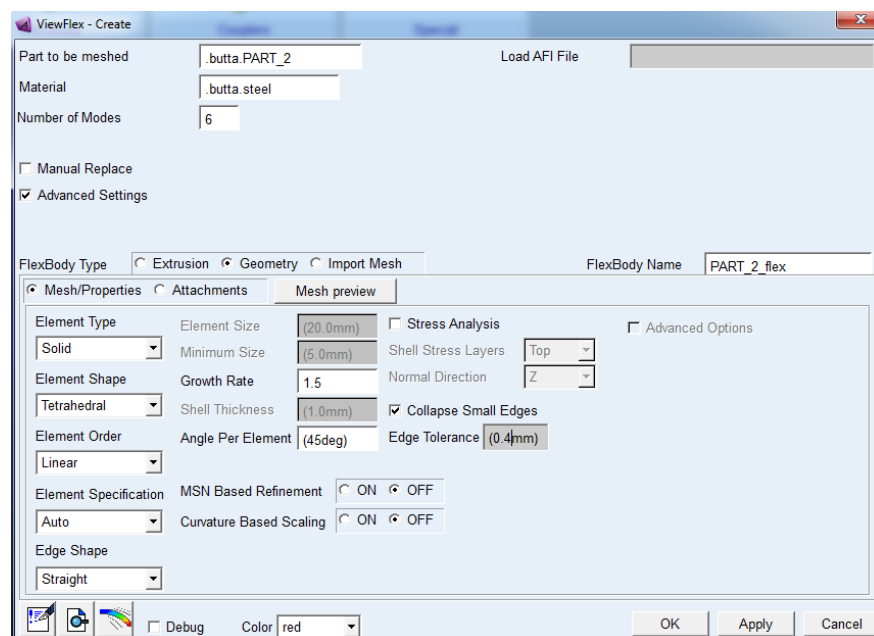
A crucial difference of the *template* under analysis compared to the example deals with the axle. It was decided to build a flexible one in *Adams/View* and then to import it in the *Adams/Car* model in order to give a certain degree of flexibility to the semitrailer.

This procedure will be now discussed.

As just said, *Adams/View* represents the generic multibody environment by *MSC* thanks to which any mechanical system can be modelled and tested.

Firstly two concentric cylinders of the same length L , corresponding were build, the first characterized by the d_{out} and the second by the d_{in} of the semitrailer axle. Thanks to one of the *boolean operators* the material referred to the inner cylinder was removed from the outer one. Then, four *harpoints* corresponding to the interface nodes, namely the two hubs and the two connections to the semitrailer arms were built.

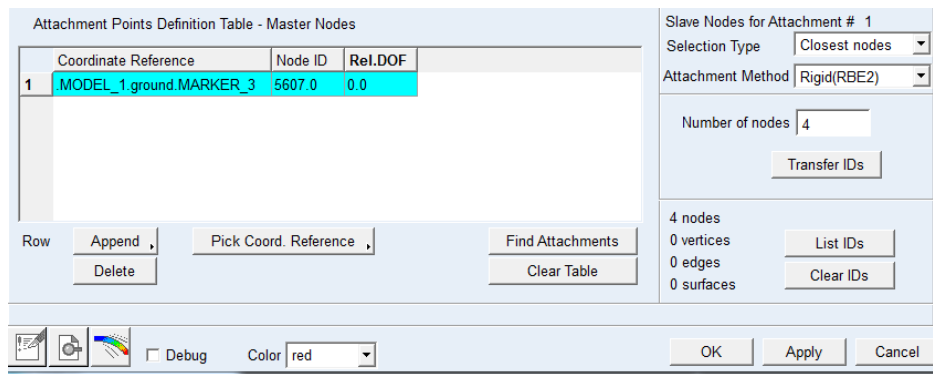
The aim of the following steps was to compute a Modal Analysis in order to obtain the *.mnf* file to include in *Adams/Car* model. First of all, the *View/Flex* panel was enabled and the *Advanced Settings* option was flagged.



Pic. 2.45 – Creation of the mesh (ADAMS/VIEW)

Firstly, it was defined the number of mode shapes to evaluate in the Modal Analysis; the default mesh parameters were left except for the *edge tolerance* in order to collapse the smallest edges of the triangles. Finally, a *mesh preview* was performed.

The last stage was to define the RBE2 entities corresponding to the attachments of the axles. As slave nodes of the hubs, the mesh nodes within a sphere of radius $d_{in} < R_1 < d_{out}$ were chosen, while as slave nodes of the semitrailer connections were the ones within a cylinder of radius $R_2 > d_{out}$ and length l , both centered on the corresponding master nodes.



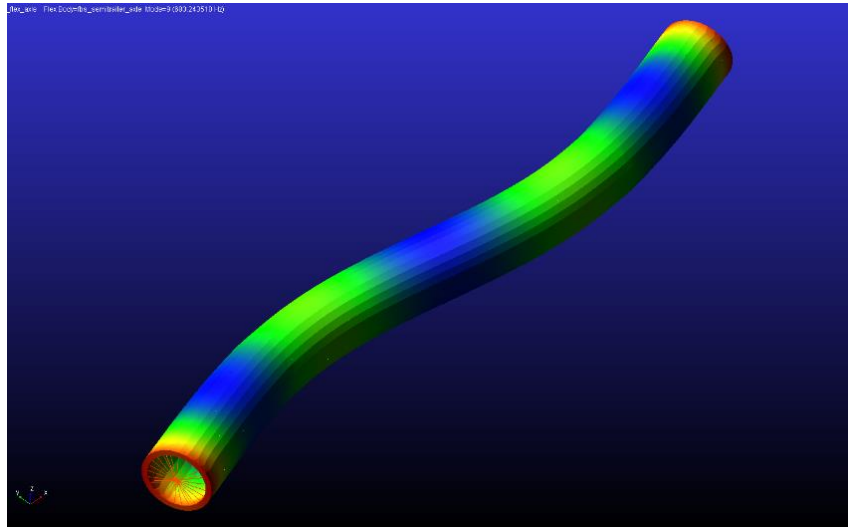
Pic. 2.46 – Definition of the master nodes (ADAMS/VIEW)

Thus, the modal analysis was launched, using the Craig-Bampton Method as for the Mode Synthesis.

The result was the *.mnf* file which was included in the semitrailer suspension *template*.

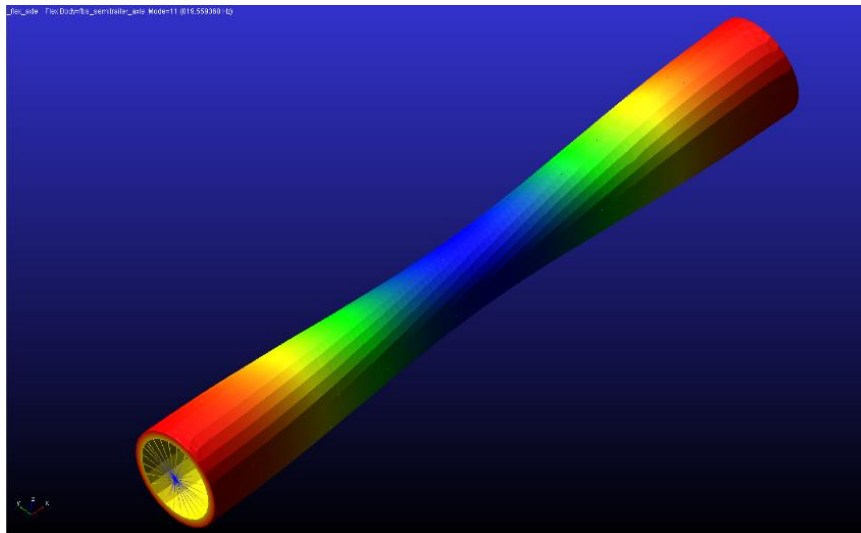
Therefore, the flexible body was placed in the correct position and orientation.

The first two shape modes, plotted in Pic. 2.49, are flessional: their natural frequency is over 250 Hz.



Pic. 2.49 - Third and fourth shape modes of the axle (ADAMS/CAR)

The third and the fourth shape modes, plotted in Pic. 2.50, are still flessional: their natural frequency is over 600 Hz.



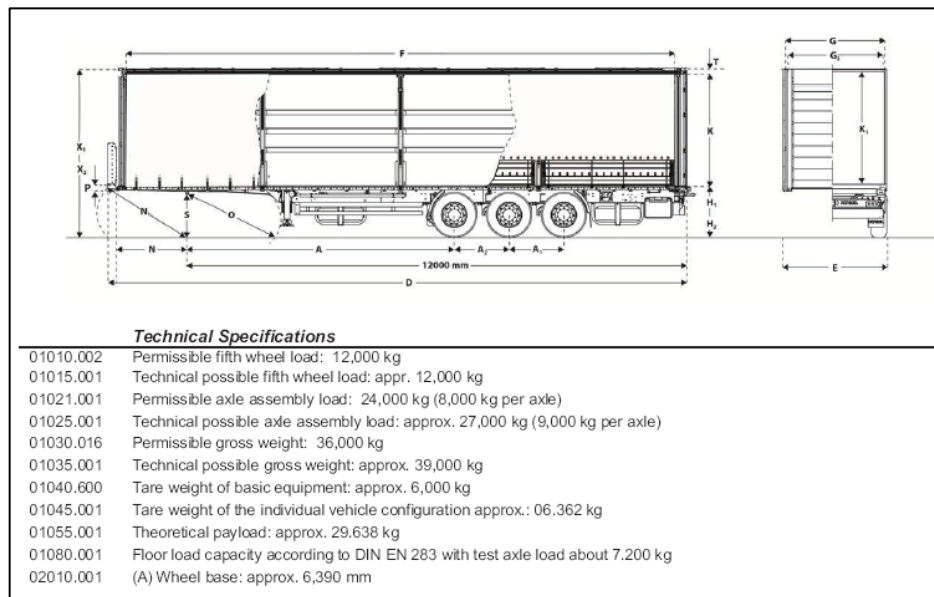
Pic. 2.50 - Fifth shape mode of the axle (ADAMS/CAR)

The fifth shape mode, plotted in Pic. 2.51, is torsional: its natural frequency is almost 1200 Hz.

2.8.2 Semitrailer

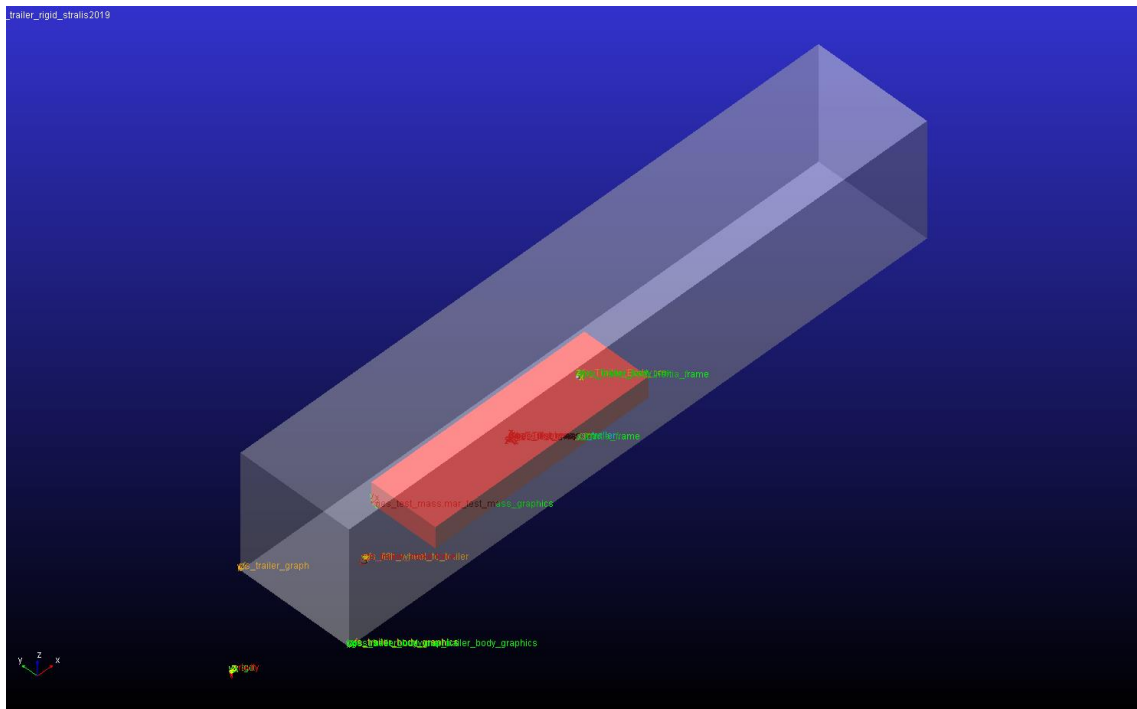
The semitrailer probably constituted the most important unknown of the problem since limited data were available: fortunately, the trailers of the commercial vehicles are standardised and some info are in common. It was decided to consider the full load configuration: if tests using the unladen configuration will be required, it will need to set the mass and the moments of inertia of the load to zero.

Firstly, commercial technical sheets were collected, like the following picture.



Pic. 2.51– Semitrailer drawing and technical Specifications

Thanks to these specifications, the mass of the semitrailer (the tare) and the maximum payload, the main lengths and the location of the suspensions were read. It remained to determine the center of the mass and the main moments of inertia both as regards the semitrailer and the test mass.



Pic. 2.52 – Semitrailer subsystem (ADAMS/CAR)

Note that, even if, the two bodies were graphically sketched as parallelepipeds, the masses are concentrated in a single point and they are not distributed.

In order to evaluate the inertia properties, two 3D *Catia* model were built.

As concerns the semitrailer, it was represented as an hollow solid: all the walls were characterized by the thickness s_1 except for the lower one, characterized by $s_2 \gg s_1$ in order to concentrate more mass where the semitrailer frame is located. Notice that the thickness values were assumed; thus, iteratively, the density of the body was changed until the real value of mass was found. The info, which were looked for, were read and included in the *Adams/Car* model. As for the modelling of the test mass, the sought-after density was the one who determines the maximum payload. The missing data were finally included in the *template*.

The mass was set, on the first attempt, at an height equal to one-third the available height inside the semitrailer.

The *template* was completed by the introduction of a bushing which stands for the fifth wheel: it was locked on the correct point of the semitrailer and referred to the fifth wheel *Interface*

Node of the frame by an *Input Communicator* in order to have the right location of the bodies in the final assembly.

As to the semitrailer tires, the one used at the front of the tractor were implemented.

2.9 Generation of the Assemblies and debugging

This phase is strongly preparatory to the simulation one since any mistake in the model has to be found and corrected.

Turning in *Standard Interface* mode, first of all, the *templates* were converted in *Subsystems*. Note that, some *Subsystems*, like the semitrailer suspension ones, were based on the same *template* but own a different *Adams Minore Role*, which distinguishes one from an other: it was necessary to define the correct location of each by the *Shift* command. Other *Subsystems* automatically took this info thanks to the *location input communicator*.

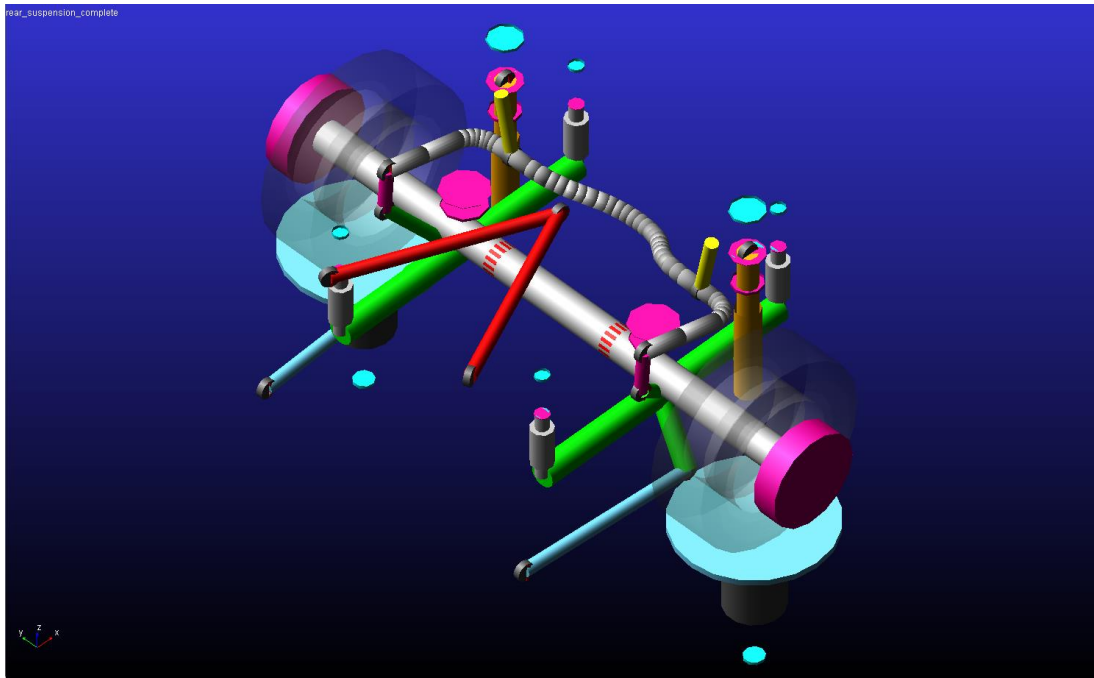
The simplest Suspension Assembly at the front and at the rear was set up and debugged.

As just said in paragraph 2.1, the helycal springs were replaced by the air springs.

The debugging phase consisted of some *Suspension Tests*, both in *Dynamic* and *Kinematic* mode, like the *Parallel Wheel* or the *Opposite Wheel Travel* in order to verify the correct behaviour of the several entities.

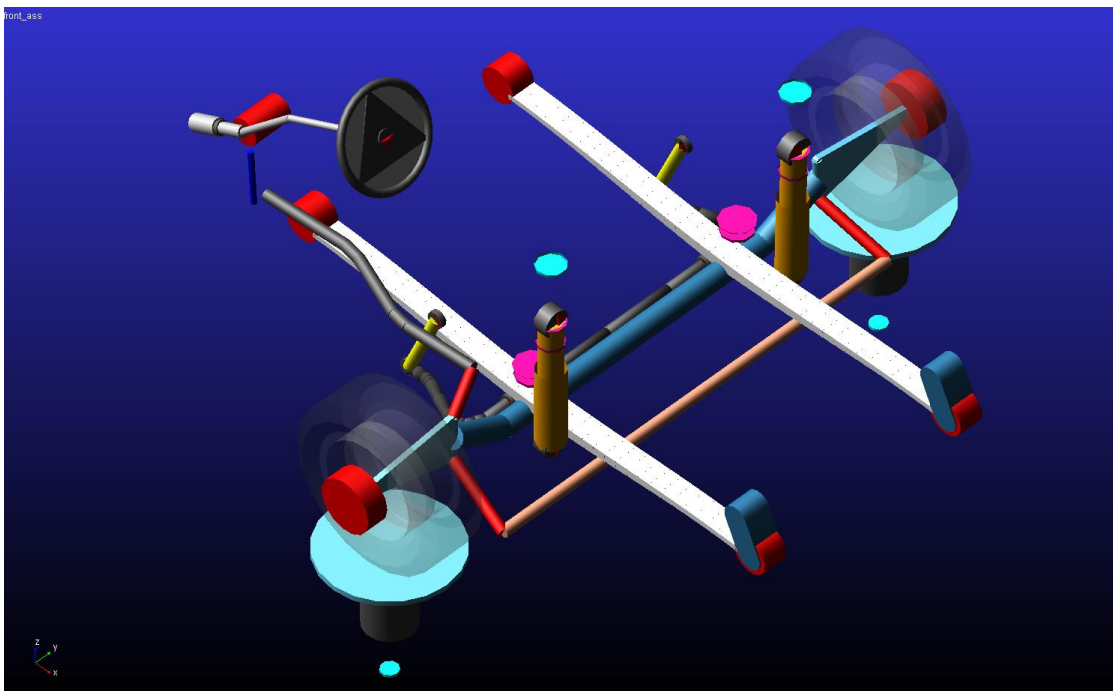
In this stage, each *Input Communicator* which did not found the corresponding *output* one was automatically hooked on the *ground*.

Then, more and more *Subsystems* were added to the original one and the procedure was iterated.



Pic. 2.53 – Rear Suspension Assembly (ADAMS/CAR)

In figure 2.54 a *Suspension Assembly* composed by the rear suspension and the rear anti-roll bar *Subsystems* was reported.

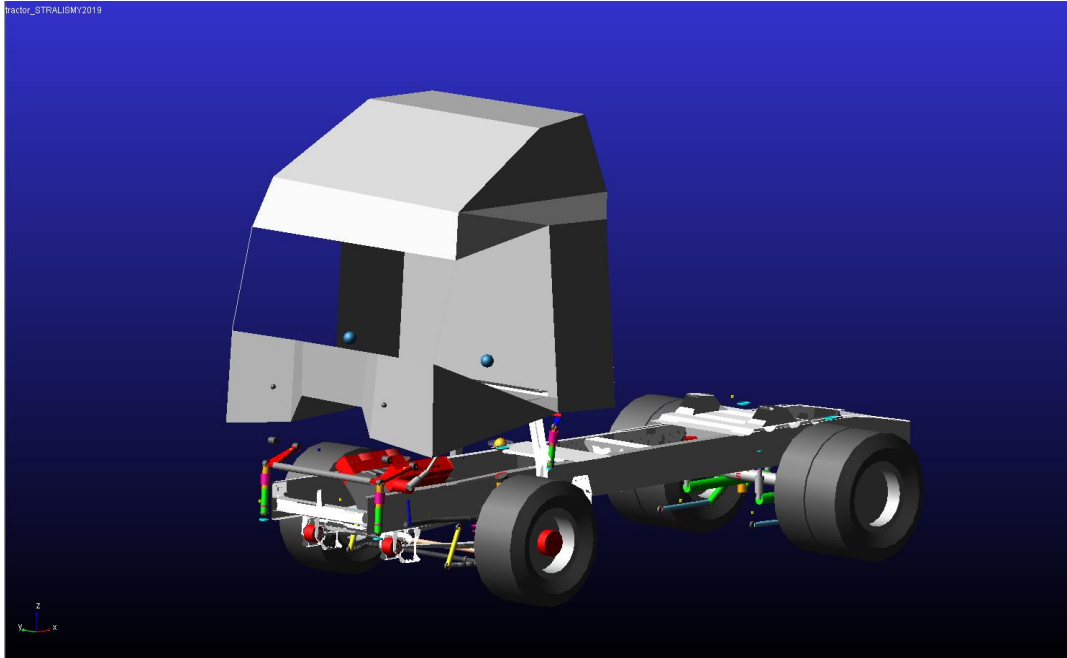


Pic. 2.54 – Front Suspension Assembly (ADAMS/CAR)

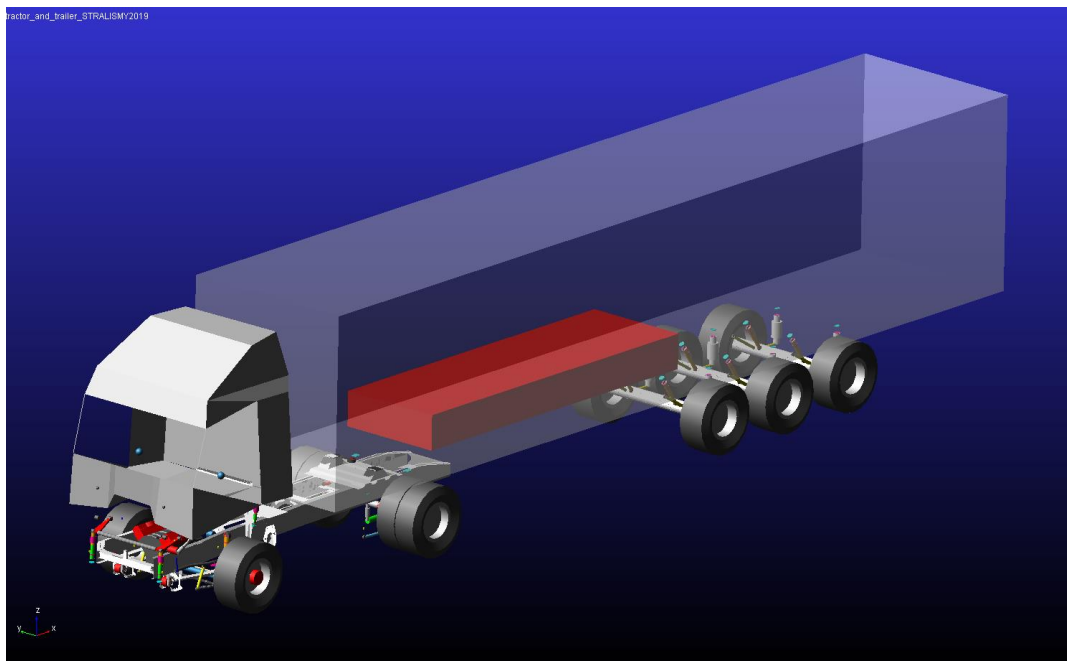
Picture 2.55 represents the collection of the steering-system, the leaf springs, the front suspension and the front anti-roll bar *Subsystems*.

Final modelling step consisted of the creation of two *Full-Vehicle Assemblies*, i.e. the tractor and the the entire vehicle composed by the tractor and the semitrailer.

The checking phases was performed thanks to simple manoeuvres like the *Strict-Line Forward* one, mantaing constant the velocity, and some *Step Steers*.



Pic. 2.55 – Tractor Assembly (ADAMS/CAR)



Pic. 2.56 – Full Truck Assembly (ADAMS/CAR)

As for the entire vehicle, it was required to iteratively translate the test mass forward and backward in order to achieve the load distribution on the semitrailer axles and the fifth wheel at drawing. Final the total mass of the tractor, of the semitrailer and of the entire vehicle was checked and compared to the design one since some values have been computed by *Adams/Car* from the geometry.

CHAPTER 3. SIMULATIONS

In the following Chapter, firstly the definition of the solver settings and their influence on the simulations will be described, secondly more details dealing with the manoeuvres performed will be given with reference to ISO standard; finally the simulation parameters both as for the tractor and the full truck will be summarized.

Preparatory to the simulation phase, it was required to modify some of the solver settings in order to achieve a good quality in the results and to prevent errors which did not eventually bring to the simulation success. The attention will be focused only on the modified ones while the others will be left at the default value.

As for the Dynamic Settings, the I3 GSTIFF INTEGRATOR was used since it is considered the most robust and efficient formulation in *Adams*. The step-size HMAX was made constant and equal to $5 \cdot 10^{-3}$ [s] in order not to skip very short events. Moreover, the default HMAX is variable and automatically computed by the Solver and this can eventually bring to spikes in the results. The ERROR, whose formula is closely depending on the kind of INTEGRATOR, defines the accuracy of the results: it was set to $5 \cdot 10^{-3}$.

Note that this two settings directly influence the time simulation: a good compromise between resonable results and time computation is advisable.

As said in Chapter 1, the Static Analysis precedes any kind of Dynamic Simulations. Since the model is composed by some flexible bodies and owns more than four wheels, the starting equilibrium configuration turns out to be challenging to find. Firstly, the STATIC approach was chosen; then, the maximum number of the Newton-Rapson iteration, named MAXIT, was increased to 500 from the default value of 20.

Finally, as to the Output Settings, the Graphics and the Request Files were flagged.

3.1 Open-loop test methods

As concerns the manoeuvres, firstly, the steady-state circular tests will be described: the reference norm is the ISO 4138:2004 ^[8], which provides the methods in order to characterize the steady-state circular driving behaviour of a road vehicle. Three main tests belonging to this category exist: the constant-radius, the constant steering-wheel angle and the constant-speed. In this set of tests the main variables consists of the speed, the steering-wheel angle and the turn radius: in each manoeuvre, one variable is hold constant, an other one is varied and the last is measured or calculated.

The following results have to be measured too:

- longitudinal velocity v_x ;
- lateral acceleration a_y ;
- steering-wheel angle δ_H ;
- yaw rate $\dot{\psi}$;
- sideslip angle β and lateral velocity v_y ;
- roll θ and pith φ angle.

Appropriate transducers in real tests and correct requests in virtual simulations have to be installated on the vehicle in order to record this data on the time base.

In this work, the Constant Speed test (Method 3) was performed: it consists of driving the vehicle under analysis at a defined speed (the standard one is 100 km/h but it can be higher or lower in 20 km/h increments) on a circular path of different radii thanks to a range of steering-wheel angles. This test can be performed with discrete or continous steering-wheel angle transition: in this case, the continous method was used which is commonly called *Ramp Steer*. The test starts bringing the vehicle to the desired speed; then the steering input is applied and constantly increased in time: note that the throttle has to be controlled since the speed has to be

hold constant. The manoeuvre ends when a test limit condition is achieved, i.e. the lateral acceleration or the stability of the vehicle.

The lateral behaviour is determined plotting the results in function of the lateral acceleration.

The attention was shifted thereafter on the lateral transient response test methods: the reference norm, as for this kind of manoeuvres, is the ISO 7401:2003 ^[9]. In this case results both in time and frequency domain are required in order to characterize the dynamic behaviour of the vehicle. It is advisable to carry out the tests at the minimum load (the mass of the driver and the instrumentation has not to exceed 150 kg) and at the maximum one (maximum authorized total mass). In this activity, only the tests at the maximum load condition were carried out. The first manoeuvre to be performed was the Step Input (generally called *Step Steer*). Firstly the vehicle is driven straight until the test speed; from the equilibrium condition, a steering input to a defined value is rapidly applied and maintained in order to measure the variables from the transient to the steady-state condition. The speed can decrease since no change in throttle position are carried out.

The last test was represented by the Continuous Sinusoidal Input (generally called Sweep Steer or Swept-Sine): at the predetermined steering-wheel angle value, sinusoidal steering-wheel inputs were applied. Even in this case, the throttle is hold constant. The frequency of the input can be increased in steps or, as in this case, continuously from an initial value of 0,2 Hz to 2 Hz; optionally, the upper frequency limit can be extended or reduced.

Note that, in this transient manoeuvres, the steering-wheel angle has to be determined performing a steady-state lateral test and reading the angle value at a defined lateral acceleration.

3.2 Manoeuvres

Both on the tractor and the full truck, a Ramp Steer, two Step Steer and two Swept-Sine Steer tests were performed.

The choice of the parameters will be described in paragraph 3.2.1 and 3.2.2.

As for the tractor simulations, two configurations were analyzed:

- the fully rigid vehicle;
- the vehicle in which the cabine and the frame are made flexible.

As for the full truck, the simulations were repeated in four different configurations:

- the fully rigid vehicle;
- the vehicle in which the cabine and the frame are flexible while the semitrailer axles are rigid;
- the vehicle in which the cabine and the frame are rigid while the semitrailer axles are flexible;
- the vehicle in which the cabine, the frame and the semitrailer axles are flexible.

Notice that all the tests start with an initial period, equal to 5 s, in which the vehicle goes straight holding the speed tests: this allow to achieve an equilibrium in the mechanical components at the beginning of the simulation: fluctuations in the results have not to be considered in this timeframe.

3.2.1 Tractor Simulations

First of all, a *Ramp Steer* simulation was performed; the parameters, reported below, were chosen according to ISO standard 4138.

Simulation parameters	Ramp Steer
Simulation Time	20 [s]
Starting Time	5 [s]
Number of Output Steps	400
Initial Velocity	60 [km/h]
Cruise Control	yes
Steering Input	angle
Steering Ramp	10 [°/s]
Quasi-Static Straight-Line Setup	yes

Tab. XI – Tractor Ramp Steer parameters

The *cruise control* was flagged in order to keep the velocity constant.

The *quasi-static straight-line setup* is useful to achieve the static steering-wheel configuration such that the vehicle go straight: the steering-wheel angle, defined in the parameter variable, was automatically summed to or subtract from this offset.

Secondly, two *Step Steer* tests were carried out, at two different steering-wheel angle, one twice the other. The steering-wheel angle were chosen in order to achieve steady-state lateral acceleration ranging from 0.2g to 0.4g.

Simulation parameters	Step Steer 1	Step steer 2
Simulation Time	30 [s]	30 [s]
Starting Time	5 [s]	5 [s]
Number of Output Steps	600	600
Initial Velocity	70 [km/h]	70 [km/h]
Cruise Control	no	no
Steering Input	angle	angle
Final Steering Angle	30 [°]	60 [°]
Step Duration	1 [s]	1 [s]
Quasi-Static Straight-Line Setup	yes	yes

Tab. XII – Tractor Step Steer parameters

Note that the *cruise control* was disabled since in this test it is the throttle to be kept constant. Finally two *Swept-Sine Steer* tests were carried out. Defined the velocity, which was the same of the *Ramp Steer* test, it was decided to investigate the frequency range between 0,2 Hz and 3 Hz by a rate of 0,1 Hz/s. The steering-wheel angle was chosen in such a way that the first lateral acceleration amplitude was respectively 0,15g as for the first test and 0,4g as for the second one. The angles of first attempt had been found plotting the steering-wheel angle against the lateral acceleration of the *Ramp Steer* test: knowing the lateral acceleration, the steering-wheel angle was read on the trend (20° and 49°). Since the *Ramp Steer* was a steady-state test (some input are kept constant like the velocity while other ones slowly change in time) and the *Swept-Sine Steer* was a very dynamic test, the steering-wheel angles which were found were not the correct ones: iteratively, some short *Swept-Sine Steer* were performed in order to find the angles which produce the specific lateral acceleration at the beginning (23 and 59,5°).

Consider that the rigid configuration was used like reference as for the choice of the angles.

Simulation parameters	Swept-Sine Steer 1	Swept-Sine Steer 2
Simulation Time	35 [s]	35 [s]
Starting Time	5 [s]	5 [s]
Number of Output Steps	750	750
Initial Velocity	60 [km/h]	60 [km/h]
Cruise Control	no	no
Steering Input	angle	angle
Steering Angle	23 [°]	59,5 [°]
Initial Frequency	0.2 [Hz]	0.2 [Hz]
Final Frequency	3 [Hz]	3 [Hz]
Frequency Rate	0.1 [Hz/s]	0.1 [Hz/s]
Quasi-Static Straight-Line Setup	yes	yes

Tab. XIII – Tractor Swept-Sine Steer parameters

3.2.2 Full Truck Simulations

The manoeuvres, previously described, were repeated using appropriate parameters on the vehicle composed by the tractor and the semitrailer. In this case the reference configuration was represented by the vehicle in which both the tractor and the semitrailer were made of rigid bodies.

Firstly a Ramp Steer test was performed.

Simulation parameters	Ramp Steer
Simulation Time	25 [s]
Starting Time	5 [s]
Number of Output Steps	500
Initial Velocity	60 [km/h]
Cruise Control	yes
Steering Input	angle
Steering Ramp	5 [°/s]
Quasi-Static Straight-Line Setup	yes

Tab. XIV – Full Truck Ramp Steer parameters

Notice that, the steering rate and the time simulation was reduced compared to the previous case since the vehicle is more unstable: nevertheless all the four simulations ended before the time limit because of the rollover of the vehicle, indicated by a specific *Adams* error.

Secondly, the Step Steer tests were carried out: it was decided to hold the velocity equal to 70 km/h and to reduce the steering-wheel angles.

Simulation parameters	Step steer 1	Step Steer 2
Simulation Time	30 [s]	30 [s]
Starting Time	5 [s]	5 [s]
Number of Output Steps	600	600
Initial Velocity	70 [km/h]	70 [km/h]
Cruise Control	no	no
Steering Input	angle	angle
Final Steering Angle	20 [°]	30 [°]
Step Duration	1 [s]	1 [s]
Quasi-Static Straight-Line Setup	yes	yes

Tab. XV – Full Truck Step Steer parameters

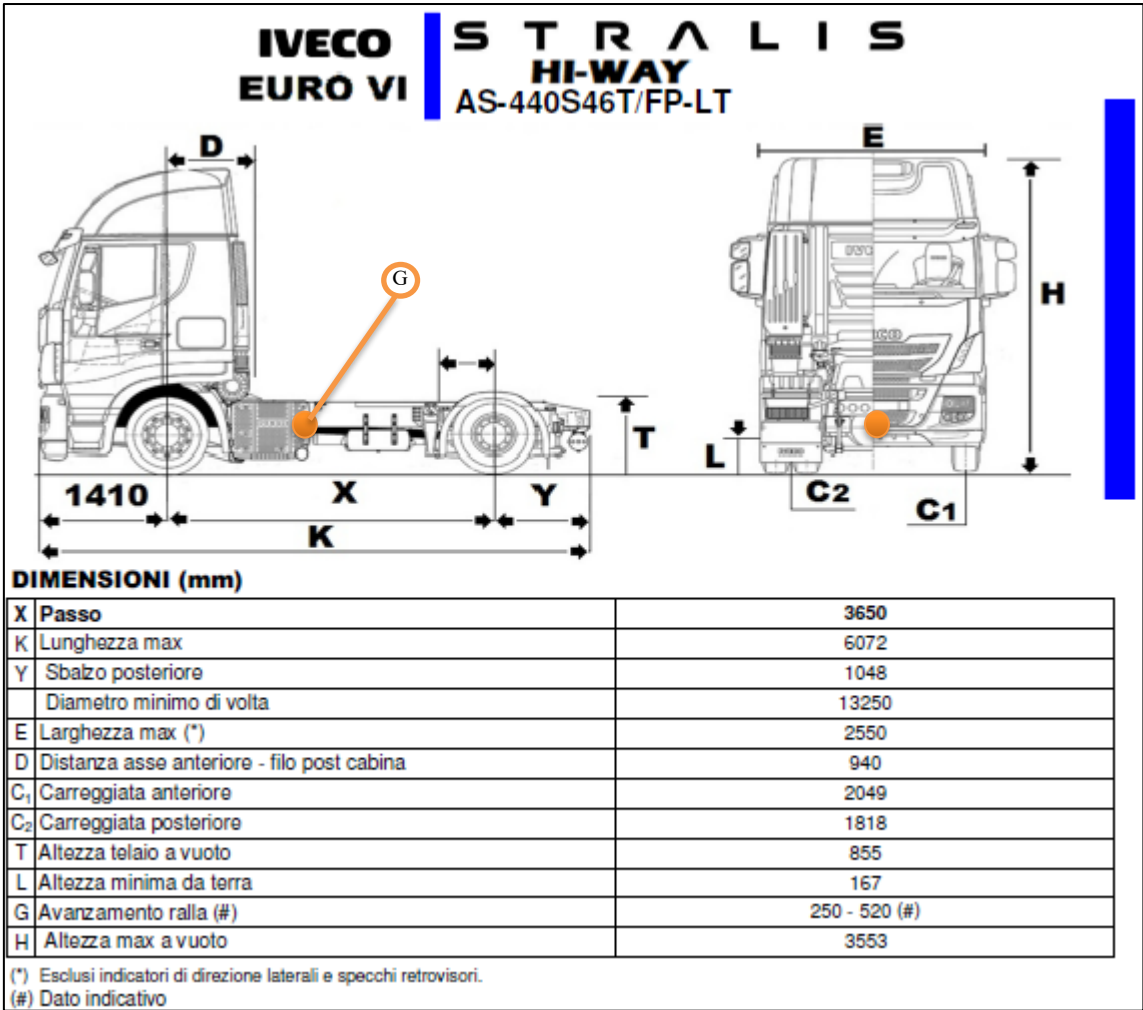
Finally the Swept-Sine Steer tests were performed: since the vehicle is more unstable, the steering-wheel angle value was researched in order to achieve 0,15g and 0,25g as the first lateral acceleration amplitude. The same procedure described in paragraph 3.2.1 was carried out.

Simulation parameters	Swept-Sine Steer 1	Swept-Sine Steer 2
Simulation Time	35 [s]	35 [s]
Starting Time	5 [s]	5 [s]
Number of Output Steps	750	750
Initial Velocity	60 [km/h]	60 [km/h]
Cruise Control	no	no
Steering Input	angle	angle
Steering Angle	25.5 [°]	42.5 [°]
Initial Frequency	0.2 [Hz]	0.2 [Hz]
Final Frequency	3 [Hz]	3 [Hz]
Frequency Rate	0.1 [Hz/s]	0.1 [Hz/s]
Quasi-Static Straight-Line Setup	yes	yes

Tab. XVI – Full Truck Swept-Sine Steer parameters

CHAPTER 4. POST-PROCESSING AND RESULTS

In this Chapter, the results are shown: particular emphasis is paid on the difference between the tests carried out using a vehicle composed by the flexible parts, discussed in Chapter 3, and the completely rigid model. It was decided to analyze the lateral acceleration a_y , the side-slip angle β , the yaw rate $\dot{\psi}$ and the roll angle θ : note that all these quantities were measured at the tractor frame center of mass which almost perfectly corresponds to the one of the entire tractor.



Pic. 4.1 - Geometrical characteristics of Iveco Stralis MY2019

The same point was used to read the *requests* even as for the full truck.

Firstly, a *Plot Configuration File* was created in the Post-Processing environment of *Adams/Car*: it consists of a generic collection of variables which the user is interested in.

Then, it was imported for each test in order to read the evolution of the variables in time in the same order and plot them on a single diagram; the trends were exported like tables (*.html*) and uploaded in Excel thereafter: for each test a *.xlsx* file was generated: it included as many spreadsheets as many vehicle configurations exist: for instance, any tractor and full truck test owns an Excel file respectively composed by two and four spreadsheets.

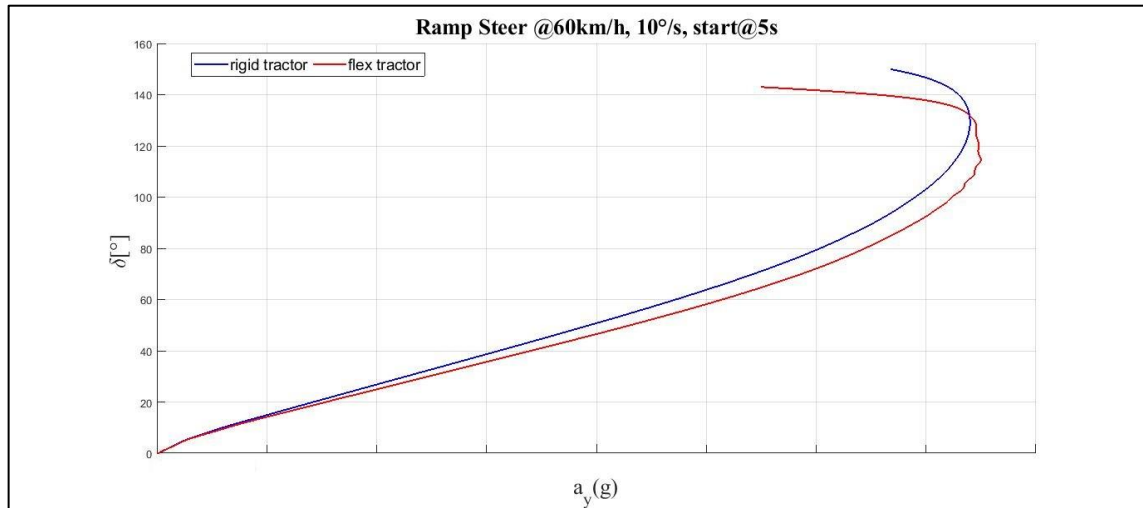
Finally, a *Matlab* script was written in order to read the Excel files and automatically generate the diagrams. Since the signals turned out to be affected by the solver techniques and showed several not physical oscillations, it was decided to use the *Matlab* low-pass filter ^[10]: the aim was to reduce the high frequency oscillations. Firstly it was defined the *order filter* (10) which represents the power of the filter to isolate the band in which the signal has to pass without being altered. Secondly, it was chosen the *cut-off frequency*, normalised for the signal frequency (0,3). The last step required before plotting the variables consisted of removing the static offsets due to the *request* definitions in *Adams/Car*.

According with the commercial and industrial secrecy, one axis of each diagram was hidden in order to keep the trends but not to allow to read a specific value; the same scale were used on the plots of the same variable in order to facilitate the comparison.

The results are divided in two paragraphs: they respectively deals with the manoeuvres performed on the tractor and the full truck; the diagrams are collected within this paper in order to compare the trends of the same variable obtained by the same kind of test in which different parameters were used.

4.1 Tractor Results

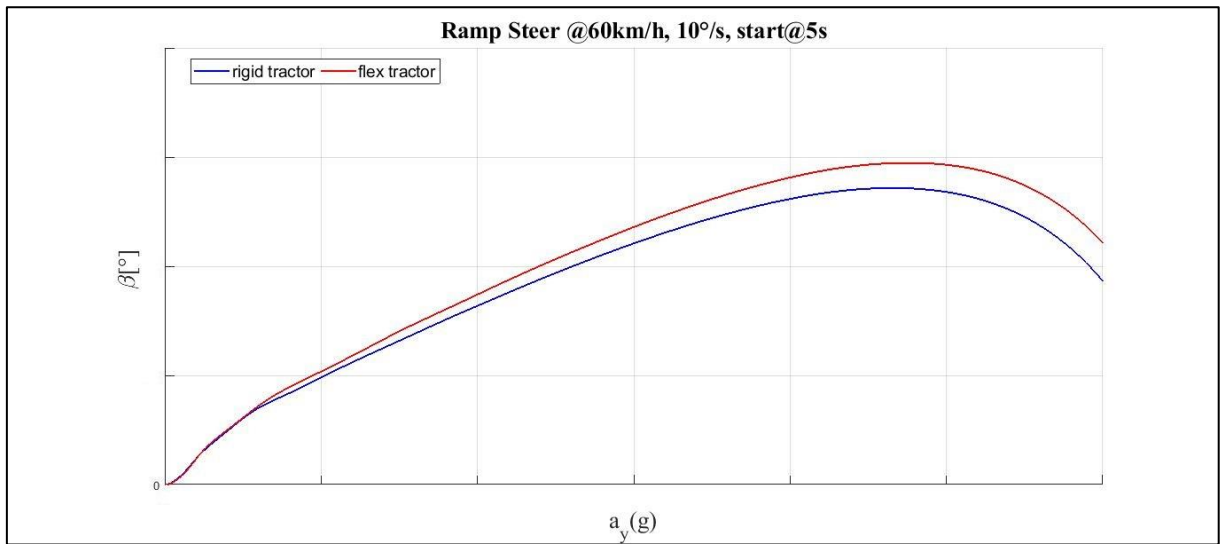
Firstly, the steering-wheel angle against the lateral acceleration obtained by the Ramp Steer test was plotted.



Pic. 4.2 – Tractor, Ramp Steer: steering-wheel angle against lateral acceleration (MATLAB)

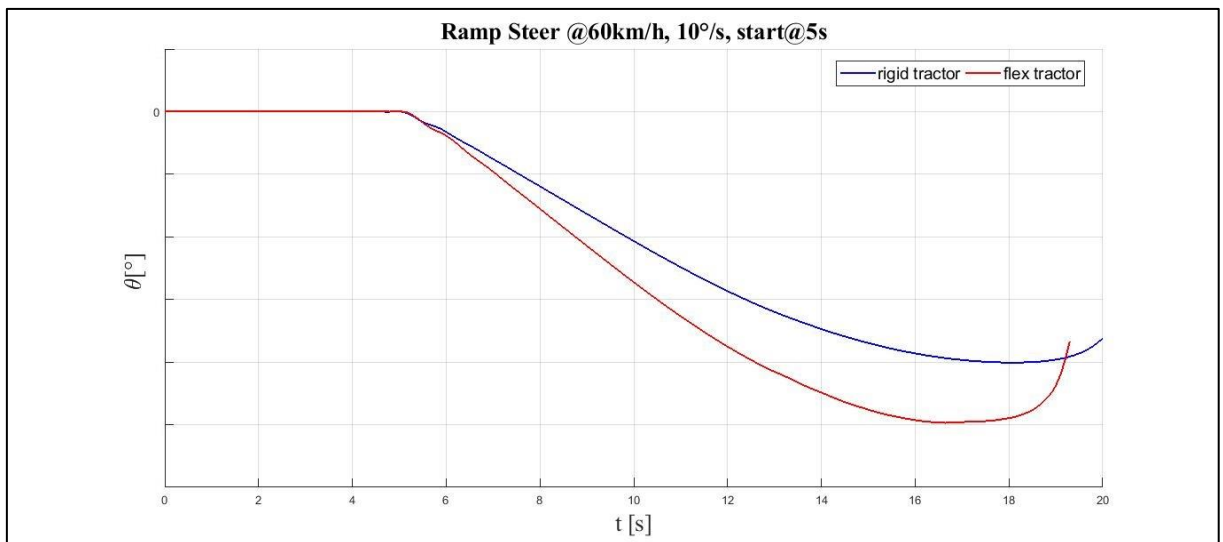
The difference between the two trends exists but it is not too much marked: the *flex tractor* can reach higher lateral accelerations for the same steering-wheel angles, which implies a more oversteering behaviour, but the loss of grip is less smooth.

The side-slip angle against the lateral acceleration and the roll angle in function of the time are reported below



Pic. 4.3 – Tractor, Ramp Steer: side-slip angle against lateral acceleration (MATLAB)

Note that the two trends differ over a certain lateral acceleration; for the same lateral acceleration the flex configuration reaches higher value of the side-slip angle.



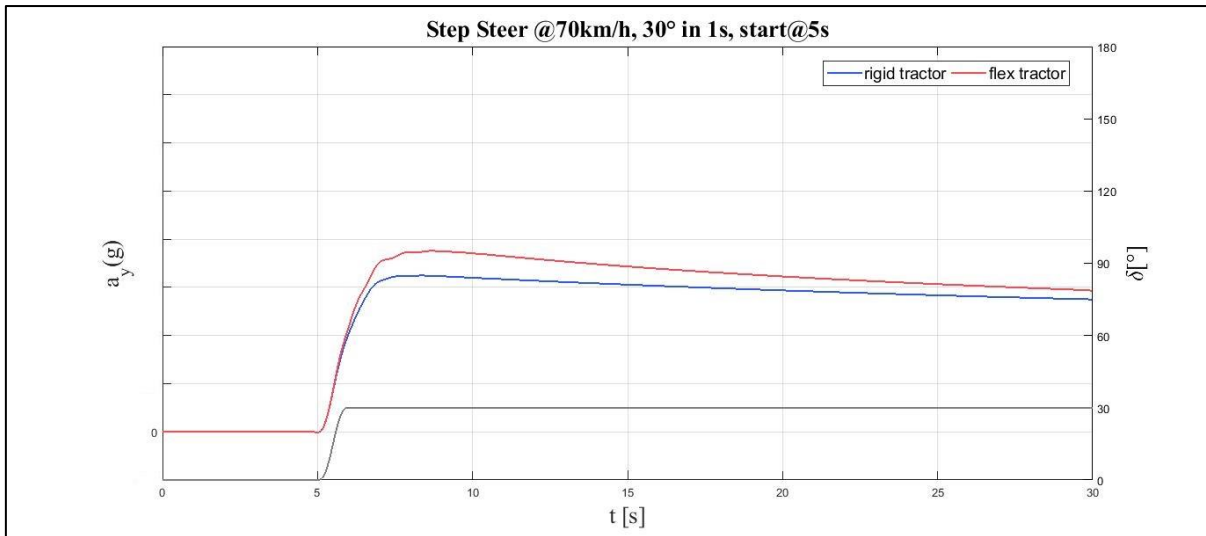
Pic. 4.4 – Tractor, Ramp Steer: time evolution of the roll angle (MATLAB)

From Pic. 4.4 it is evident that the test does not end with the rollover of the vehicle for both the configuration.

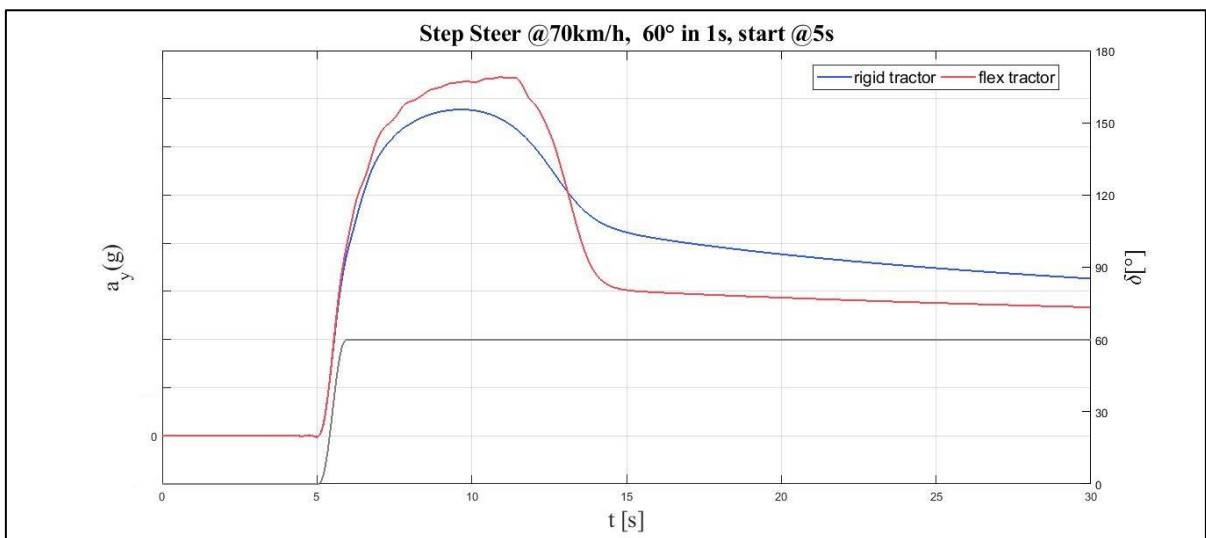
Secondly the results coming from the two Step Steers are described.

Note that the second Step Steer was more challenging than the first one.

The lateral acceleration trends are reported below.



Pic. 4.5 - Tractor, Step Steer1: time evolution of the lateral acceleration (MATLAB)

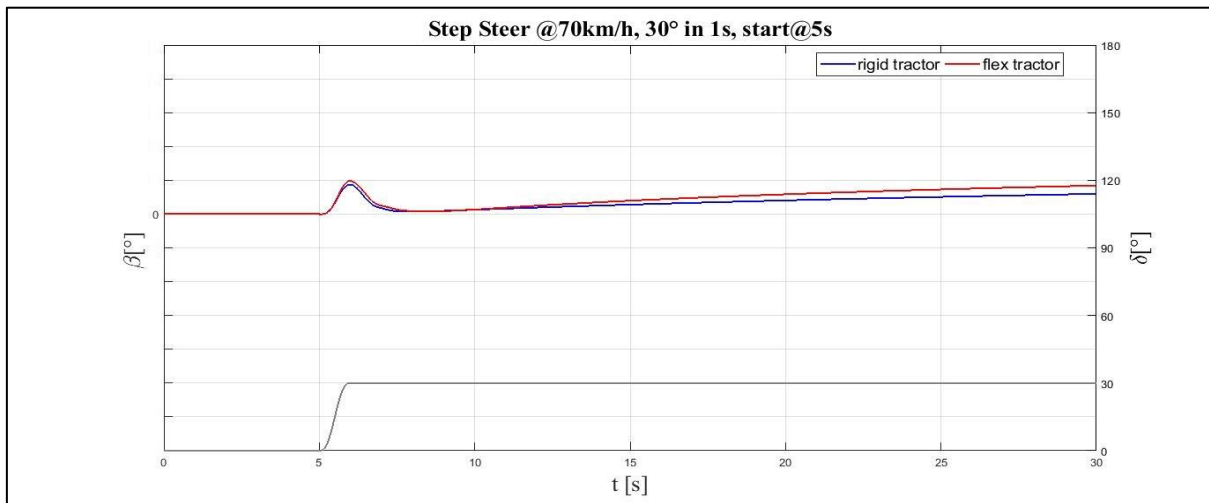


Pic. 4.6 - Tractor, Step Steer2: time evolution of the lateral acceleration (MATLAB)

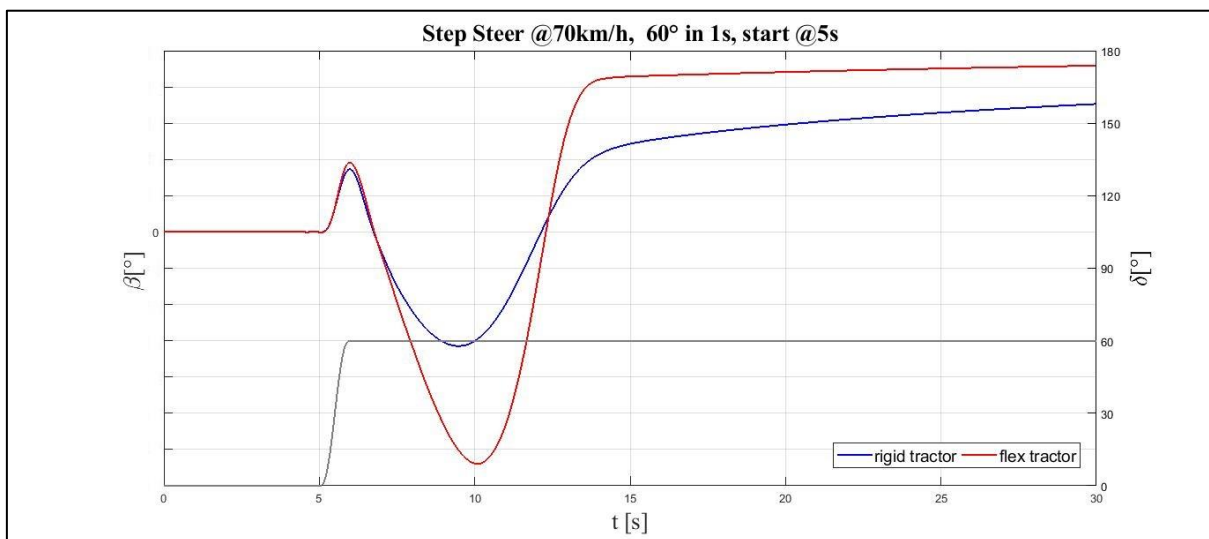
In the first test, the steady-state condition, which is higher in the flex configuration, was pretty fast achieved.

In the second test the higher steady state value corresponds to the rigid configuration even though the flex configuration achieves the higher peak value. The system seems to be overdamped; the difference between the two configurations is more evident in the second test.

The side-slip angle plots follow.



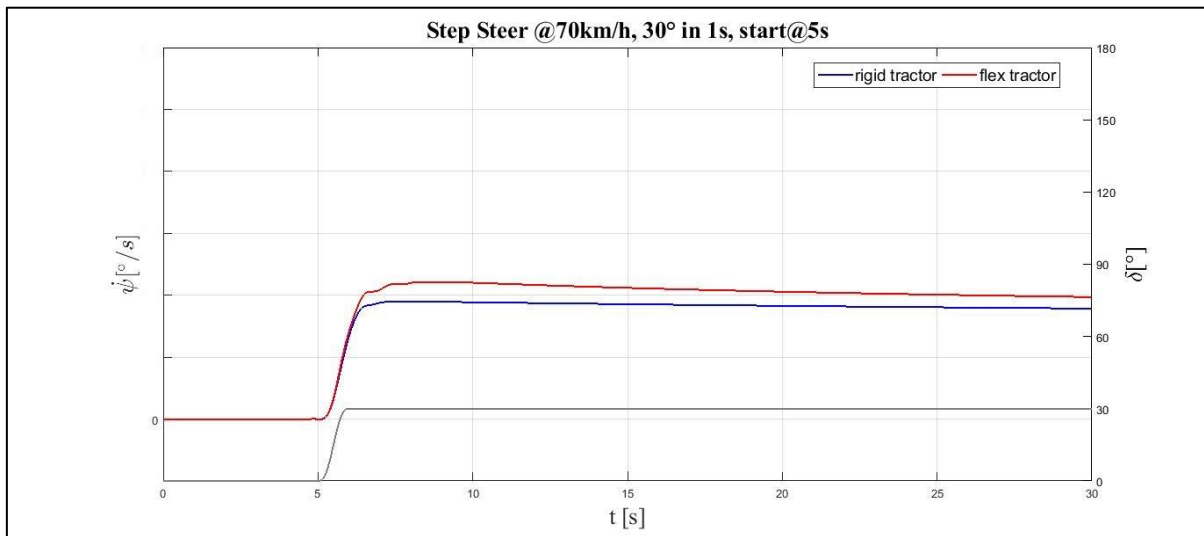
Pic. 4.7 - Tractor, Step Steer1: time evolution of the side-slip angle (MATLAB)



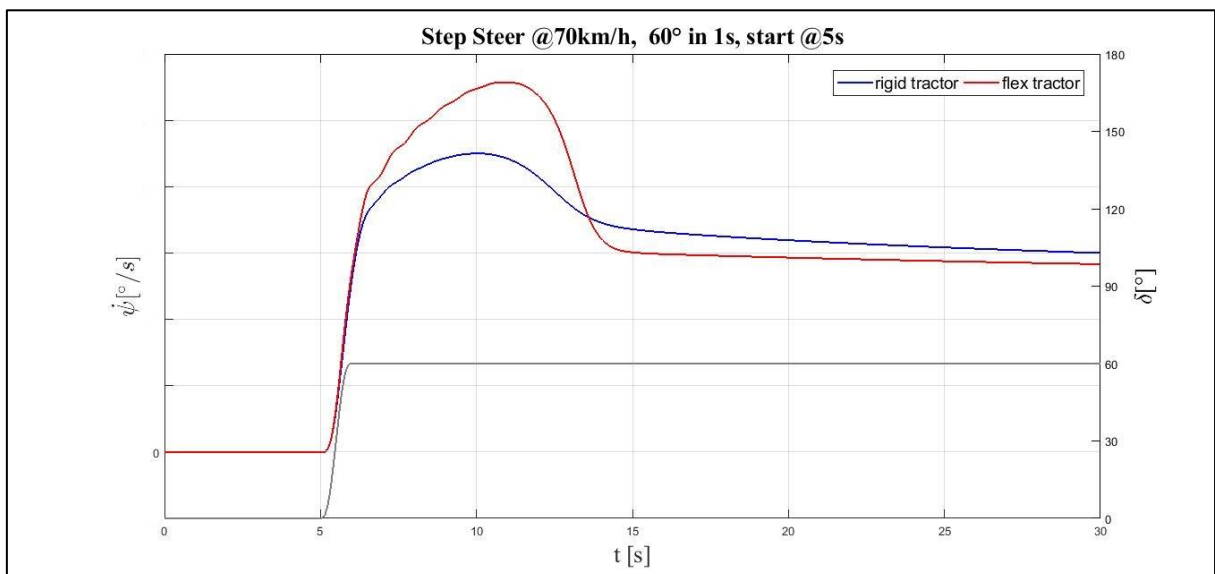
Pic. 4.8 - Tractor, Step Steer2: time evolution of the side-slip angle (MATLAB)

In both the tests, the flex configuration gets the higher peak and steady-state value. The trend are consistent with the the previous ones.

Then, the yaw rate trends are plotted.



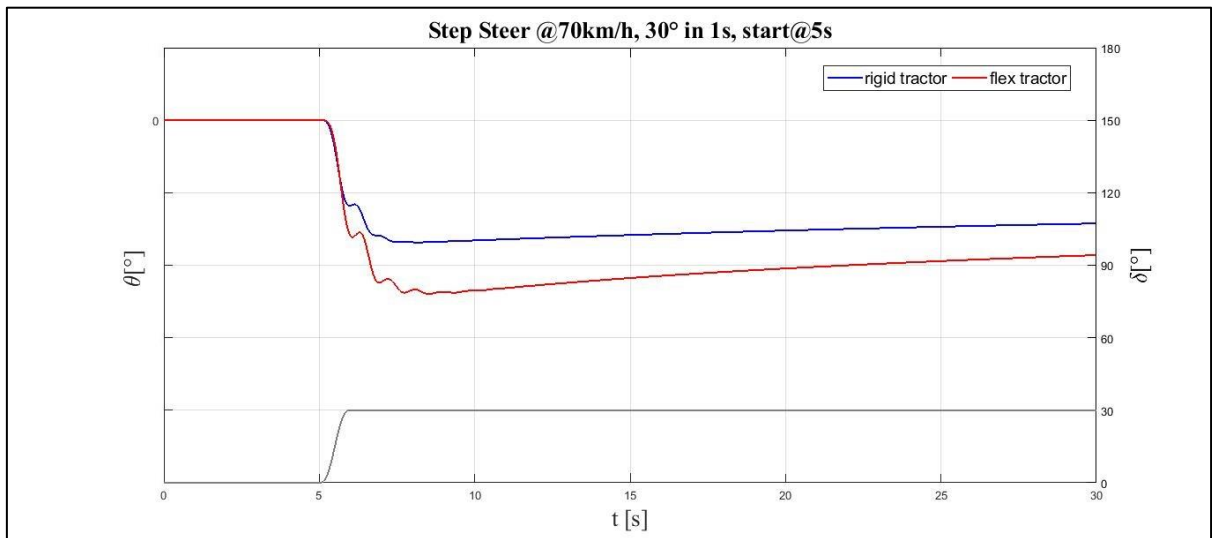
Pic. 4.9 - Tractor, Step Steer1: time evolution of the yaw rate (MATLAB)



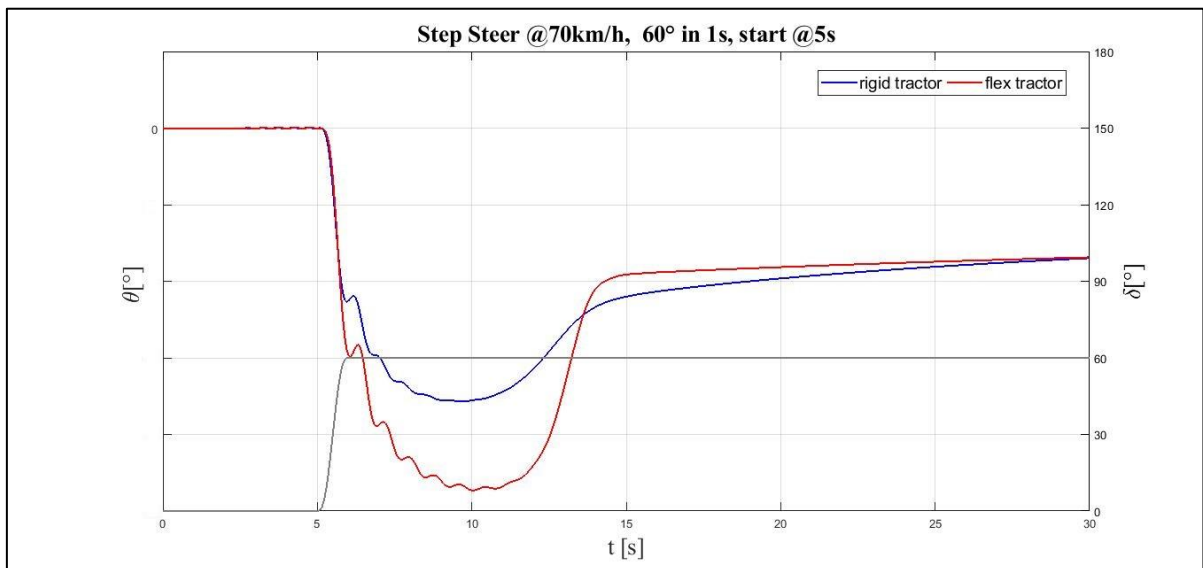
Pic. 4.10 - Tractor, Step Steer2: time evolution of the yaw rate (MATLAB)

The trends are quite similar to the lateral acceleration ones and it is coherent: the same comments are applicable even to this case.

Finally the roll angle charts are shown.



Pic. 4.11 - Tractor, Step Steer1: time evolution of the roll angle (MATLAB)



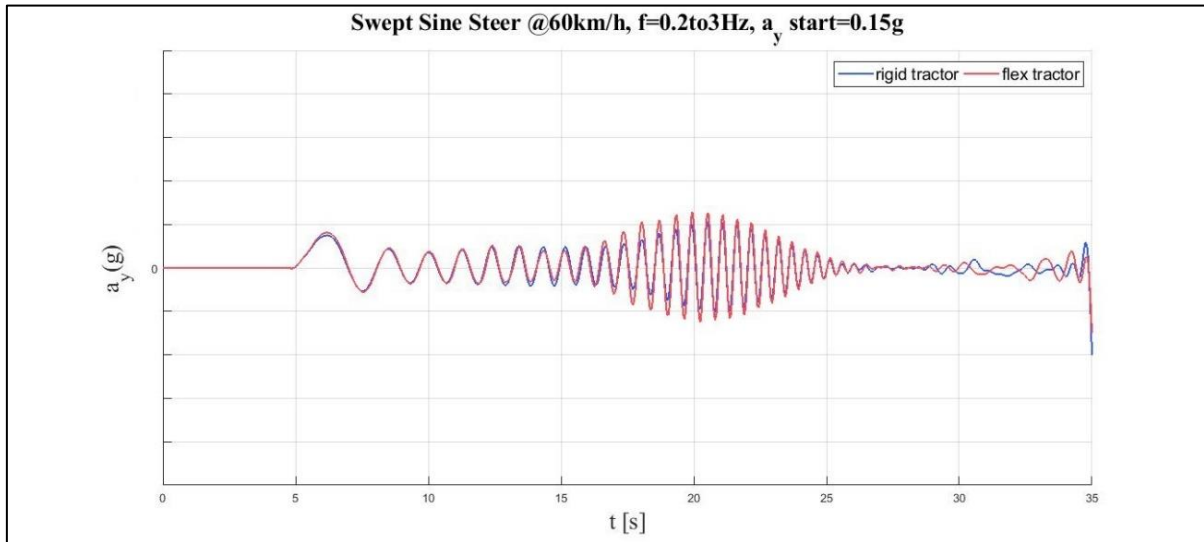
Pic. 4.12 - Tractor, Step Steer2: time evolution of the roll angle (MATLAB)

Even in this case, the peak value is higher for the flex configuration both in the first and in the second Step Steer test. Notice that, in the Pic. 4.12, the two splines move towards the same asymptotical value. It is evident from Pic. 4.11 and Pic. 4.12 that a more challenging steering-wheel angle turns the behaviour of the mechanical system from linear to non-linear, probably

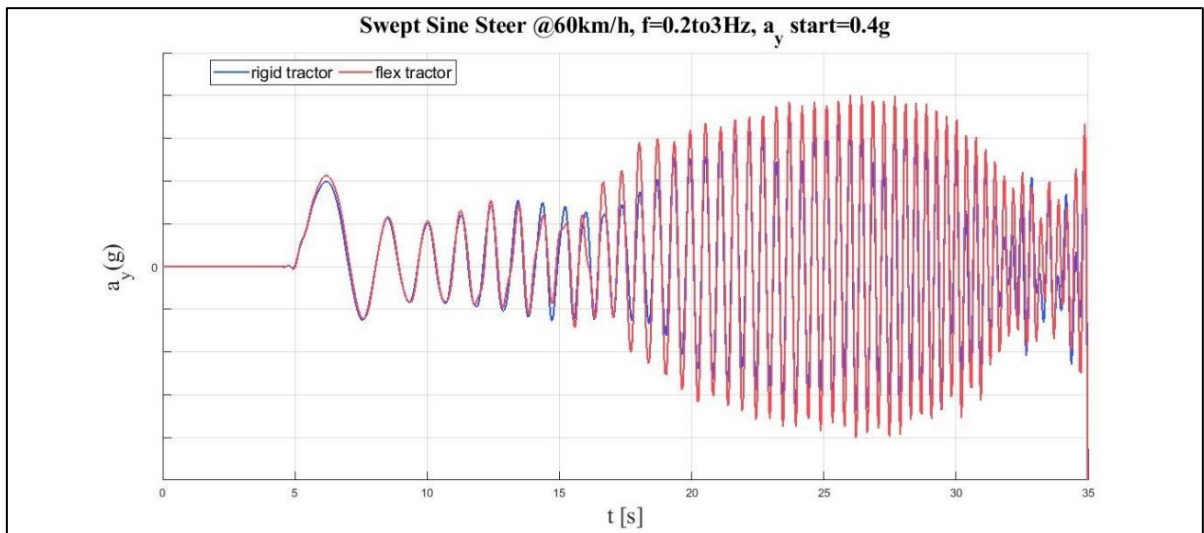
because of the contribution of the non-linear elements like the boundstop and the reboundstop of the suspensions.

Lastly, the results of the two Swept-Sine Steer manoeuvres are analyzed.

Firstly, the lateral acceleration charts are displayed.



Pic. 4.13 - Tractor, Sweep Steer1: time evolution of the lateral acceleration (MATLAB)

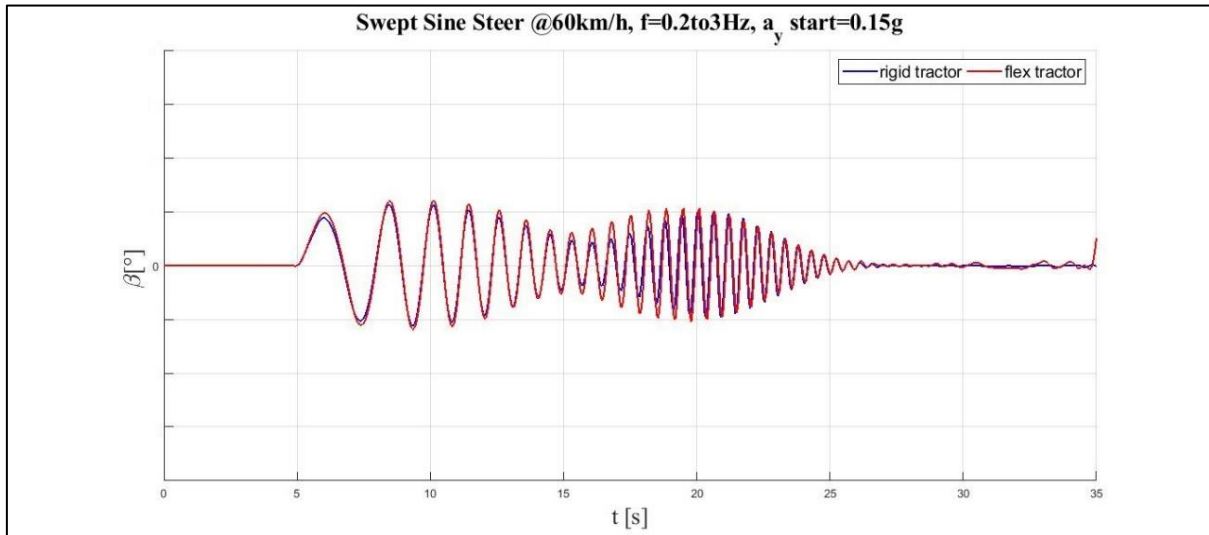


Pic. 4.14 - Tractor, Sweep Steer2: time evolution of the lateral acceleration (MATLAB)

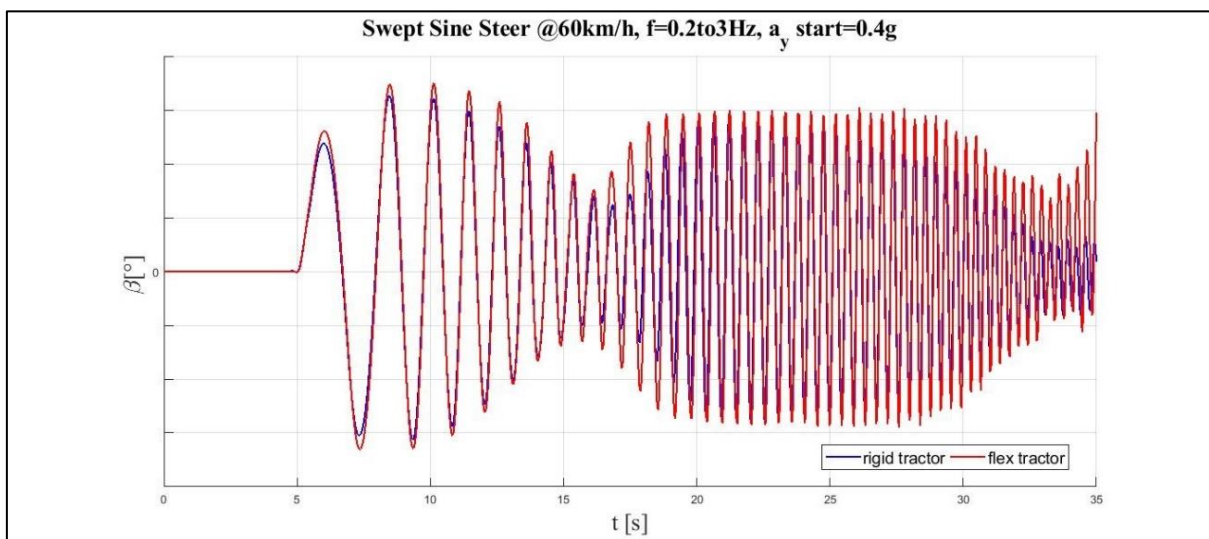
Both in the two test, the lateral acceleration owns a decreasing evolution from a starting high value, then it raises and decreases again. On average, the *flex tractor* always reaches higher

peaks than the rigid configuration and the difference is accentuated using a larger value of steering-wheel angle. Notice that at the low frequencies the dynamic behaviour of the two configurations almost perfectly corresponds while it diverges in the high frequency field.

The side-slip angle plots follow.



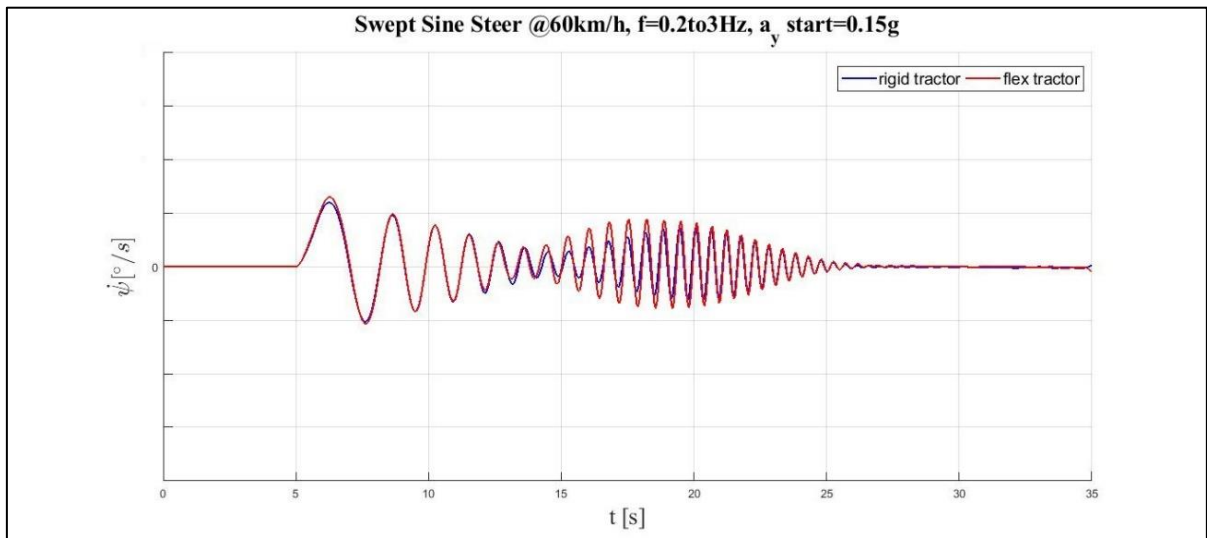
Pic. 4.15 - Tractor, Sweep Steer1: time evolution of the side-slip angle (MATLAB)



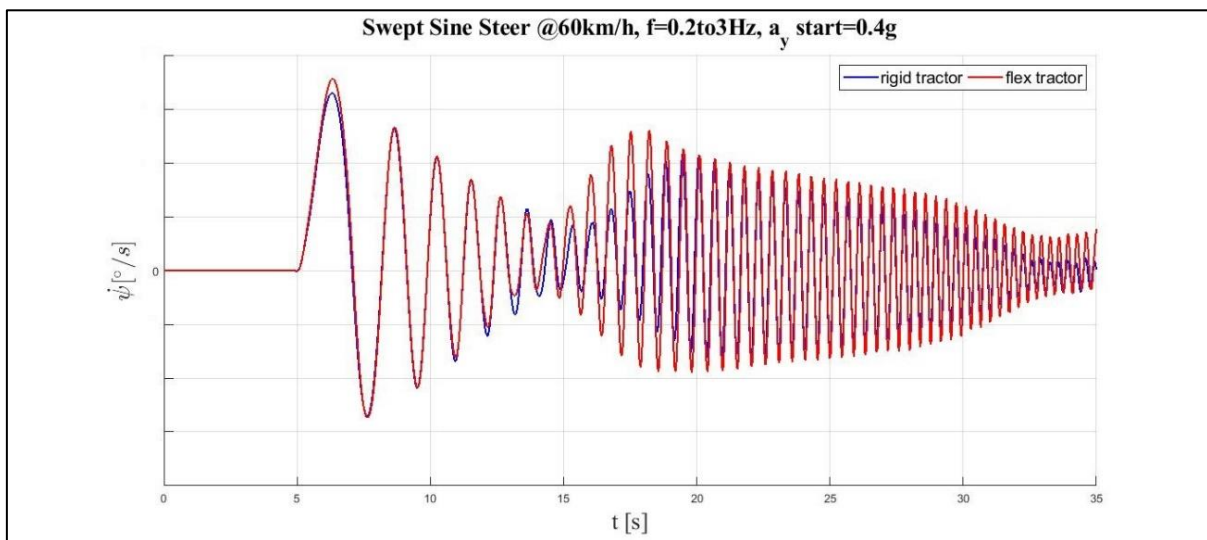
Pic. 4.16 - Tractor, Sweep Steer2: time evolution of the side-slip angle (MATLAB)

The comments previously discussed as regards the lateral acceleration are extended to the side-slip angle diagrams. Notice that, in the second test, the variable decreases much more around 1 Hz frequency while from the 1,5 Hz to 2,5 Hz is kept quite high and constant.

The yaw rate trends are shown below.



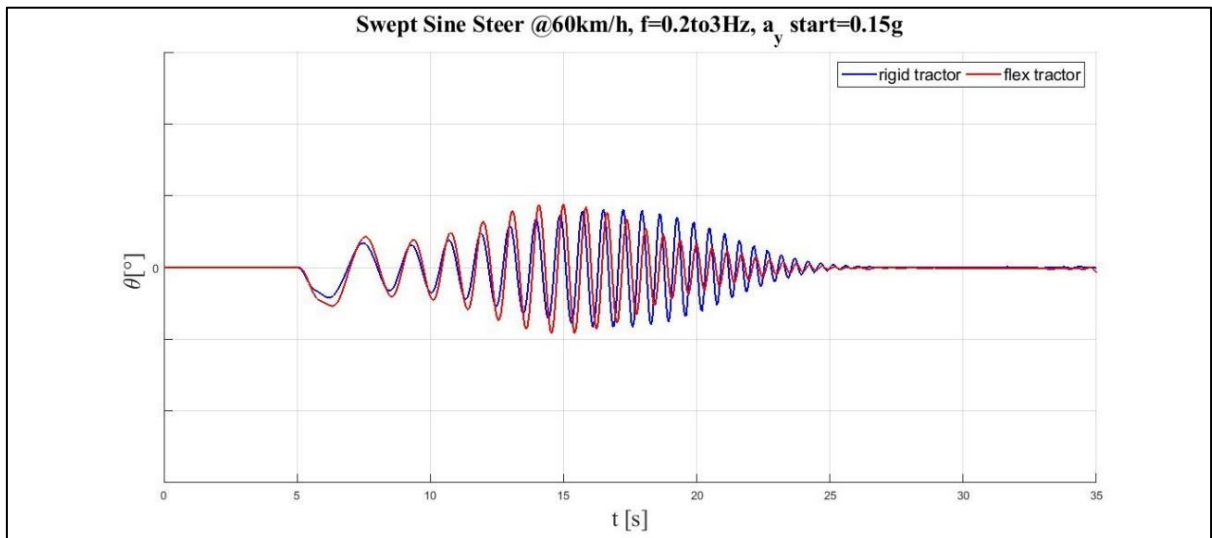
Pic. 4.17 - Tractor, Sweep Steer1: time evolution of the yaw rate (MATLAB)



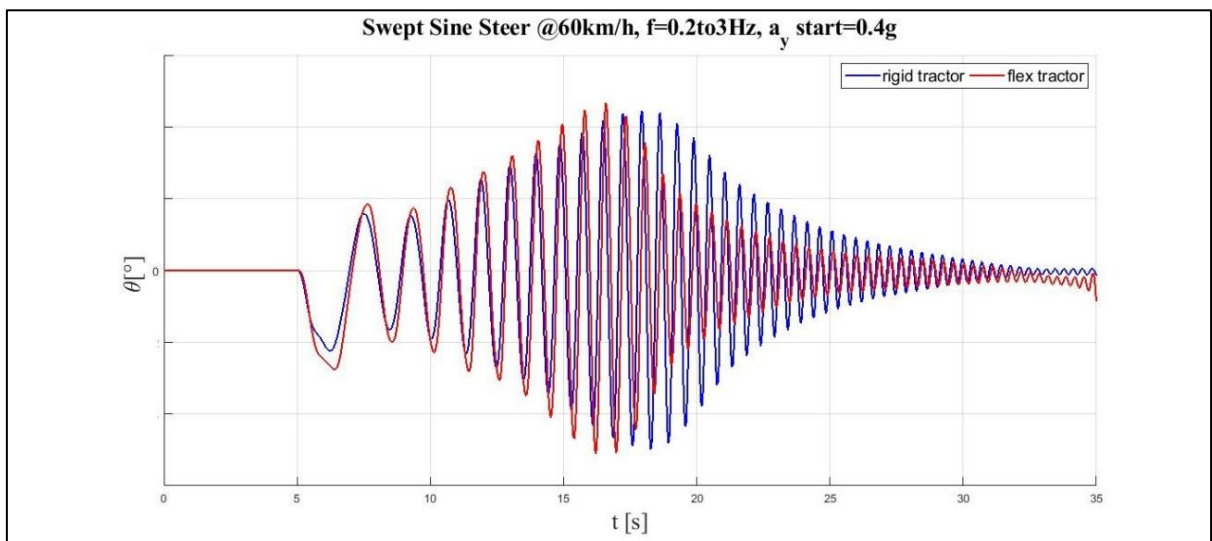
Pic. 4.18 - Tractor, Sweep Steer2: time evolution of the yaw rate (MATLAB)

The oscillations are similar to the lateral acceleration as for both the tests. Note that, both as to the flex and the rigid configuration, the larger the steering-wheel angle is, the higher the frequency corresponding to zero oscillation is. Moreover, the oscillations seem not to settle down in the second test, especially in the flex configuration.

Finally, the roll angle trends are presented.



Pic. 4.19 - Tractor, Sweep Steer1: time evolution of the roll angle (MATLAB)



Pic. 4.20 - Tractor, Sweep Steer2: time evolution of the roll angle (MATLAB)

Several considerations can be discussed watching Pic. 4.19 and 4.20. First of all, the peaks in the flex configuration are later compared to the rigid configuration ones, probably because of the damping in the cabine and in the frame. Secondly, in contrast to the other variables under analysis, the frequency which produce the highest peak value in the flex and in the rigid configuration is different: namely the resonance frequency of the flex configuration is lower

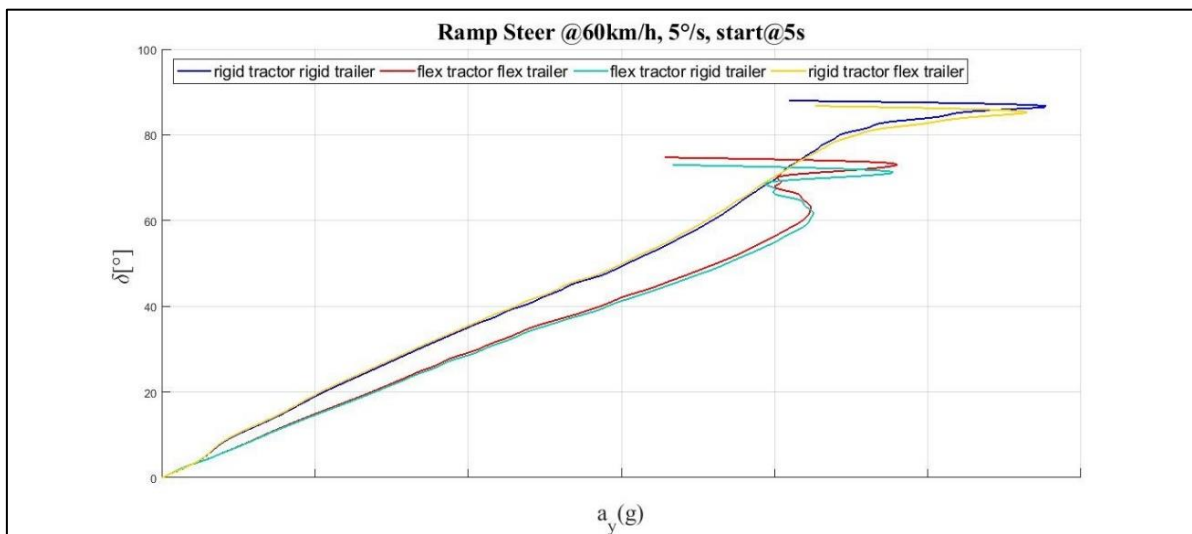
then the rigid configuration one. Finally the highest peak value corresponds to the flex configuration trend.

Note that the second Sweep Test, at high frequency, involved the non-linearity of some elements like the *bumpstop* or *reboundstop* or the *tires* and it is evident, for instance, from Pic. 4.13 and 4.16 which represent the lateral acceleration and the side slip trends. Nevertheless, there are no consequence on the yaw rate and the roll angle plots.

4.2 Full Truck Results

In this paragraph, the results coming from the Full Truck tests are shown.

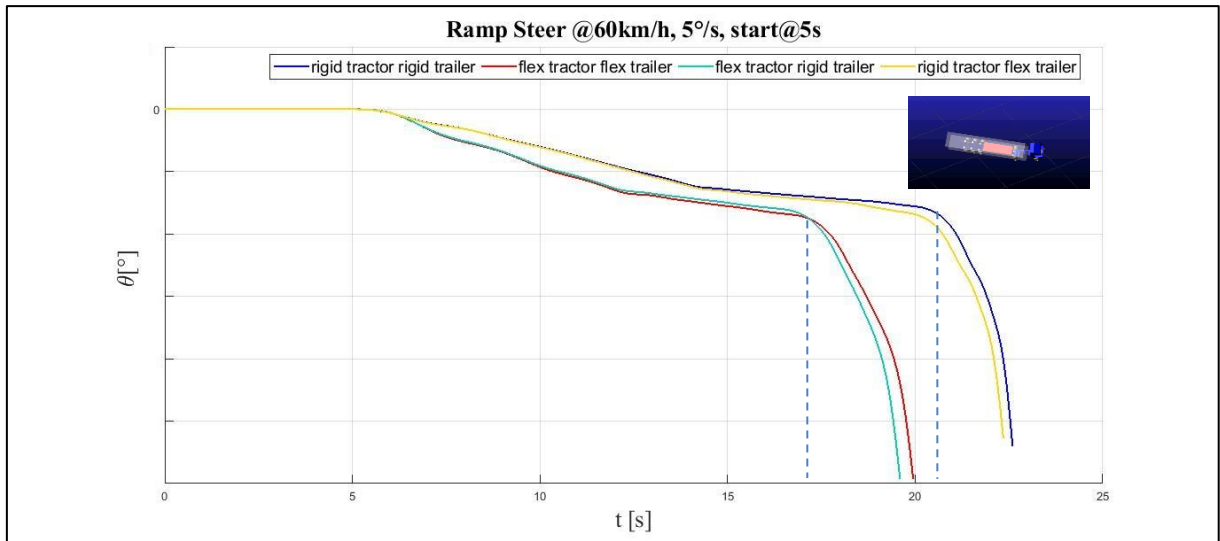
Firstly, the Ramp Steer test was carried out. The steering-wheel angle against the lateral acceleration plot follows.



Pic. 4.21 – Full Truck, Ramp Steer: steering-wheel angle against lateral acceleration (MATLAB)

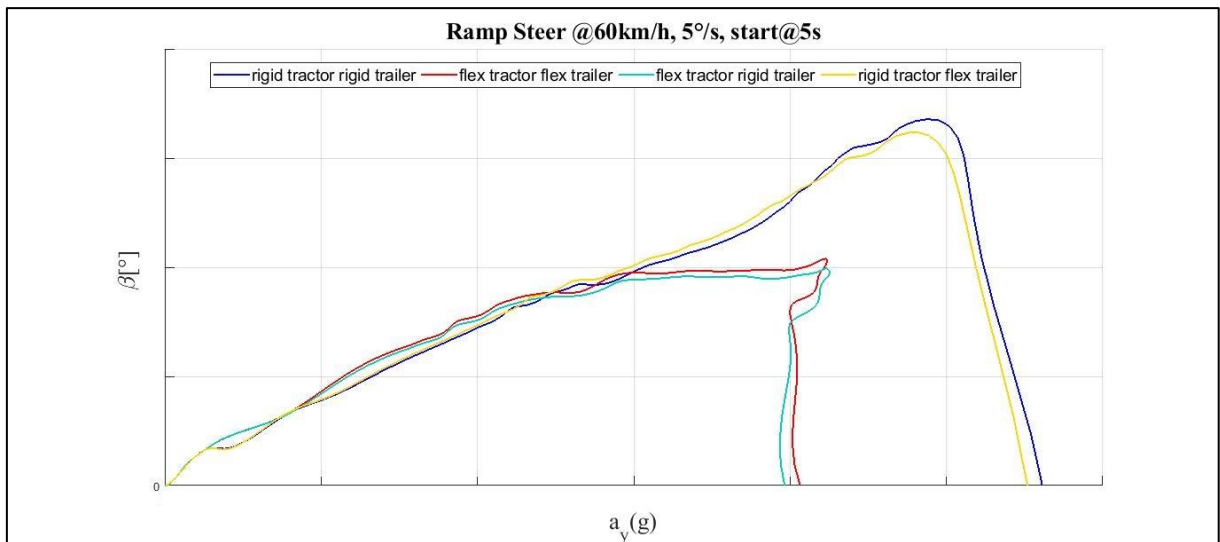
As can be seen from Pic. 4.21, the flexibility of the semitrailer axles gives a little contribution compared to the influence of the flexible tractor frame: in this case, the flexible axles make the vehicle more understeering while the flexible tractor frame and cabine continue to imply a more oversteering behaviour. Comparing Pic. 4.21 to Pic. 4.1, the flexibility of the frame and the cabine has a larger impact on the full truck than the tractor alone. Lastly, note that the loss of

stability was always characterized by a final rollover which happens at a different steering-wheel angle according to the configuration and it is evident seeing the roll angle trend (Pic. 4.22).



Pic. 4.22 - Full Truck, Ramp Steer: time evoluion of the roll angle (MATLAB)

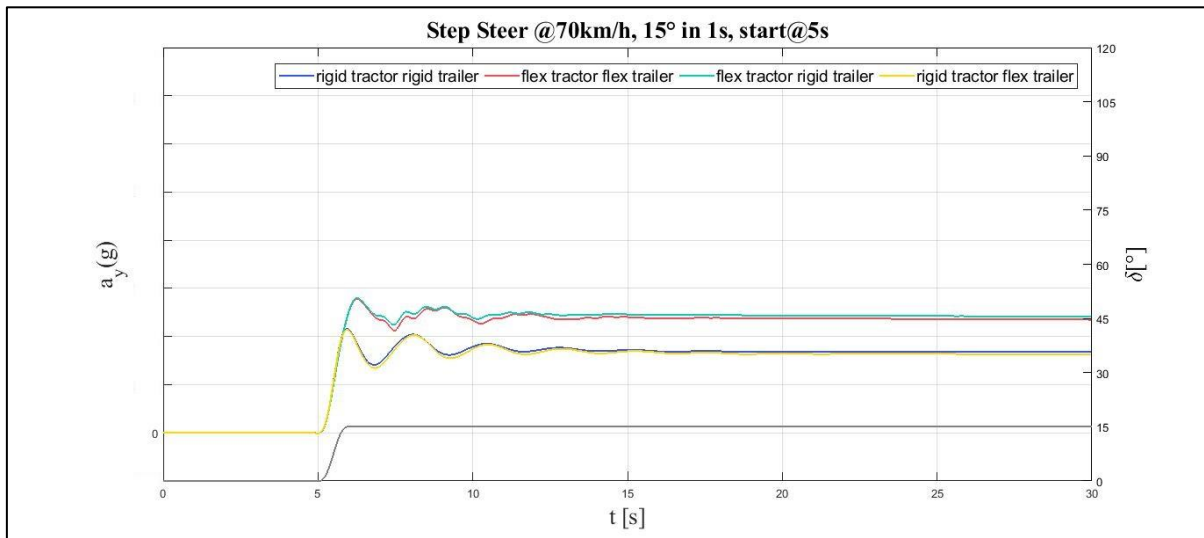
The side-slip angle against the lateral acceleration trend is reported below.



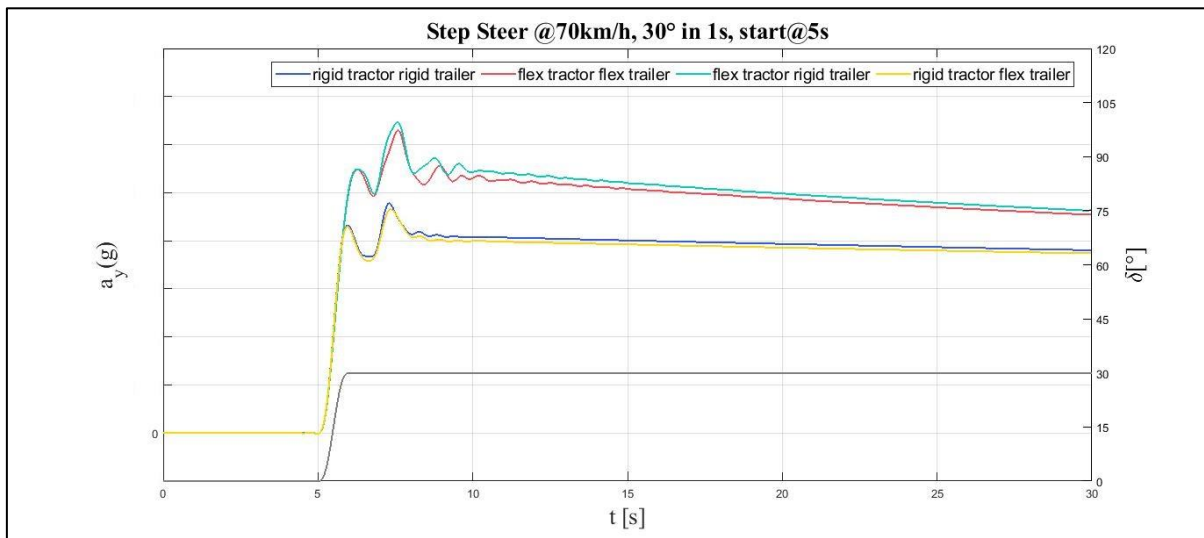
Pic. 4.23 – Full Truck, Ramp Steer: side-slip angle against lateral acceleration (MATLAB)

Secondly, the Step Steer results are analyzed.

The Pictures reported below represent the lateral acceleration against the time.



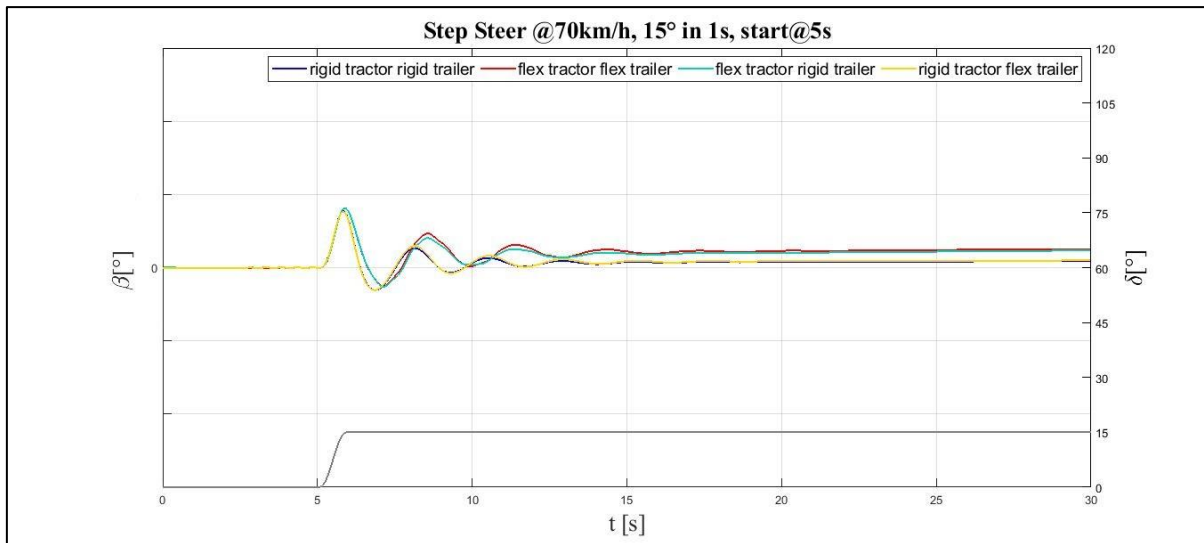
Pic. 4.24 – Full Truck, Step Steer1: time evoluion of the lateral acceleration (MATLAB)



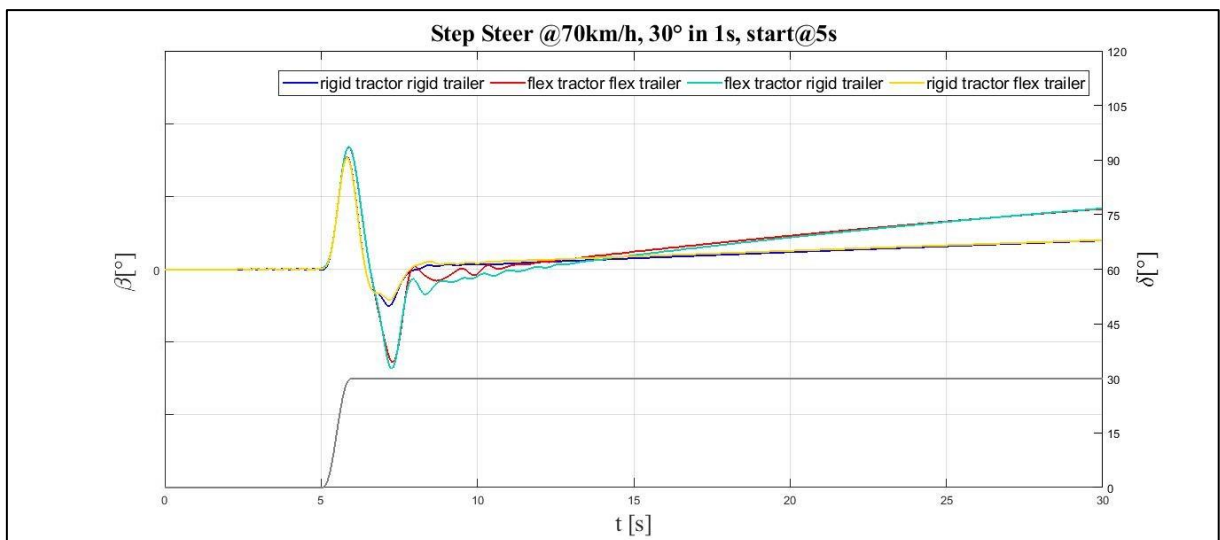
Pic. 4.25 – Full Truck, Step Steer2: time evoluion of the lateral acceleration (MATLAB)

Even in this case, the flexible semitrailers axles do not influence so much the results: the largest difference is in the second test which is more challenging than the first one. Note that in Pic. 4.25 the second peak is higher than the first one, which is probably due to the semitrailer inertia.

The side-slip angle charts are reported below.



Pic. 4.26 – Full Truck, Step Steer1: time evolution of the side-slip angle (MATLAB)



Pic. 4.27 – Full Truck, Step Steer2: time evolution of the side-slip angle (MATLAB)

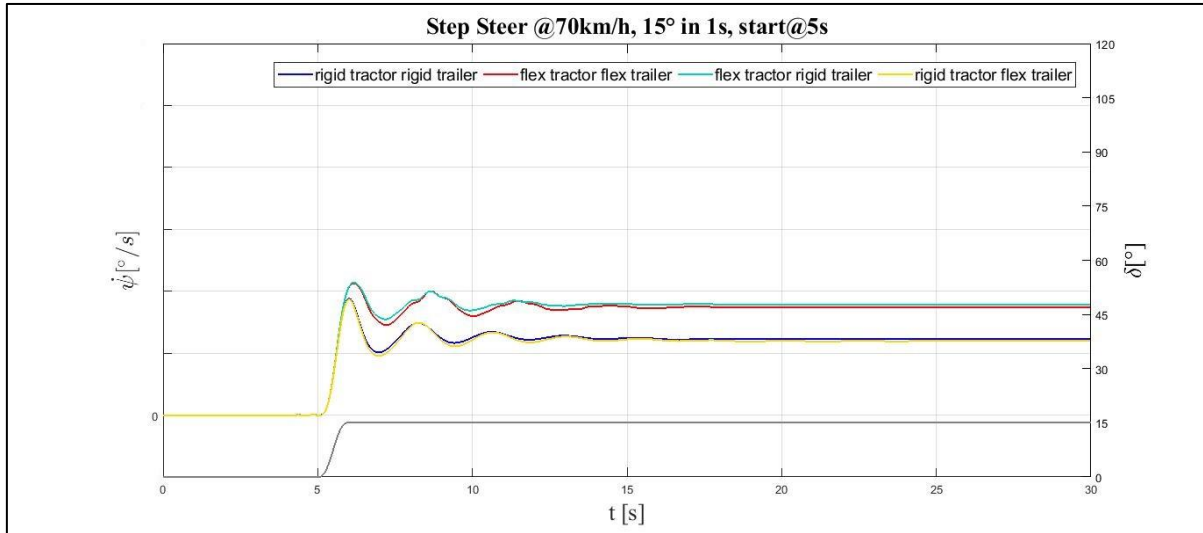
All the previous comments are valid even in these diagrams.

In Pic. 4.26, the oscillations of the *flex tractor* are higher and later than the rigid configuration ones. In Pic. 4.27, the flex configuration owns a second peak comparable to the first one while using the rigid tractor it is quickly dampened. Note that in both the tests and especially in the flex configuration, the tractor cannot reach a stationary value: the longitudinal velocity

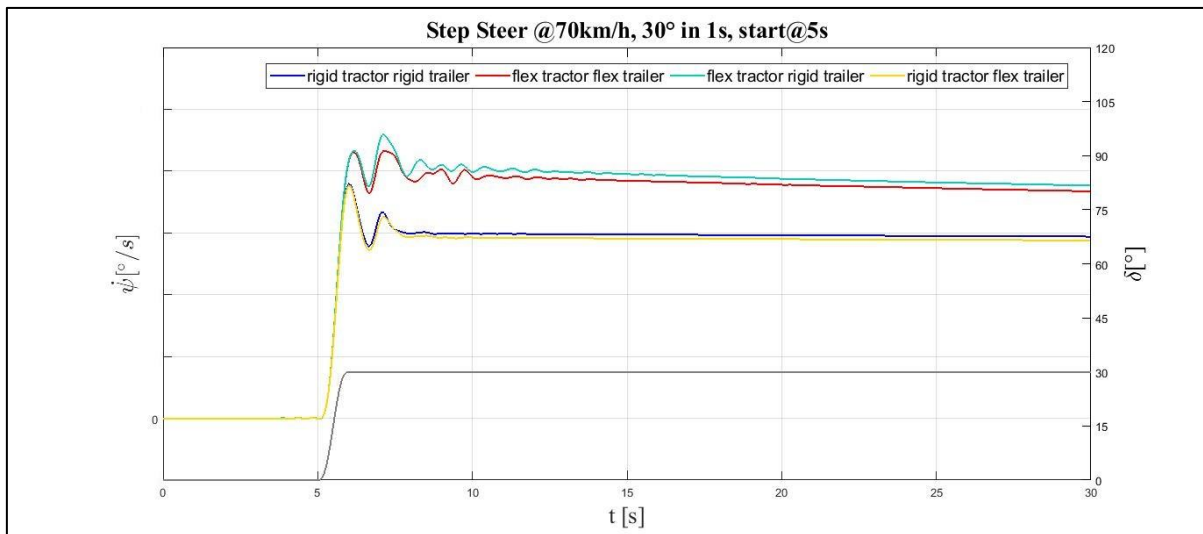
decreases since, according to the test methodology, the accelerator pedal travel is hold constant.

Thus, the lateral velocity being equal, the side-slip angle grows.

Then, the time evolution of the yaw rate is plotted.



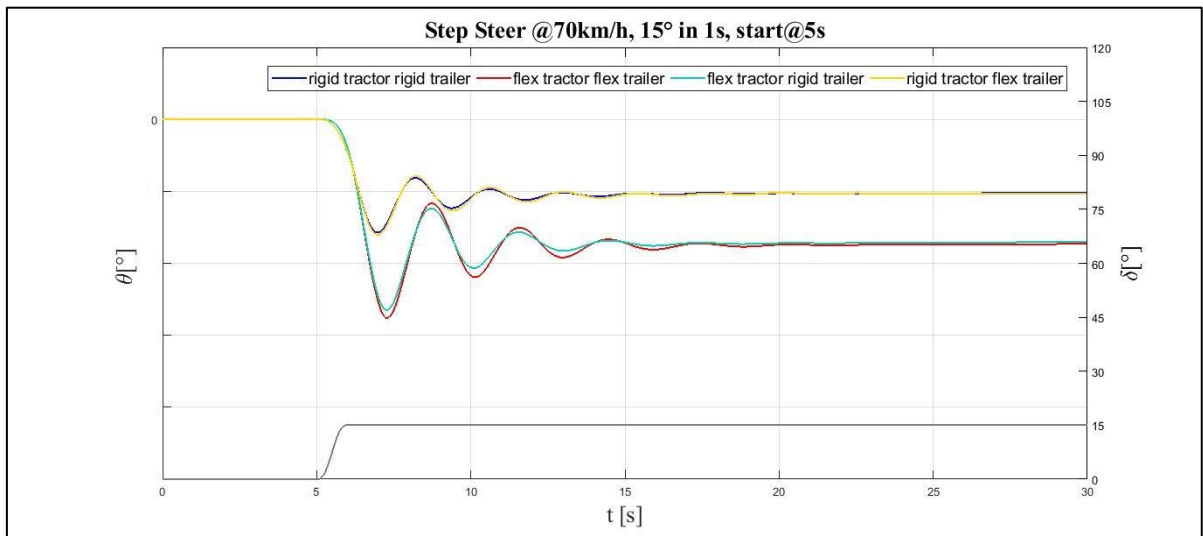
Pic. 4.28 – Full Truck, Step Steer1: time evoluion of the yaw rate (MATLAB)



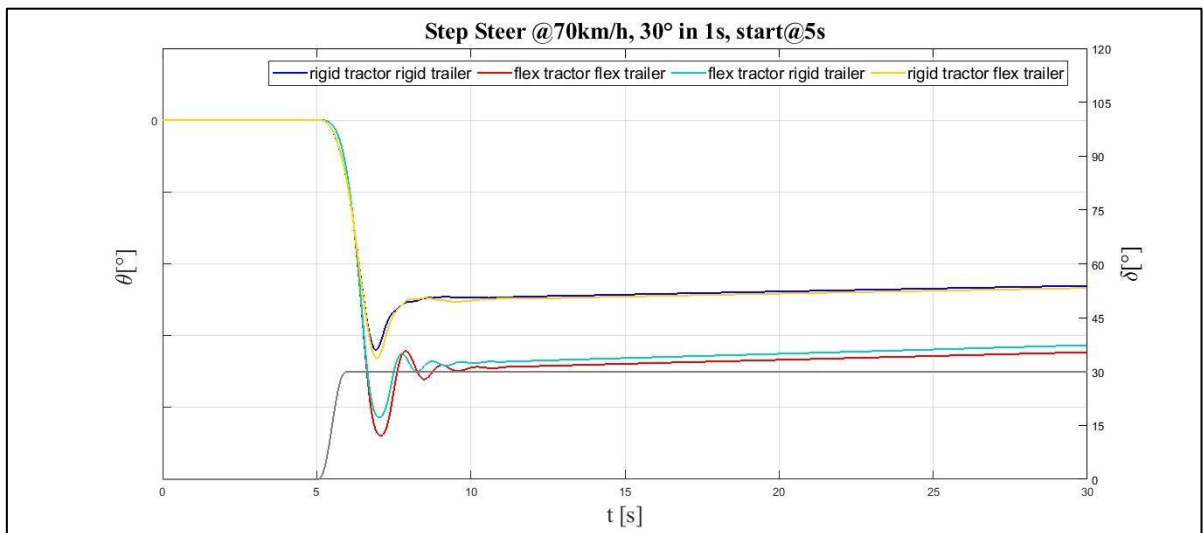
Pic. 4.29 – Full Truck, Step Steer2: time evoluion of the yaw rate (MATLAB)

The same considerations can be applied to these charts.

Finally, the roll angle trends are reported.



Pic. 4.30– Full Truck, Step Steer1: time evoluion of the roll angle (MATLAB)

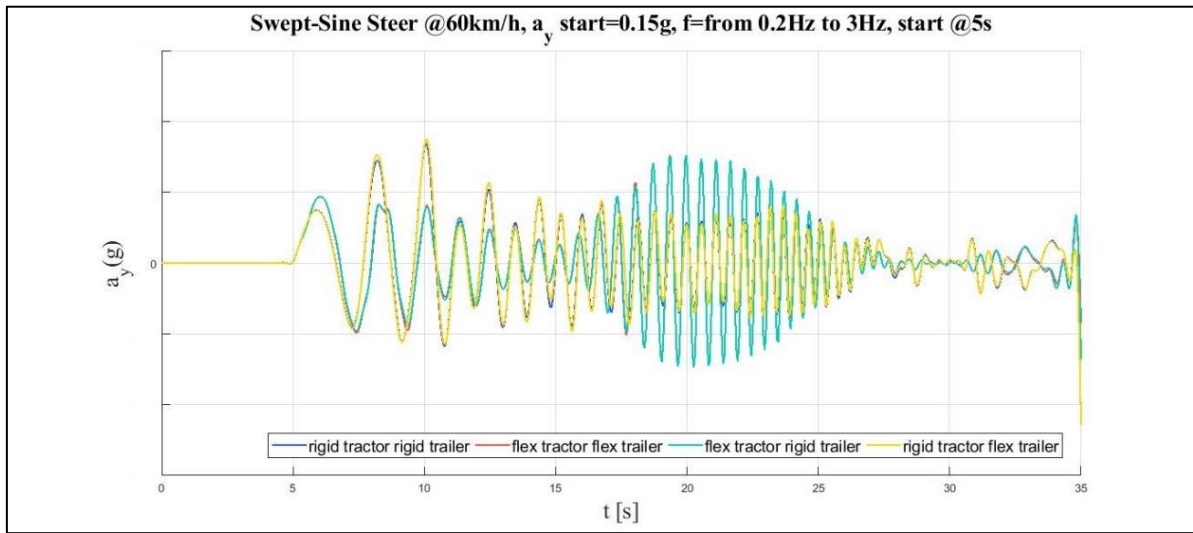


Pic. 4.31 – Full Truck, Step Steer2: time evoluion of the roll angle (MATLAB)

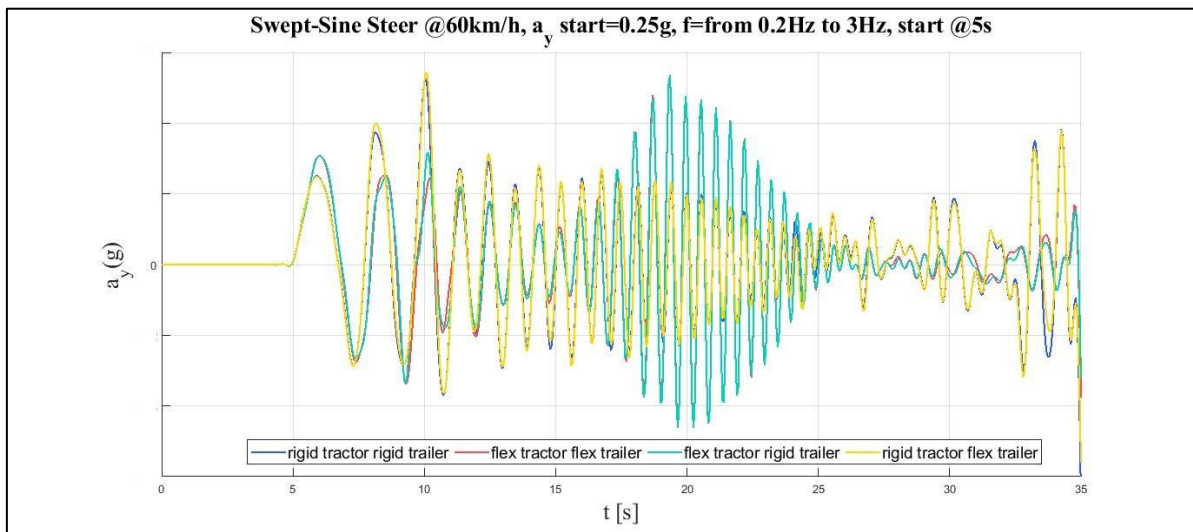
In Pic. 4.30 and Pic. 4.31, the gap in terms of values and lateness of the flex tractor configuration is remarkable. Notice again that in the first test the vehicle acts like an underdampened system while using a larger value of steering-wheel angle the oscillations are dampened like an overdampened system.

The last results to be analysed come from the two Sweep Steer tests.

The first diagrams to be plotted refer to the lateral acceleration.



Pic. 4.32 – Full Truck, Sweep Steer1: time evolution of the lateral acceleration (MATLAB)

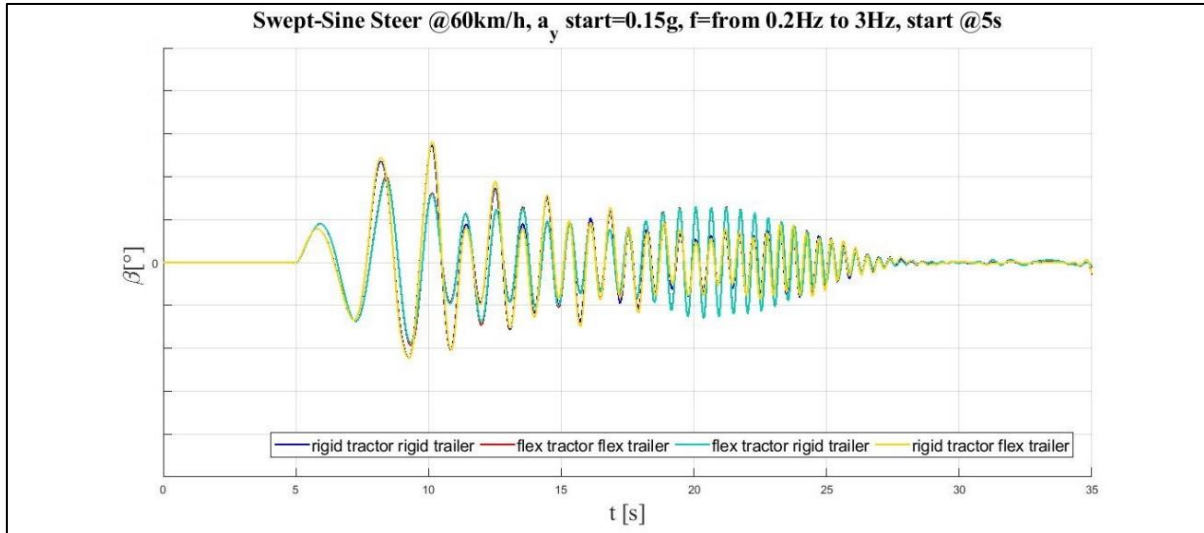


Pic. 4.33 – Full Truck, Sweep Steer2: time evolution of the lateral acceleration (MATLAB)

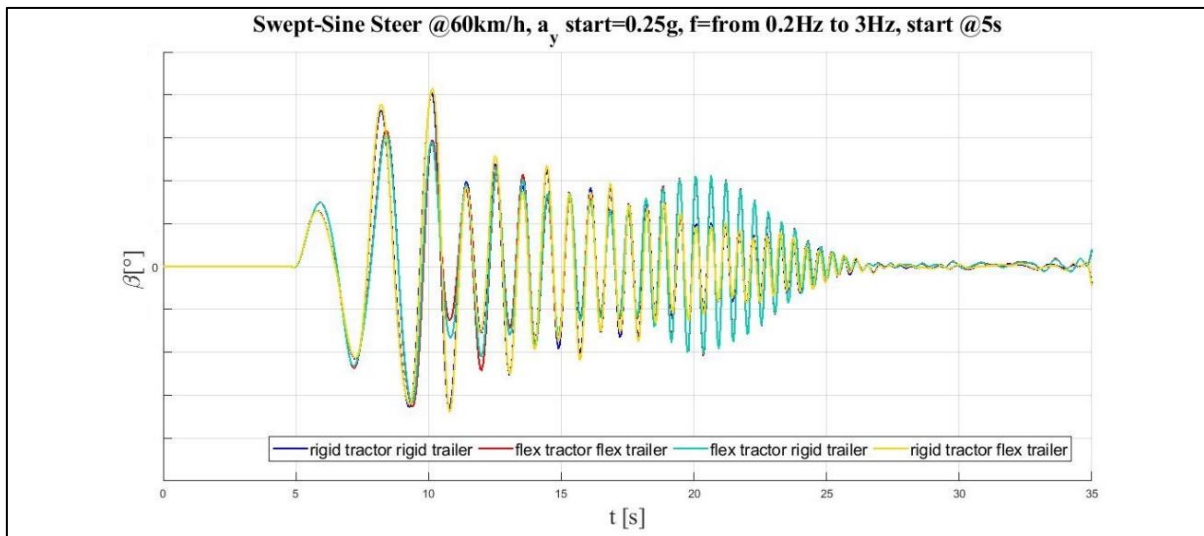
From Pic. 4.32 and 4.33, it is clear that the full truck in the *flex tractor* configurations owns two resonances, one in the low and an other one in the middle frequencies, while the rigid tractor configurations have a closely decreasing trend: the different behaviour could derive from the impact of the semitrailer on the tractor frame. The peaks of the flex tractor configurations are always later than the ones of the rigid configurations.

Notice that the non-linearities get involved at the end in both the manoeuvres and in all the four configurations.

Then, the side-slip angle diagrams are reported.



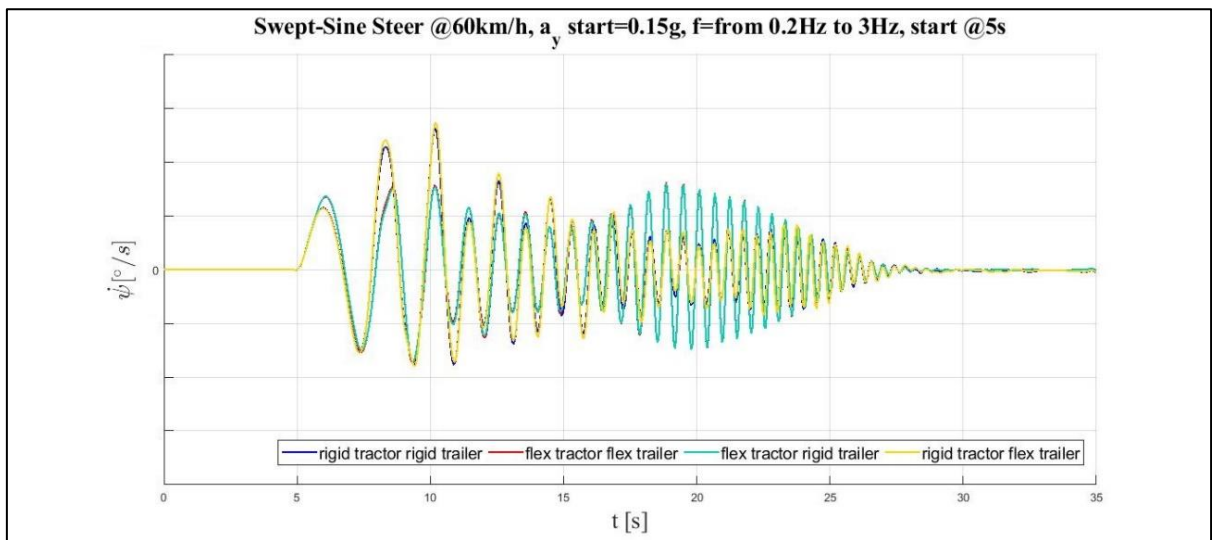
Pic. 4.34 - Full Truck, Sweep Steer1: time evoluion of the side-slip angle (MATLAB)



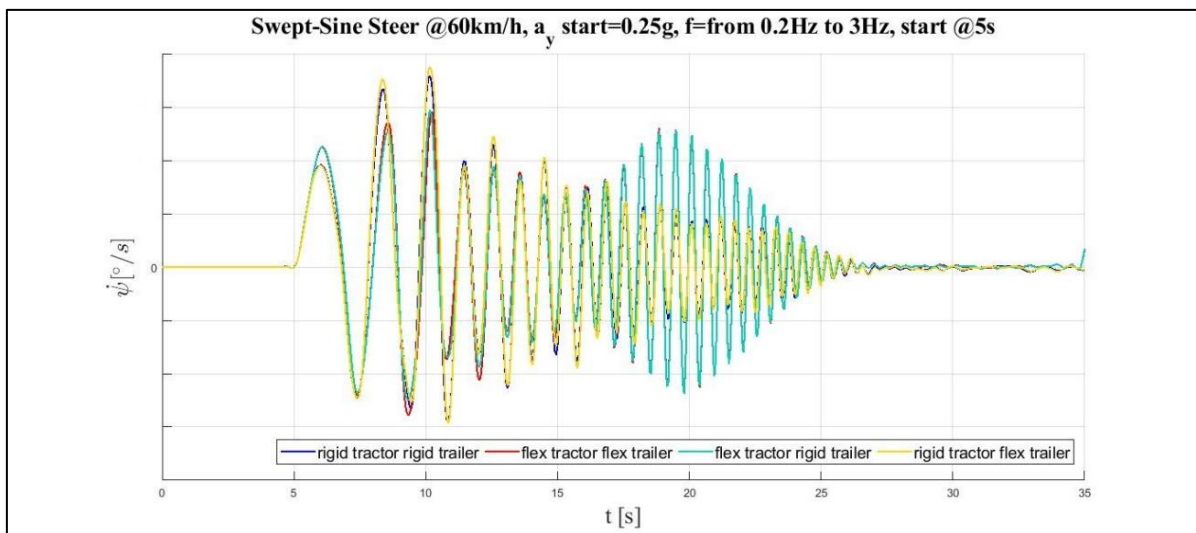
Pic. 4.35 - Full Truck, Sweep Steer2: time evoluion of the side-slip angle (MATLAB)

Pic. 4.34 and 4.35 confirm the considerations discussed as for Pic. 4.32 and 4.33.

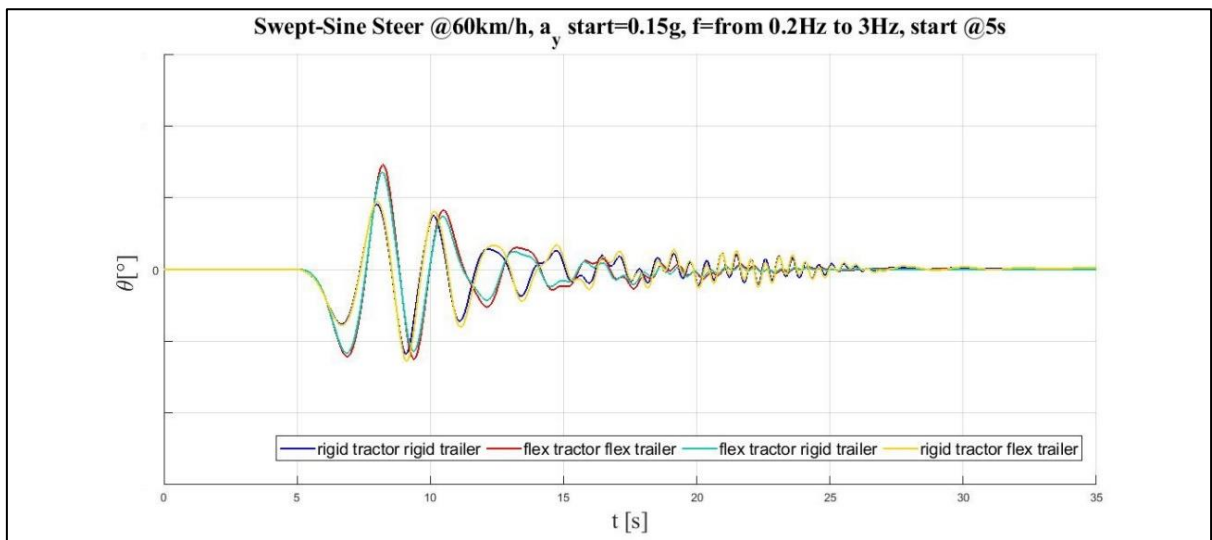
For completeness, the yaw rates (Pic. 4.36 and 4.37) and the roll angle diagrams (Pic. 4.38 and 4.39) are reported below.



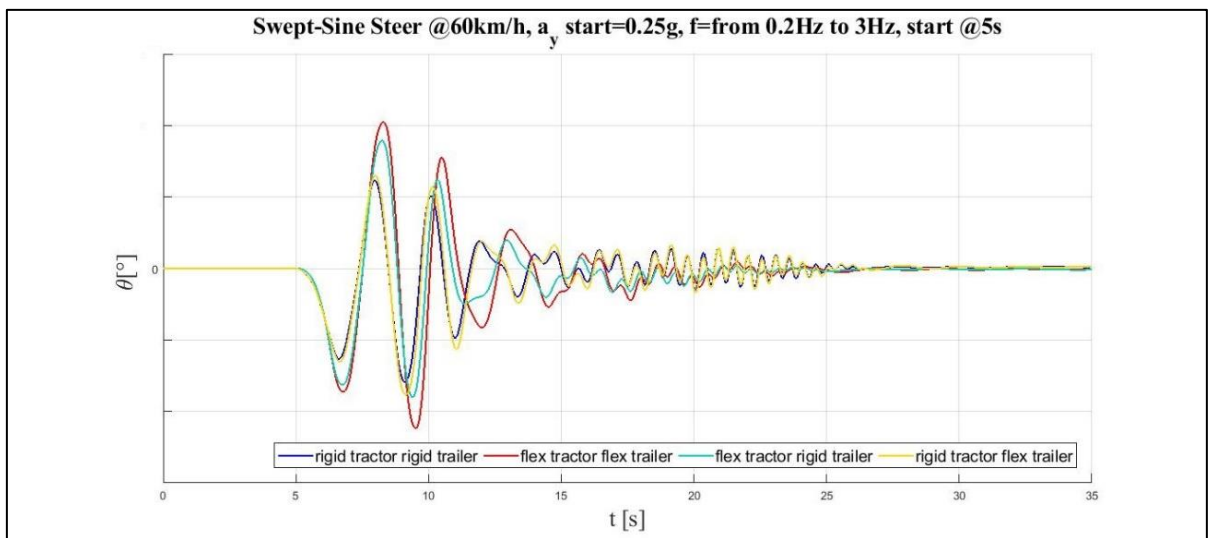
Pic. 4.36 - Full Truck, Sweep Steer1: time evoluion of the yaw rate (MATLAB)



Pic. 4.37 - Full Truck, Sweep Steer2: time evoluion of the yaw rate (MATLAB)



Pic. 4.38 - Full Truck, Sweep Steer1: time evolution of the roll angle (MATLAB)



Pic. 4.39 - Full Truck, Sweep Steer1: time evolution of the roll angle (MATLAB)

A small but remarkable difference between the flexible and the rigid semitrailer axles is noted as regards Pic. 4.39 which describes the roll angle evolution in time, especially in the *flex tractor* configurations.

CONCLUSIONS

The predetermined goal of this thesis work, namely the development of the multibody model of *Iveco Stralis model year 2019*, can be considered achieved. All the modelling strategies and the methodology exploited in the activity were aimed at making a model as much versatile and changeable as possible in order to facilitate the future updates.

The main strenghts of the final model consist of the use of a specific tool used as for the front leaf spring suspension and the implementation of several flexible bodies, namely the tractor cabine and frame and the semitrailer axles. All these points are targeted at approximating in the best way the dynamic behaviour of the vehicle under analysis.

The multibody model of the Stralis can be moved to the Iveco Engineering Office in order to carry on their dynamic studies.

Since the model was not calibrated because of the lack of the experimental data, the work has been focused on the influence of the flexible bodies in the rigid model in terms of lateral dynamics. Several manoeuvres according to standard ISO were simulated both on the tractor and the full truck. The differences in the results are more evident in the full truck tests: the main role was played by the flexibility of the tractor frame while semitrailer axles have a small impact: it is recommended to set them as rigid bodies in the future analysis. Both on the tractor and the full truck, the different dynamics are more remarkable in the lateral transient manoeuvres than the steady-state ones and choosing more challenging test parameters since the shape modes of the flexible bodies are more excited.

After the calibration of the virtual model, comparing the simulation results to the on-road ones, further steps in the modelling could be still carried out in order to make the model more complete and realistic: the integration of the semitrailer frame as flexible body, the driveline, the brake system and the active controls like ABS and ESP. This study could be also extended to the longitudinal dynamics performing other kind of tests.

Moreover, having the property files of the tires according to the Pacejka 5.2 formula for different pressure levels, the influence of the tire pressure on vehicle dynamics can be analyzed. Finally, other tire models, like the Swift Tyre for the comfort studies or the FTire or CDTire for the durability ones, can be implemented in order to represent the tire dynamics in a more accurate way during the vehicle simulations.

APPENDIX A

In this Appendix, more details will be given about the flexible bodies, both as concern the Modal Analysis and the management in *Adams*.

Modal Superposition

The purpose of this paragraph is to explain the procedure used by the FEM solver *Nastran*, in order to compute the Modal Analysis and the Dynamic solution.

The theoretical background was collect from the “Elementi Finiti” ^[4] and the “Theory of Flexible Bodies” ^[5].

The assumption which underlines FEM theory consists of considering the deformation of the body as small and linear. The approximation of using a finite element method lies in the fact that a body, constituted by an infinite number of DOF, is represented thanks to a model with a finite number of DOF.

In a Dynamic Analysis which deals with FEM model, the displacement of the nodes can be written as linear combination of the mode shapes. In matrix notation:

$$\{\mathbf{s}\} = \{\mathbf{x}\}[\Phi] \quad (51)$$

The vector $\{\mathbf{x}\}$ collects what are called modal coordinates and represents the amplitudes of the shape modes, gathered in columns in the matrix $[\Phi]$.

This approach to solve the dynamic problem is generally called Modal Superposition and substantially consists of turning from the physical space to the modal one.

Since the procedure is as much expensive as the number of nodes is high and the dynamic characterization of a body requires a smaller number of DOF than the static analysis, it is advisable the using of a reduction method in order to decrease the dimension of the problem. Many algorithm are available: in this work the Craig-Bampton, which is the Nastran default one, was used.

The idea which underlies any reduction method is to choose some nodes and to implode the others in these ones. The difference deals with the criteria used to distinguish the two node families.

The Craig-Bampton method partiones the DOF into a *boundary* or *interface* family $\{\mathbf{s}_B\}$ and into an *interior* one $\{\mathbf{s}_I\}$.

First of all, the *constraint modes* are obtained by the Modal Analysis giving each boundary DOF a unit displacement while holding all the others fixed: they will not be subjected to a reduction in order not to miss boundary information. Notice that, in this phase of the Modal Analysis, there is a one to one corrispondence between the attachment mode coordinate and its respective displacemnt.

The *normal modes* are extracted by fixing the boundary DOF and computing an eigensolution; the user can choose how many modes of this type have to be expanded: the quality of the modal reduction is proportional to the number of normal modes required.

The solution can be rewritten as:

$$\begin{Bmatrix} \mathbf{s} \end{Bmatrix} = \begin{Bmatrix} \mathbf{s}_B \\ \mathbf{s}_I \end{Bmatrix} = \begin{bmatrix} I & 0 \\ \Phi_{IC} & \Phi_{IN} \end{bmatrix} \begin{Bmatrix} \mathbf{x}_C \\ \mathbf{x}_N \end{Bmatrix} \quad (52)$$

where:

$\{\mathbf{s}_B\}$ is the array of the boundary DOF;

$\{\mathbf{s}_I\}$ is the array of the interior DOF;

$[I]$ is the identity matrix;

$[0]$ is the zero matrix;

$[\Phi_{IC}]$ is the matrix which contains the shape modes of the interior DOF in the constraint modes;

$[\Phi_{IN}]$ is the matrix which contains the shape modes of the interior DOF in the normal modes;

$\{\mathbf{x}_C\}$ is the array of the modal coordinates of the constraint modes;

$\{\mathbf{x}_N\}$ is the array of the modal coordinates of the fixed-boundary normal modes.

Then, the generalized stiffness and mass matrices, according to the Craig-Bampton method, can be obtained as:

$$[\hat{\mathbf{k}}] = [\Phi]^T [\mathbf{k}] [\Phi] \quad (53)$$

$$[\hat{\mathbf{m}}] = [\Phi]^T [\mathbf{m}] [\Phi] \quad (54)$$

$[\hat{\mathbf{k}}]$ is a block diagonal matrix since there is no stiffness coupling between the constraint modes and the normal ones while $[\hat{\mathbf{m}}]$ is not because of the inertia coupling.

Notice that the Craig-Bampton modes are not orthogonal and this is clear since the two generalized matrices are not diagonal. The orthogonalization procedure of the eigenvectors requires a matrix transformation which influences also the generalized coordinates. Finally, the shape modes referred to the rigid body motions can be identified and disabled.

Flexibility in Adams/Solver

In this paragraph, how *Adams* manage a FEM model, downstream from the Craig-Bampton Analysis, will be discussed in terms of differences respect to a rigid bodies.

Firstly, *markers*, which are a sort of *construction frames* set up on the bodies, are associated with all the nodes of the model: each of them monitors the location and the orientation of its own node. The reason consists of satisfying the joint equations, evaluating internal forces and measuring physical quantities according to the user-defined requests.

As for the applied loads, only the point ones, which can be tranfered by the joints to the model, will be mentioned; a point force or torque acts on a marker of the flexible body: it needs to be projected on the corresponding generalized coordinate in order to obtain the generalized force as previously described in Chapter 1.

The equation of motion is the Lagrangian one as for the rigid body. The kinetic energy can be approximated for a flexible body as:

$$T \approx \frac{1}{2} \sum_{j=1}^n (\mathbf{v}_j^T \mathbf{m}_j \mathbf{v}_j + \boldsymbol{\omega}_j^T \mathbf{I}_j \boldsymbol{\omega}_j) \quad (55)$$

where

j is the node index;

\mathbf{v}_j is the vector of the translational velocity of j -node;

\mathbf{m}_j is the j -nodal mass tensor;

$\boldsymbol{\omega}_j$ is the vector of the angular velocity of j -node

\mathbf{I}_j is the j -nodal inertia tensor.

Summarizing the angular and the translational vectors in the single array $\dot{\mathbf{x}}$, the kinetic energy can be written as:

$$T \approx \dot{\mathbf{x}}^T \mathbf{M}(\mathbf{x}) \dot{\mathbf{x}} \quad (56)$$

In the generalized mass matrix \mathbf{M} , nine inertia invariants figure: they depend on several quantities, like the mass and the undeformed location of the nodes or the shape modes. Moreover, it directly depends on the modal coordinates and so it is not a constant quantity.

As the regards the potential energy U , the two terms are the gravity and the elasticity.

$$U = U_g(\mathbf{x}) + \frac{1}{2} \mathbf{x}^T \mathbf{K} \mathbf{x} \quad (57)$$

\mathbf{K} represents the generalized stiffness matrix of the body written respect to the modal coordinates and is generally constant.

In a flexible body even damping dissipation can be included in the following term:

$$F \approx \dot{\mathbf{x}}^T \mathbf{D} \dot{\mathbf{x}} \quad (58)$$

where \mathbf{D} is the damping matrix, normally constant and symmetric; if the mode shapes are orthogonal, \mathbf{D} can be a diagonal matrix.

Finally, the equation which governs the motion in terms of generalized coordinates is written as:

$$\mathbf{M} \ddot{\mathbf{x}} + \dot{\mathbf{M}} \dot{\mathbf{x}} - \frac{1}{2} \left[\frac{\partial \mathbf{M}}{\partial \mathbf{x}} \dot{\mathbf{x}} \right]^T \dot{\mathbf{x}} + \mathbf{K} \mathbf{x} + \mathbf{f}_g + \mathbf{D} \dot{\mathbf{x}} + \left[\frac{\partial \boldsymbol{\Psi}}{\partial \mathbf{x}} \right]^T \boldsymbol{\lambda} = \mathbf{Q} \quad (59)$$

BIBLIOGRAPHY

- [1] Arbor A., Dyer N., Negrut D. (2004). “ADAMS/Solver Primer”
- [2] Galvagno E., Velardocchia M. (2017). “Meccanica del Veicolo”, CLUT Editrice
- [3] MSC Software Japan (2015). “Leaf Spring Toolkit for Adams 2015.1 User’s Guide”.
- [4] Gugliotta A. (2002). “Elementi Finiti Parte III”. Otto Editore, Chapter 8.
- [5] MSC Software (2015). “Theory of Flexible Bodies”
- [6] Galvagno E., Mauro S., Velardocchia M., Vigliani A. “Notes of the Vehicle Dynamics course”. Polytechnic of Turin, Italy.
- [7] Pacejka H.B. “Tyre and Vehicle Dynamics”. Delft University of Technology, Netherlands.
- [8] Association Française de Normalisation (2004). “Norme Internationale ISO 4138”, Third Edition, ISO Editeur
- [9] Association Française de Normalisation (2003). “Norme Internationale ISO 7401”, Second Edition, ISO Editeur
- [10] Capitelli E., Nosenzo V. (2018). “MissionElab – User Manual”

RINGRAZIAMENTI

La tesi di laurea magistrale rappresenta in un certo modo l'atto finale della vita universitaria di uno studente: giornate di studio intenso, corse frenetiche la mattina per assicurarsi un posto nelle prime file a lezione, attese che sembrano un'eternità per il voto di un esame, scrivendo questa ultima manciata di pagine, realizzi che tutto sta per concludersi. Se prima non desideravi altro che la fine, ora ti aggrappi al filo dei ricordi e non vuoi allentare la presa. Ma fa parte del processo di crescita che inesorabilmente investe ognuno di noi, che da una parte intimorisce e al tempo stesso incuriosisce ed entusiasma. E sono convinto che anche questa fase della vita non ha fatto altro che arricchirmi sia a livello universitario ma soprattutto umano.

Ripercorrendo con un velo di nostalgia gli ultimi due anni e mezzo, che sono parallelamente coincisi con il mio trasferimento a Torino, è doveroso ringraziare tutti coloro che hanno contribuito, ognuno a proprio modo, al raggiungimento dell'obiettivo finale.

E vorrei iniziare proprio da Torino, una città tanto ostile specialmente nei periodi iniziali che ha saputo a poco a poco farsi apprezzare e accogliermi.

La mia famiglia. I miei genitori, mia sorella *Maria*, nonni e zii, che mi hanno sempre supportato e incoraggiato in ogni decisione importante, con la loro saggezza ed il loro affetto; nonostante la lontananza hanno trovato sempre un modo di farsi sentire vicini, che sia con una visita inaspettata o con una telefonata serale.

Vorrei ringraziare i miei compagni di viaggio in questa magica avventura torinese.

Alessia, con la quale condivido un viaggio molto più importante e lungo ormai più di quattro anni insieme. Per te qualche riga di ringraziamento nelle pagine finali di una tesi è riduttiva, troppo... L'Università ha voluto prima farci incontrare. Poi la decisione di cambiare, come in ogni cosa sempre fianco a fianco, l'uno dell'altro. Sento che anche questa esperienza, dai momenti difficili a quelli felici, non ha fatto altro che rafforzare ulteriormente il nostro legame.

E poi gli amici, in particolare *Daniele*, con il quale ho una splendida amicizia sin dai primi anni di Ingegneria; anche se le nostre strade universitarie si sono divise, ti sei sempre dimostrato l'amico che tutti vorrebbero avere, una persona su cui poter sempre contare.

Ringrazio *La Compagnia*, il mio coinquilino *Danilo*, *Domenico* e *Antonio*, per aver reso la nuova casa una vera Casa, con tanti momenti di condivisione: un pomeriggio di studio, una cena, un film e tanto altro da tramandare ai posteri.

Vorrei ringraziare infine *Simone*, primo nuovo amico in quel di Torino, punto di riferimento per ogni consiglio in ambito professionale, senza il quale dubito sarei venuto a conoscenza della possibilità di svolgere questa attività di tesi.

Arrivo dunque agli amici, vorrei ringraziarvi tutti, vicini e lontani, uno ad uno, perchè chi con una gita di pochi giorni o chi con un semplice messaggio ha cercato sempre di ridurre la distanza che ci separava.

Un particolare ringraziamento va a chi ha materialmente contribuito al conseguimento di questo risultato: in primis il team del dipartimento di Meccanica Applicata del Politecnico di Torino, con particolare riguardo al *Prof. Mauro Velardocchia*, al *Prof. Enrico Galvagno* e al *Prof. Elvio Bonisoli* che mi hanno seguito con estrema disponibilità e professionalità.

Ringrazio poi il mio tutor aziendale, il *Dott. Vladi Massimo Nosenzo*, la *Dott.ssa Enrica Capitelli* e l'*Ing. Andrea Morello*, per aver creduto nelle mie capacità, per tutto l'aiuto nel corso degli ultimi mesi e per avermi offerto la preziosissima possibilità di affacciarmi al mondo del lavoro da studente.

In ultimo ringrazio lo staff della *MSC Software* di Torino ed in particolare l'*Ing. Angelo Casolo*, per la formazione ed il supporto tecnico che mi sono stati offerti in questo lavoro di tesi.